PNC TN9420 92-005

INTRODUCTION of NUCLEAR INSTRUMENTATIONS and RADIATION MEASUREMENTS in EXPERIMENTAL FAST REACTOR "JOYO"

Toshihiro ODO and Soju SUZUKI

April, 1992

Experimental Reactor Division
O-arai Engineering Center
Power Reactor and Nuclear Fuel Development Corporation

PNC TN9420 92-005
April, 1992

INTRODUCTION of NUCLEAR INSTRUMENTATIONS and RADIATION MEASUREMENTS in EXPERIMENTAL FAST REACTOR "JOYO"

Toshihiro ODO* and Soju SUZUKI*

ABSTRACT

This report introduces the nuclear instrumentation system and major R&D (research and development) activities using radiation measurement techniques in Experimental Fast Reactor "JOYO".

In the introduction of the nuclear instrumentation system, following items are described;

- system function
- roles as a reactor plant equipment
- specifications and characteristics of neutron detectors,
- construction and layout of the system

For reactor dosimetry at various irradiation tests and surveillance tests, multi-foil method employed in "JOYO", neutron fluence evaluation using activation foils and HAFM (Helium Accumulation Fluence Monitor) under development are described briefly. The failed fuel detection system and some experimental equipments using radiation measurement techniques are also introduced here with main results obtained by a series of fuel failure simulation experiments.

In addition, following R&Ds are picked up as some examples based on radiation measurement technology;

- burn-up measurement of spent fuel subassembly
- measurement and evaluation of radiation source distributions (radioactive corrosion products)

* Reactor Technology Section, Experimental Reactor Division,
O-arai Engineering Center, PNC

PNC TN9420 92-005
１９９２年　４月

高速実験炉「常陽」の核計装設備と放射線計測入門

大戸 敏弘*、鈴木 惣十*

要　旨

本報告書は、高速実験炉「常陽」の核計装設備および実験炉部で実施している広範な研究開発のうち、放射線計測が主要な測定技術となっている代表的な研究開発の内容を紹介するものである。

核計装設備の紹介では、原子炉プラント設備としての核計装の機能と位置付け、使用している中性子検出器の仕様と特性、システム構成と機器配置等について記述した。各種照射試験やサーベイランス試験に対する中性子照射量を実測ベースで評価するための原子炉ドシメトリーでは、実験炉部が採用している多重放射化法とその測定解析評価法および目下開発中のＨＡＦＭ（ヘリウム蓄積モニタ法）について概説した。また、放射線計測技術がキーとなる破損燃料検出技術の開発では、「常陽」の燃料破損検出設備と各種実験装置の説明に加え、現在までに実施した一連の燃料破損模擬実験の主な成果を紹介した。

さらに、放射線計測を基礎技術として用いている研究開発として

・使用済燃料の燃焼度測定
・被曝源（放射性腐食生成物）分布の測定と評価

について、その概略内容を記述した。

＊動力炉・核燃料開発事業団　大洗工学センター　実験炉部技術課

INTRODUCTION of NUCLEAR INSTRUMENTATIONS and RADIATION MEASUREMENTS in EXPERIMENTAL FAST REACTOR "JOYO"

Tosihiro ODO and Soju SUZUKI

CONTENTS

1. INTRODUCTION ---- 1

2. PLANT DESCRIPTION ---- 6

3. NUCLEAR INSTRUMENTATION SYSTEM (NIS) ---- 11

4. NEUTRON FLUENCE MEASUREMENT WITH DOSIMETRY USING ACTIVATION METHOD --- 22

5. HELIUM ACCUMULATION FLUENCE MONITOR (HAFM) ---- 35

6. FUEL FAILURE DETECTION (FFD) SYSTEM ---- 38

7. FAILED FUEL DETECTION AND LOCATION (FFDL) SYSTEM ---- 63

8. BURN-UP DISTRIBUTION MEASUREMENT OF JOYO SPENT FUEL ---- 68

9. MEASUREMENT OF RADIOACTIVE CORROSION PRODUCTS (CP) ---- 78

ACKNOWLEDGMENT ---- 83

1. INTRODUCTION

JOYO is a sodium-cooled fast reactor which was constructed at the Oarai Engineering Center (OEC) of PNC. Preliminary design studies began in 1964 and construction started in January, 1970. JOYO attained initial criticality in April, 1977 with a breeder core (Mark-I core). The reactor initially operated at 50 MWt and then 75 MWt. This MK-I core operations (50MWt and 75 MWt) were completed at the end of 1981, with a natural convection test from 75 MWt. During the MK-I operations, the reactor experienced total 260 start-ups, conducting tests on reactor physics, reactor dynamics, power ascent and transient behaviors. The maximum burn-up level of MK-I driver fuels reached to 40,500 MWd/t, while the design limit was 42,000 MWd/t.

In 1982, the initial MK-I core was replaced by the MK-II irradiation core for FBR fuels and materials irradiation tests. The rated thermal power for the MK-II is 100 MWt. The transfer from the MK-I to the MK-II core was completed in 10 months with handling approximately 600 subassemblies. Since then, JOYO has operated twenty three duty cycles without any fuel failures and serious plant troubles. The operating history of JOYO is shown in Fig. 1.1 and the accumulated operational data as of November, 1991 in Table 1.1.

A new program, what is called a Mark-III project, is going on in Experimental Reactor Division to enhance the irradiation test capability and to demonstrate advanced technologies for competitive FBRs. The output power of the reactor will rise up to 140 MWt to increase neutron flux and extend irradiation capacity. The fuel handling system will be replaced by new one to reduce the outage days. The outline and the schedule of the MK-III project are illustrated in Figs. 1.2 and 1.3, respectively. Basic design studies and experiments required for the modification of the plant have been started in 1987. The completion of the MK-III project is scheduled for the end of 1990s.

The present paper introduces the activities and the experiences focused on the nuclear instrumentation system and the radiation measurements such as neutron dosimetry, fuel failure detection (FFD) and location (FFDL), burn-up of spent fuel, and behavior of radioactive corrosion products in JOYO.

Table 1.1 JOYO Operational Experience Data (as of Nov.,1991)

Accumulated Reactor Operation Time	45,393 hrs
Accumulated Heat Generation	3,645,999 MW • hr
Fuel Irradiation Maximum Fuel Burn-Up Achieved Number of Fuel Assemblies Discharged from Reactor	 70,000 MWd/t (Fuel element Average) 422 (Core Fuel)
Number of Start-Ups	450 (Including Critical Test)
Number of Annual Inspections	8

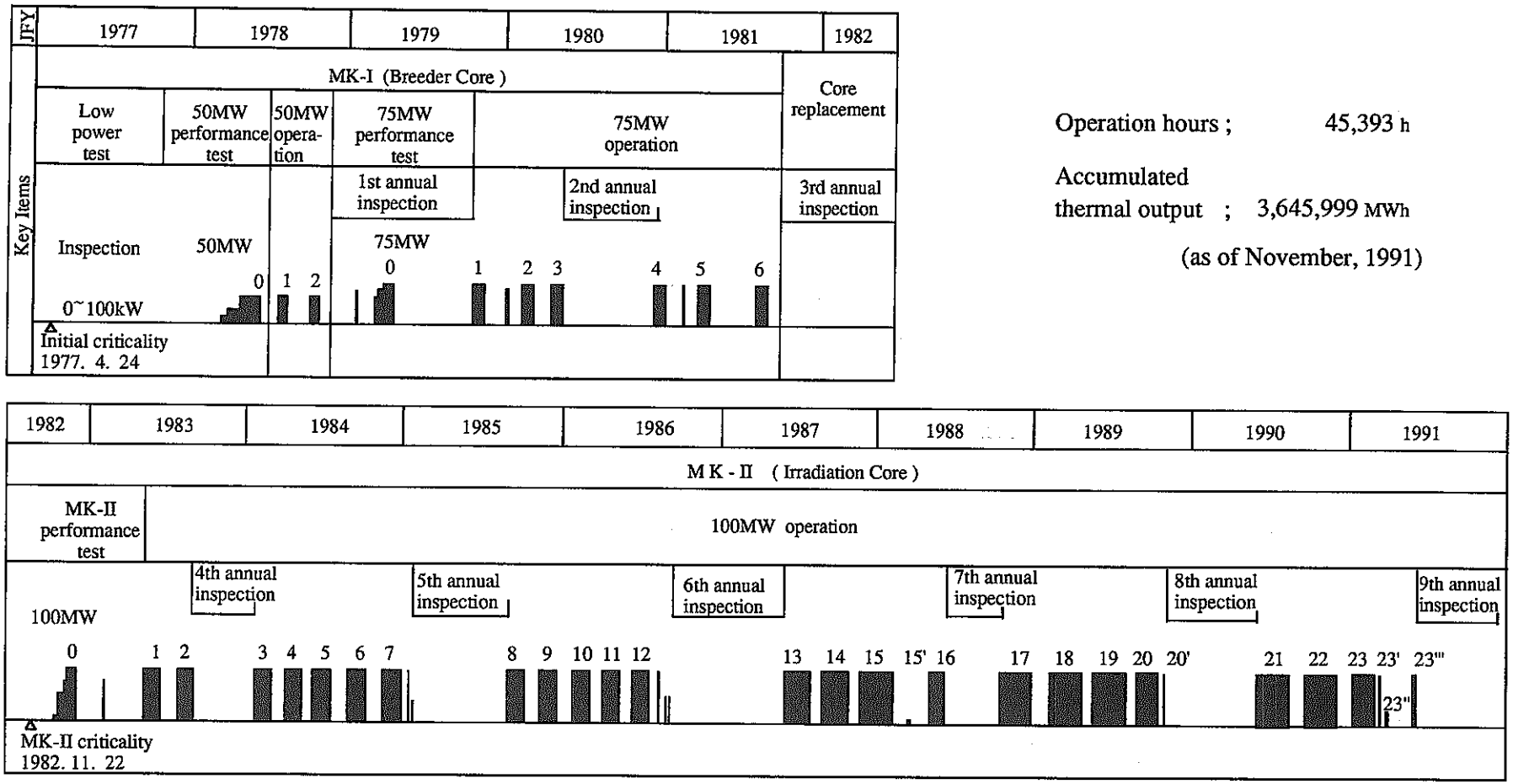

Operation hours ; 45,393 h

Accumulated thermal output ; 3,645,999 MWh

(as of November, 1991)

Fig. 1.1 Operational History of Experimental Fast Reactor JOYO

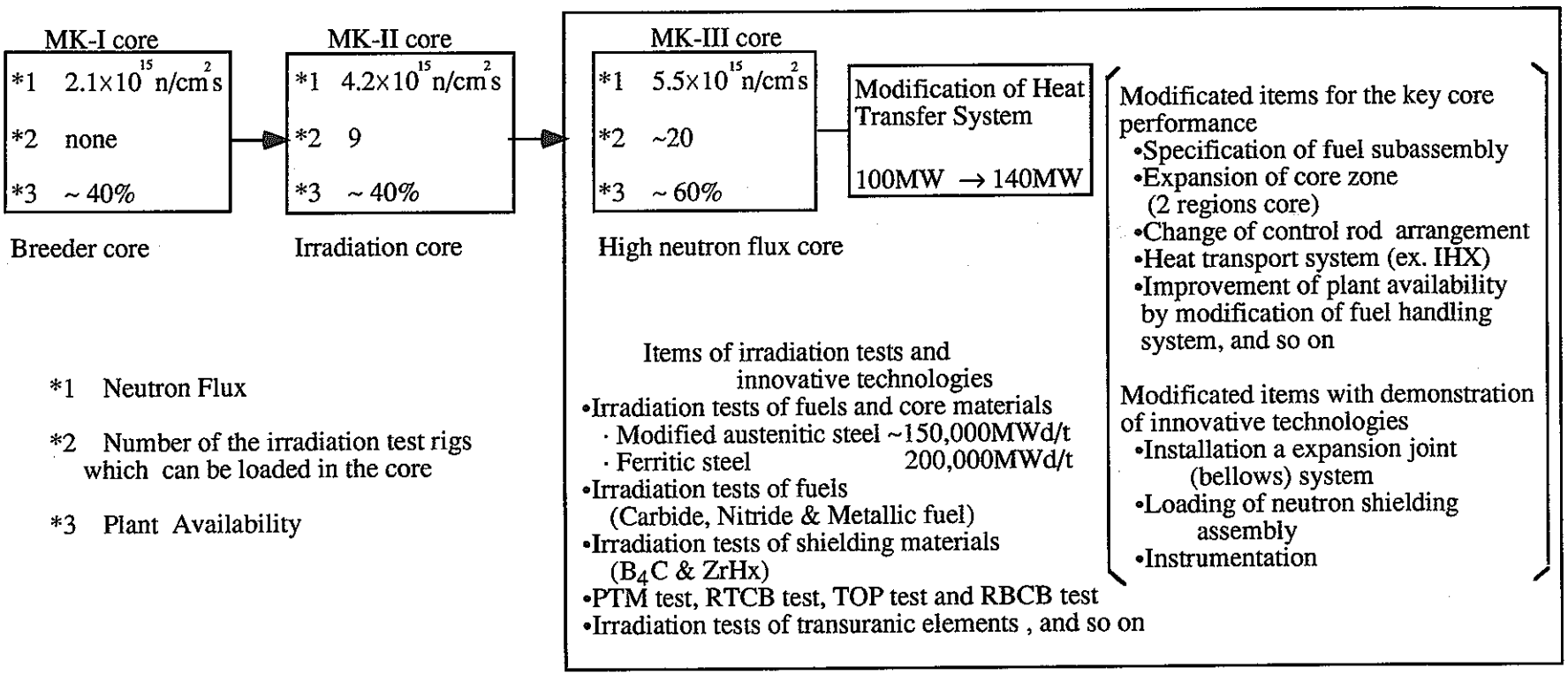

Fig. 1.2 Outline of the MK-III Project

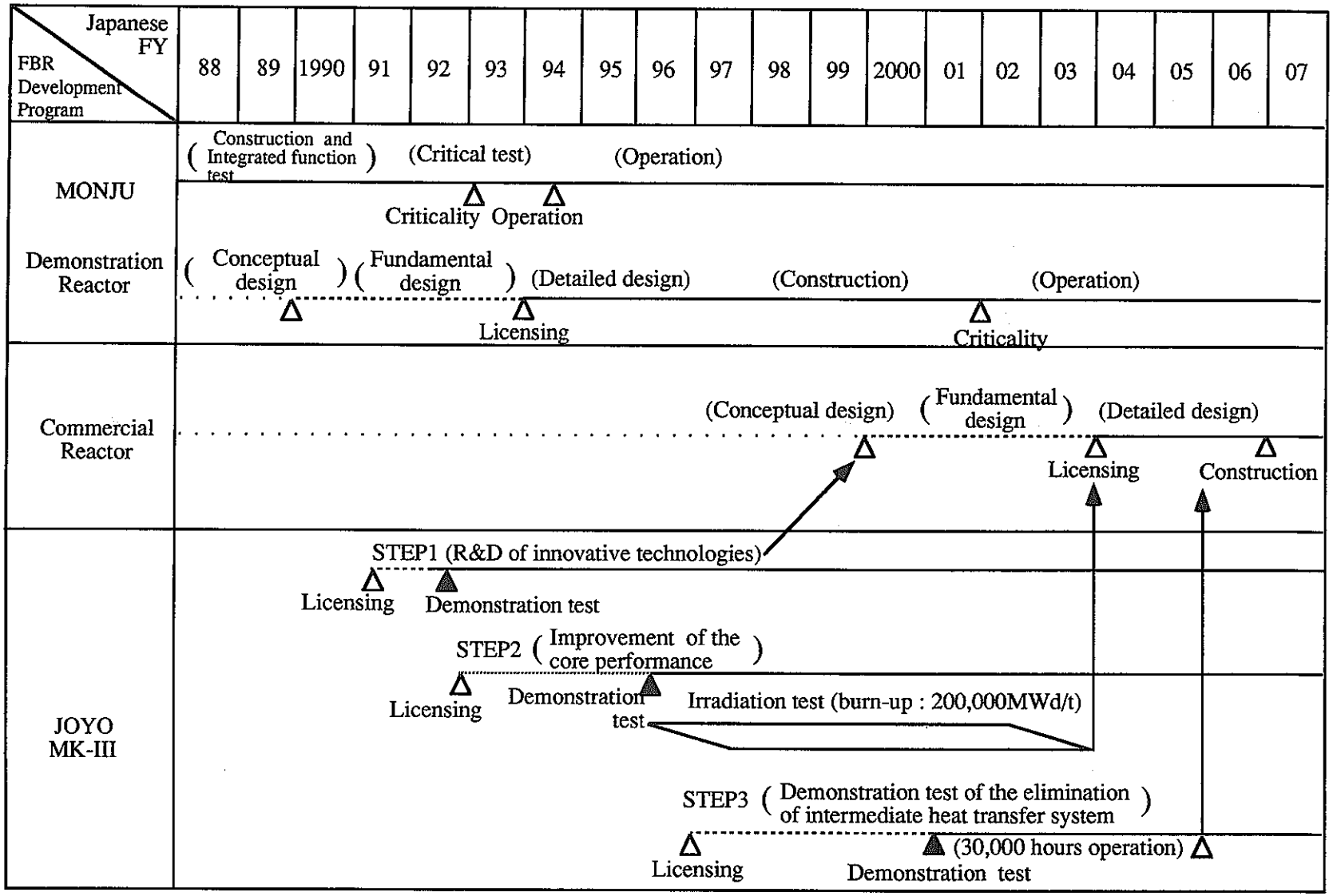

Fig. 1.3 Schedule of the MK-III Project

2. PLANT DESCRIPTION

JOYO is a Plutonium-Uranium mixed oxide fueled fast reactor with two main primary sodium loops, two secondary loops, and an auxiliary system. The auxiliary system consisting of primary and secondary loops is used for decay heat removal in case that the main cooling systems are not available. Approximately 200 tons of sodium are used for the JOYO cooling systems. The sodium flows into the core at 370°C at a flow rate of 1100 tons/hr/loop, and flows out the reactor vessel at 500°C through 20 inch diameter piping. The maximum outlet temperature of fuel assembly is about 570°C. An intermediate heat exchanger (IHX) separates radioactive sodium in the primary system from non-radioactive sodium in the secondary system. Secondary sodium loops transport the heat generates in the core from the IHX to the air-cooled dump heat exchangers.

A flow sheet of the cooling system, a cut away view and a horizontal cross section of reactor are shown in Fig. 2.1, 2.2 and 2.3, respectively. The main reactor parameters of MK-I, MK-II and MK-III are shown in Table 2.1.

Table 2.1 Main Core Parameters of JOYO

Items \ Core (Fuel)		MK-I		MK-II	MK-III
		First	Second		
Reactor Output	MWt	50	75	100	140
Primary Coolant Flow Rate	t/h	2,200	2,200	2,200	2,680
Reactor Inlet Temperature	°C	370	370	370	350
Reactor Outlet Temperature	°C	435	470	500	500
Core Stack Length	cm	60	60	55	50
Core Volume (max.)	ℓ	294	304	231	262
Linear Heat Rate (max.)	W/cm	210	320	400	430
Fuel Pin Diameter	mm	6.3	6.3	5.5	5.5
$PuO_2/(PuO_2+UO_2)$	w/o	18	18	~30	~30
^{235}U Enrichment	w/o	23	23	~12 (J1) ~18 (J2)	~10 (Inner Core) ~16 (Outer Core)
Total Neutron Flux (max.)	$n/cm^2/sec$	$1.9x10^{15}$	$3.2x10^{15}$	$4.2x10^{15}$	$5.5x10^{15}$
Fast Neutron Flux (>0.1MeV)	$n/cm^2/sec$			$3.1x10^{15}$	$4.1x10^{15}$
Max. Excess Reactivity	%Δk/k	~4.5	~4.5	~5.5	~4.5
Control Rod Worth	%Δk/k	Safety Rod ~5.6 Regulating Rod ~2.8	Safety Rod ~5.6 Regulating Rod ~2.8	~9	~8
Max. Burn-up(pin av.)	MWd/t	25,000	42,000	75,000	90,000
Operation Cycle (days)	Operation	45	45	70	60
	Outage	15	15	23	15

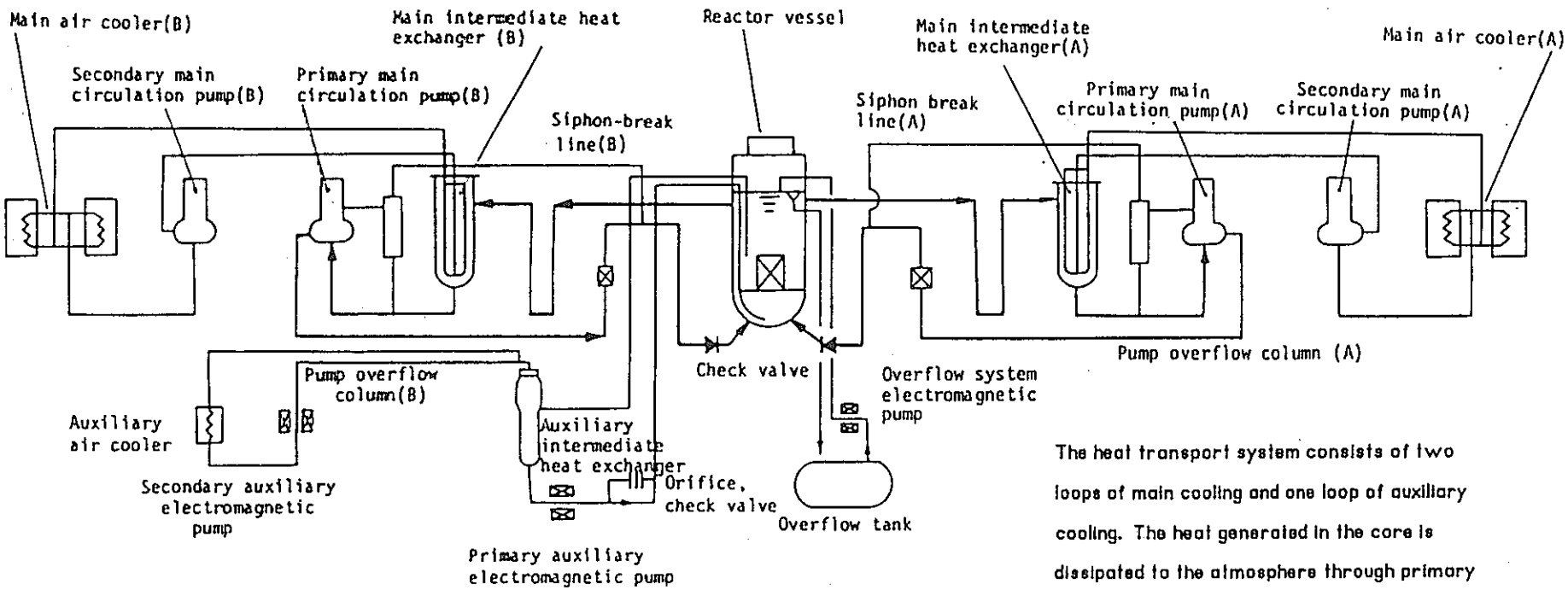

The heat transport system consists of two loops of main cooling and one loop of auxiliary cooling. The heat generated in the core is dissipated to the atmosphere through primary sodium and secondary sodium.

Fig. 2.1 Reactor Cooling System

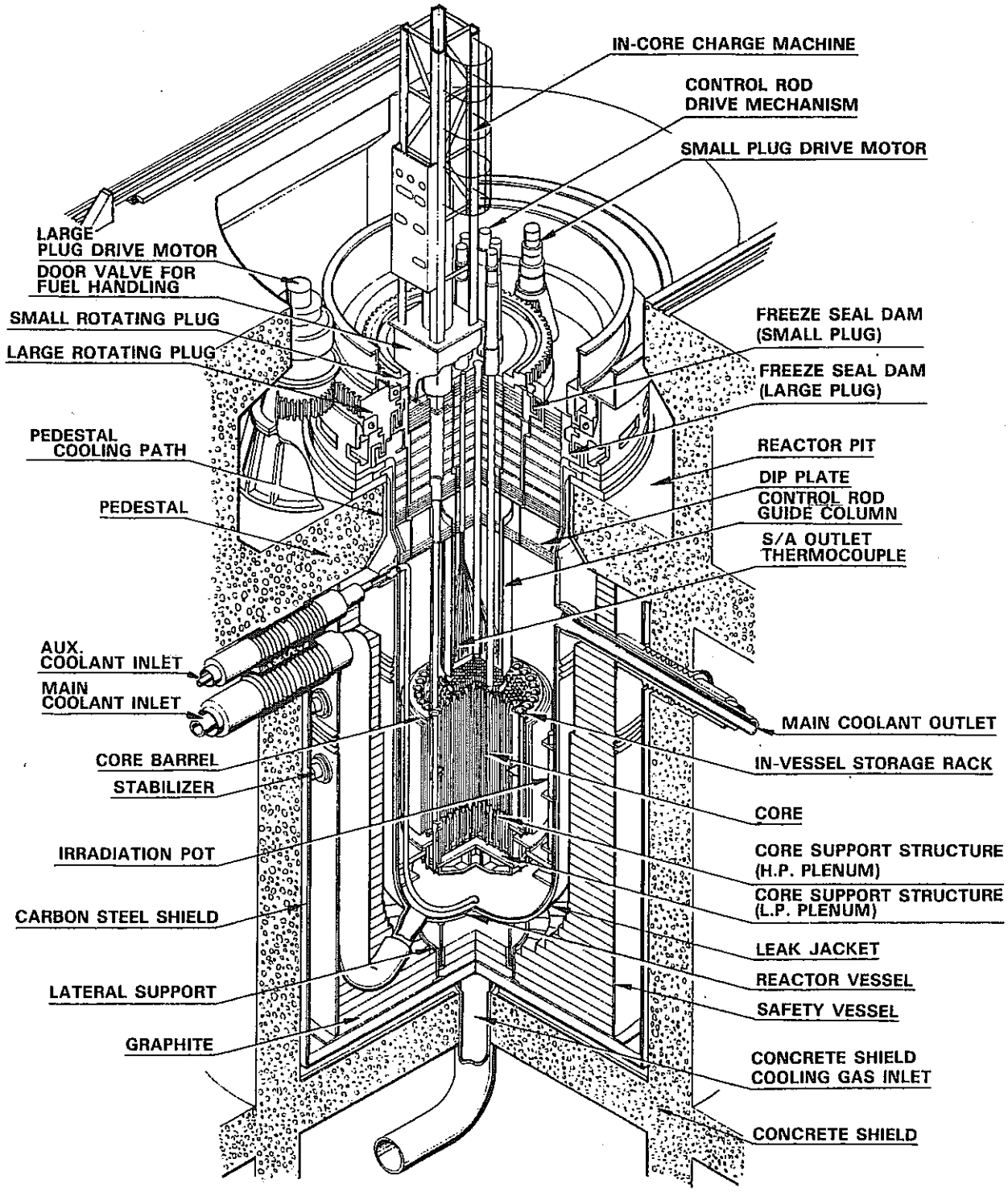

Fig. 2.2 Cut Away View of JOYO Reactor System

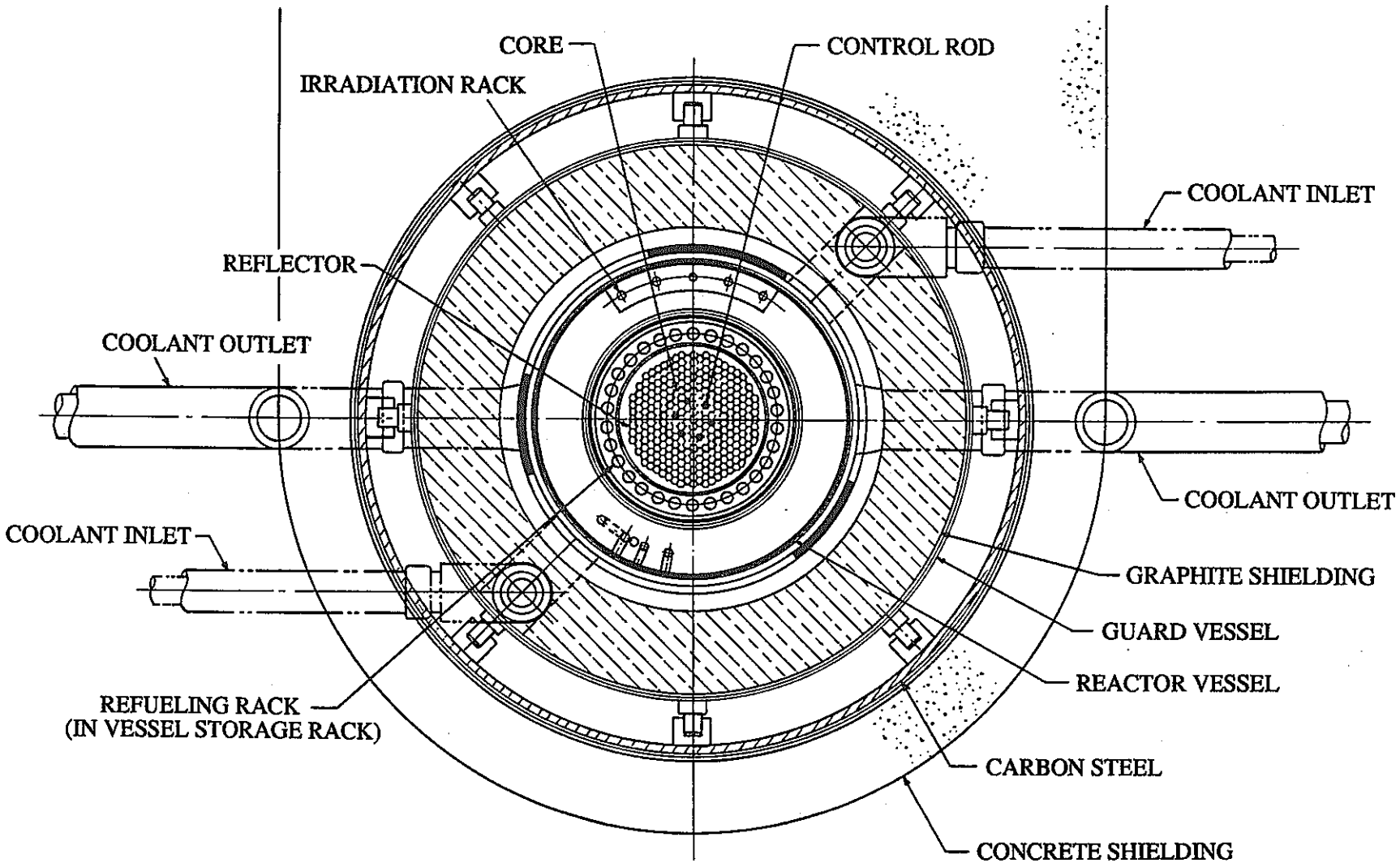

Fig. 2.3 Horizontal Cross Section of Reactor

3. NUCLEAR INSTRUMENTATION SYSTEM (NIS)

3.1 Introduction

The nuclear instrumentation system (NIS) in JOYO is designed to monitor neutron flux from start-up to the rated power of the reactor. It indicates and records the neutron level and reactor period, and it also initiates safety actions when any abnormality occurs.

The dynamic range of neutron flux in the core is about 10 decades from the neutron source level at reactor shut down to the neutron flux corresponding to the maximum rated reactor power. The entire neutron flux level can be covered by three different systems : 1) the Source Range Monitoring System (SRMS), 2) the Intermediate Range Monitoring System (IRMS), and 3) the Power Range Monitoring System(PRMS).

3.2 System Description

All of the neutron detectors are installed outside the reactor vessel. As shown in Fig. 3.1, the fission chamber of the SRMS, corresponding to ch.1 and ch.2, and the IRMS, corresponding to ch.3, ch.4 and ch.5, are located in the graphite shield, 2.9m far from the core center. The gamma ray compensated ionization chambers of the PRMS, corresponding to ch.6, ch.7 and ch.8, are located in nitrogen atmosphere outside the safety vessel, 3.55m far from the core center. All detector centers are leveled at the core center level in the vertical direction.

The neutron detectors of the SRMS and the IRMS are inserted on the core midplane for use at start-up and during low power operation. During high power operation, those detectors are withdrawn about 1.8m to extend their lifetime. For this purpose, the detectors are provided with a drive mechanism.

The specification of the fission chamber (FC) and the gamma ray compensated ionization chamber (CIC) employed in JOYO are shown in Table 3.1 and Table 3.2. The block diagram of nuclear channels and the layout of nuclear channel equipments are shown in Fig.3.2 and Fig.3.3, respectively.

The SRMS can cover a range from the neutron source level to about 3×10^{-3}% of the rated reactor power. The output pulse signal from the fission chamber is transmitted through a preamplifier to a monitor. The monitor consists of a pulse-height discrimination, a logarithmic amplifier, a reactor period amplifier, etc., in a nuclear instrumentation panel. The logarithmic count rate and reactor period are displayed and recorded at the reactor control panel.

The IRMS can cover a range from about $1x10^{-3}$% to 10% of the rated reactor power. The measurement principle of this system is based on the Campbell's method in which the square of the D.C. output fluctuation component is proportional to the reactor power. The D.C. output signal from the fission chamber is supplied through a preamplifier to a monitor consisting of a band pass amplifier, wide band rectifier, etc., in a nuclear instrumentation panel. The logarithmic output and reactor period signal are displayed and recorded at the reactor control panel.

The PRMS is supplied the D.C. output from the gamma ray compensated ionization chamber (CIC), and can monitor a flux range from about 0.1% to 125% of the rated reactor power. The D.C. output from the CIC is directly proportional to the reactor power. The signal of the linear output is displayed and recorded at the reactor control panel.

The reactor control panel contains various recorders and indicators which are essential for operation supervision, and annunciators which serve to signal any existing abnormality in the nuclear instrumentation system.

3.3 Design Basis

The nuclear instrumentation system should be designed to measure the neutron flux from start-up to the rated power of the reactor. The design bases of the NIS in JOYO are as follows.

1) The overlap in the monitoring ranges of the SRMS and the IRMS, and the IRMS and the PRMS should be more than one decade.
2) The NIS response should be linear over the full range of the power using the SRMS, the IRMS, and the PRMS.
3) Each channel should have independent preamplifiers, nuclear instrumentation panels, cables, and power supply systems.
4) The reactor must be shut down whenever the NIS detects any abnormality. The Table 3.3 is a list of control rod scram parameters measured by the NIS.

3.4. NIS Operating Experience

3.4.1 Characteristic Tests during Performance Test of the MK-I Core

For the confirmation of the characteristics of the NIS, several tests were carried out during low power test and power ascension test at JOYO. Some results obtained from the tests are described here.

(1) SRMS and IRMS Calibration

The SRMS and the IRMS of the NIS were calibrated by the nuclear calibration method during low power nuclear testing (up to 50 kW). The absolute nuclear power was determined by the relationship between the calculated neutron flux distribution in the core and the neutron flux measured by the calibrated fission chamber at the core center.

The calibration of SRMS was carried out to determine the relationship between pulse count rate and the absolute nuclear power. The monitor output voltage of the IRMS was adjusted to correspond to absolute nuclear power.

The results of the calibration test on the NIS confirmed as followings; 1) SRMS has linear response up to 10^5 cps, 2) IRMS corresponds to the absolute nuclear power, except below 1 kW, and 3) the overlap range between SRMS and IRMS is more than one decade.

(2) NIS Thermal Power Calibration

The thermal power calibration test was performed to confirm the characteristics of the IRMS and the PRMS. The IRMS and the PRMS were calibrated by measuring the reactor thermal power at several levels from low power through the rated power. The reactor thermal power was determined by measuring the inlet and the outlet temperature, and the flow rate of the main primary coolant.

After this procedure the IRMS and the PRMS were made coincide, based on the reactor power, by adjusting the electronic amplifier.

This testing was carried out during the 50MW power ascension test program. After the calibration, the reactor power was gradually decreased and increased to confirm the linearity over the full range of the reactor power. The following major items were confirmed ; l) the PRMS shows good linearity with the reactor thermal power, 2) the range of the PRMS overlaps the range of the IRMS by three decades, and 3) using the SRMS, the IRMS and the PRMS, the NIS is linear over the full range of the reactor power, with more than one decades overlap of each system.

(3) Measurement on Operational Condition of Neutron Detectors

1) Neutron Flux

The neutron flux at the each position was measured to be about $5x10^9 n/cm^2/sec$ at the FC, and about $3x10^8 n/cm^2/sec$ at the CIC at 75MW. From these results, it is estimated

that the neutron flux at 100MW would be about 6.7×10^9n/cm^2/sec at the fission chamber, and about 4×10^8n/cm^2/sec at the CIC. The measured neutron fluxes were about one-tenth of that estimated in the design stage.

2) Gamma Dose

The gamma dose at the FC and the CIC positions were measured to be about 2×10^5R/h and about 2×10^4R/h, respectively, resulting in that the gamma heating is not significant and temperature increases of the neutron detector are expected to be low.

3) Temperature of the Neutron Detector

The temperature was measured, with a Chromel-Alumel thermocouple installed about 2.5cm above each neutron detector during the 75MW power ascension test, to be 115°C at the FC for the SRMS and the IRMS, and 48°C at the CIC for the PRMS. The measured temperatures were very low, compared with ones estimated in the design stage ; 280°C at the FC position, and 200°C at the CIC position.

4) Withdrawal Characteristic of the FC

The FC withdrawal drive mechanism is provided to extend the FC life-time by enabling withdrawal of the FC about 1.8m from the core midplane level. During the design stage, the neutron flux ratio between the upper position and the lower position due to withdrawal (2m) is presumed to be about 0.1. However, based on the results of the test the ratio is found to be 0.38 to 0.25.

On the other hand, the measured neutron flux at the lower position of FC is less than one-tenth of the designed neutron flux. Therefore, as a whole the lifetime of the FC is estimated to be greater than the design value. The withdrawal characteristic of the FC is shown in Fig. 3.4.

3.4.2 Operational and Maintenance Experience of NIS

(1) Overview

Two cycles of 50MW rated power operations and six cycles of 75MW rated power operations had been continued with the MK-I core before the end of 1981, then the replacement of the MK-I core with the MK-II core was conducted in ten months. Since then, twenty three duty cycles of 100MW rated power operations have been conducte with the MK-II core until November, 1991 and the 9th annual inspection is now under way.

During the 6th annual inspection, the five imported FCs initially installed were all replaced with domestic FCs instruments and cables were replaced with new ones and several characteristics tests were performed.

(2) Replacement of Detectors and Instruments

Table 3.5 shows the accumulated operational data of neutron detectors. Although a fluence of each detector is much less than that of the design lifetime, all of the five imported FCs has been replaced with domestic detectors with the reasons as follows ; 1) the FC of ch.2 replaced by a spare P7A because a pulse height decreases due to the deterioration of insulation performance at a connector, 2) the FCs of ch.1 and ch.4 replaced by the domestic KSA-51 detectors because of a necessity to get higher sensitivity for measuring the subcriticality during the MK-II core constriction work, and 3) the FCs of ch.3, ch.5 and ch.2 replaced by the KSA-51 detectors because of the expiration of license.

Meanwhile, all of the CICs initially installed have been successfully operated without replacement.

Three linear power monitors, three power supply units and cables for IRMS and PRMS of NIS were replaced by new ones at 6th annual inspection in 1987.

As for the new linear power monitors, their electronit circuits were basically the same as the old ones but followings were improved;

1) all of NIS instruments are grounded at one point,
2) high voltage supply systems were separated from other circuits with electrical shielding boards to eliminate a possibility of occurring noise,
3) the output cables from a monitor to the output devices, such as indicators and computers, to prevent the influence caused by those output devices.

As for the new power supply units of ±21 Volt D.C., a method of rectification was changed from one with switching to another with diode to eliminate a high frequency noise.

(3) Characteristic Tests

The thermal power calibration tests were carried out several times during the 75MW power ascension test and the 100MW power ascension test and also after the replacement of each FC; in the same manner as described in (2) of section 3.4.1.

Overlapping characteristics of NIS response were measured in detail at the beginning of the tenth cycle of MK-II operation. From the test result as shown in Fig. 3.5, the overlaps in the monitoring ranges between SRMS and IRMS, IRMS and PRMS, were confirmed to be more than one decade.

Table 3.1 Specification of Fission Chambers

	P 7 A	KSA - 51
Electron Collection Time	250 ns	80 ns
Filling Gas	Argon	Argon + N_2
Filling Gas Pressure	7 atom	7 atom
Neutron Pulse Peak Current	0.88 μA	2.05 μA
Neutron Pulse Electric Charge	1.1×10^{-13} coul.	0.82×10^{-13} coul.
Thermal Neutron Sensitivity	0.1 cps/nv	0.12 cps/nv
Operating Voltage	200 V	200 ~ 300 V
Sensitivity Material	93% Enriched ^{235}U, (U_3O_8), 132mg	89% Enriched ^{235}U, (UO_2), 336mg
Max. Operating Temperature	400 °C	400 °C
Active Length	224 mm	214 mm
Detector Dimension	38.1 mmϕ x 547 mmL	38 mmϕ x 515 mmL
Cable Dimension	4.8 mmϕ	5 mmϕ

Table 3.2 Specification of CIC (SK-400)

Thermal Neutron Sensitivity	3×10^{-14} A/nv
Uncompensated Gamma Sensitivity	3×10^{-11} A/R/h
Gamma ray Compensation	97% ~ 99.5% to 10^4 R/h
Sensitivity Material	92% enriched ^{10}B
Filling Gas	90% Ar + 10% N_2
Operating Voltage	+HV 200~800 V - HV 100~300 V
Operating Temperature	385 °C
Thermal Neutron Flux Range	1×10^{-3} nv ~ 1×10^{10} nv
Gamma Flux Range	10 to 10^7 R/h
Detector Dimension	77 mmϕ x 403 mmL
Cable Dimension	4.8 mmϕ

Table 3.3 List of Scram Parameters

Trip Title	Logic to Scram	Setpoint	Notes
Reactor Period (SRMS)	1 of 2	+ 5 sec	Reactor period bypasses low and high power operation mode.
Reactor Period (IRMS)	2 of 3	+ 5 sec	Reactor period bypasses high power operation mode.
High Flux Level (SRMS)	1 of 2	9.5 x10^5 cps	High flux level bypasses low and high power operation mode.
High Flux Level (IRMS)	2 of 3	95%	High flux level bypasses high power operation mode.
High Flux Level (PRMS)	2 of 3	106%	———

Table 3.4 Accumulated Operational Data of Neutron Detectors

ch.	Detector Type	Irradiation Period	Accumulated Thermal Power (MWh)	Neutron Fluence (n/cm^2)	% of Design Life Time (%)
1	P7A	78.04 ~ 81.12	6.693×10^5	6.27×10^{16}	2.09
	KSA-51(1)	83.02 ~ 91.07	2.955×10^6	1.23×10^{18}	41.00
	KSA-51(2)	91.09 ~ 91.11	1.771×10^4	7.00×10^{15}	0.23
2	P7A(1)	78.04 ~ 79.08	2.132×10^5	2.00×10^{16}	0.67
	P7A(2)	80.01 ~ 86.12	1.802×10^6	5.30×10^{17}	17.6
	KSA-51	87.08 ~ 91.11	1.615×10^6	6.63×10^{17}	22.1
3	P7A	78.04 ~ 83.12	9.554×10^5	1.66×10^{17}	5.53
	KSA-51	84.04 ~ 91.11	2.691×10^6	1.12×10^{18}	37.33
4	P7A	78.04 ~ 81.12	6.693×10^5	6.27×10^{16}	2.09
	KSA-51(1)	83.02 ~ 91.07	2.955×10^6	1.23×10^{18}	41.00
	KSA-51(2)	91.09 ~ 91.11	1.771×10^4	7.00×10^{15}	0.23
5	P7A	79.04 ~ 83.12	9.544×10^5	1.66×10^{17}	5.53
	KSA-51	84.04 ~ 91.11	2.691×10^6	1.12×10^{18}	37.33
6	SK-400	78.04 ~ 91.11	3.646×10^6	1.8×10^{17}	1.8
7	SK-400	78.04 ~ 91.11	3.646×10^6	1.8×10^{17}	1.8
8	SK-400	78.04 ~ 91.11	3.646×10^6	1.8×10^{17}	1.8

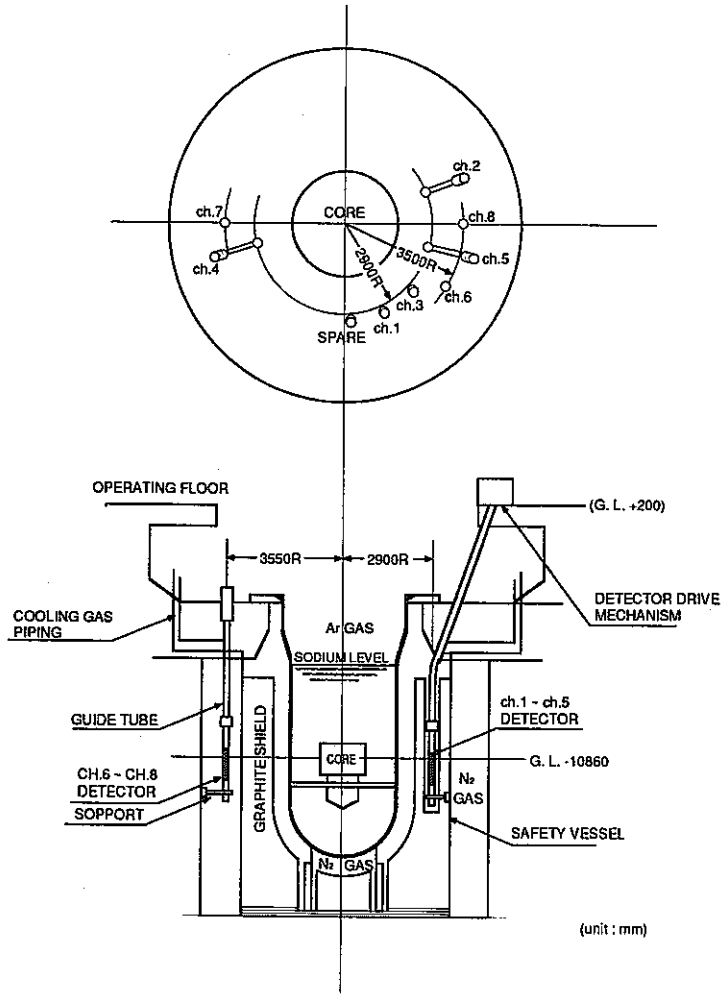

Fig. 3.1 Neutron Detector Location

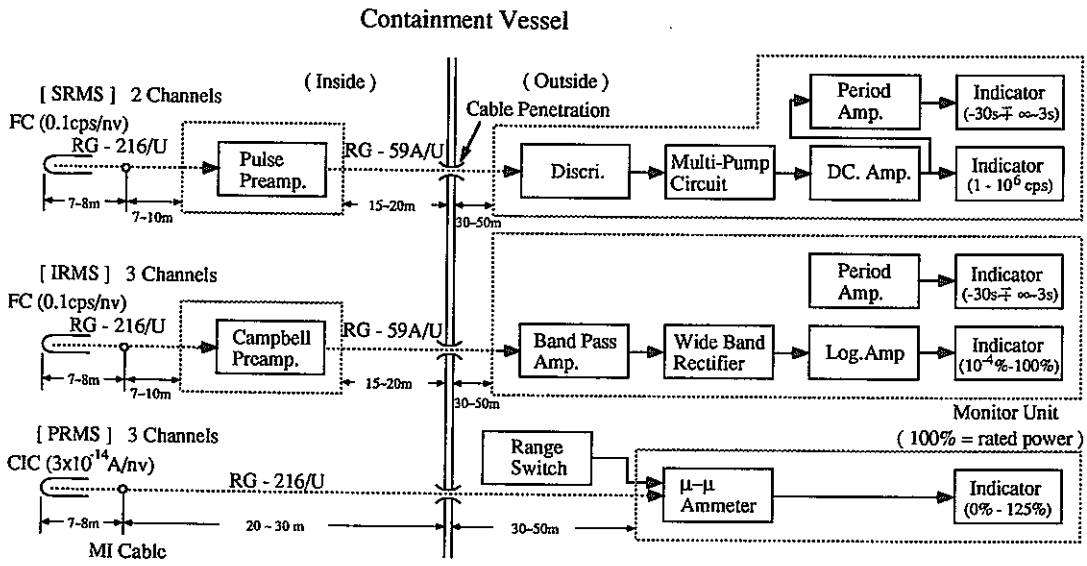

Fig. 3.2 Block Diagram of Nuclear Channels

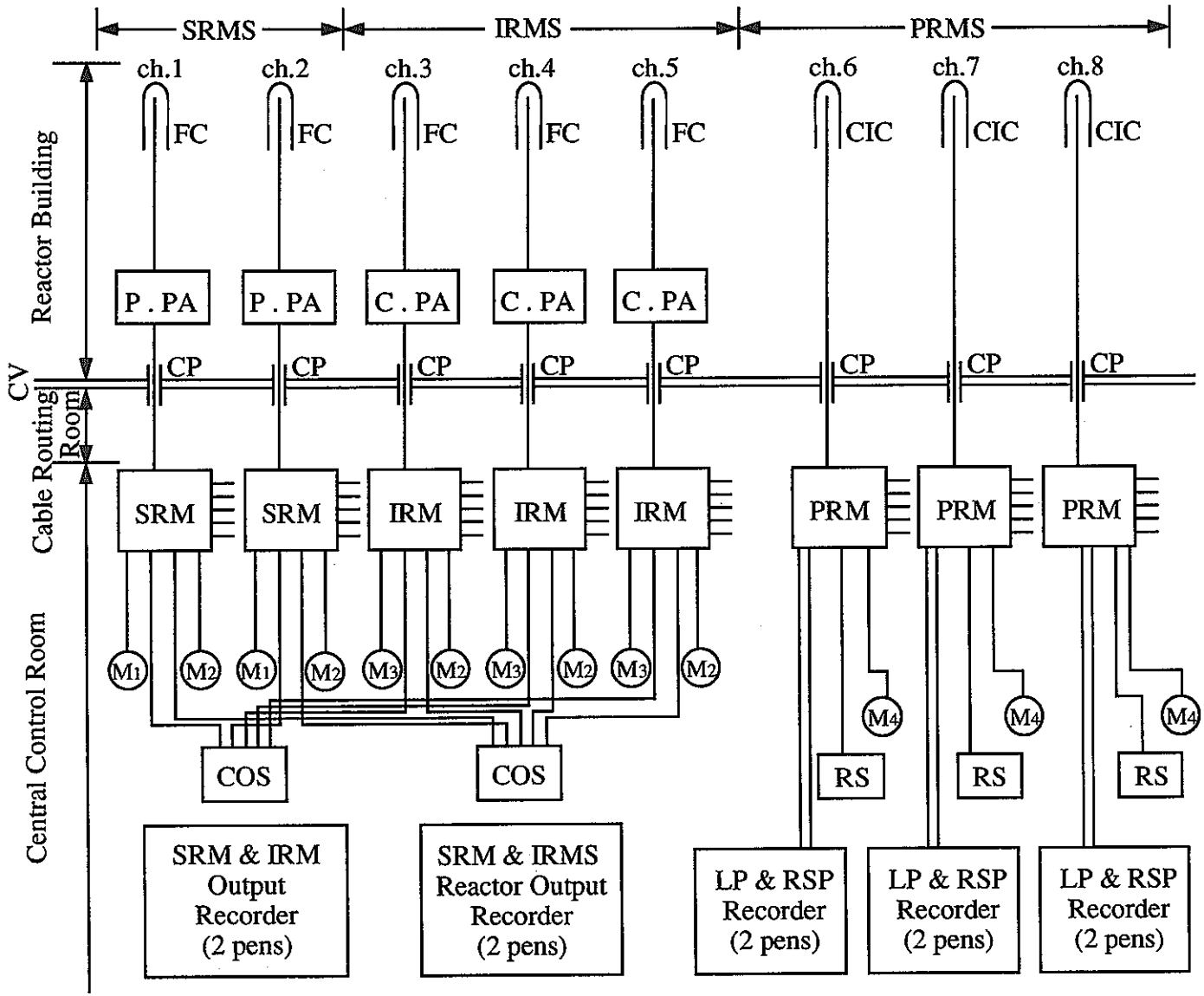

ch	Channel
FC	Fission Chamber
CIC	Gamma Compensated Ionization Chamber
P.PA	Pulse Preamplifier
C.PA	Campbell Preamplifier
CP	Cable Penetration
CV	Containment Vessel
SRM	Source Range Monitor
IRM	Intermediate Range Monitor
PRM	Power Range Monitor
COS	Cross Over Switch
RS	Range Switch
LP	Linear Power
RSP	Range Switch Position
M1	SRM Output ($1\sim10^{6}$cps)
M2	Reactor Period (+3sec~∞~-30sec)
M3	Output (10^{-4}% to100%)
M4	Output (0% ~ 125%)
SRMS	Source Range Monitoring System
IRMS	Intermediate Range Monitoring System
PRMS	Power Range Monitoring System

Fig. 3.3 Layout of Nuclear Channel Equipment

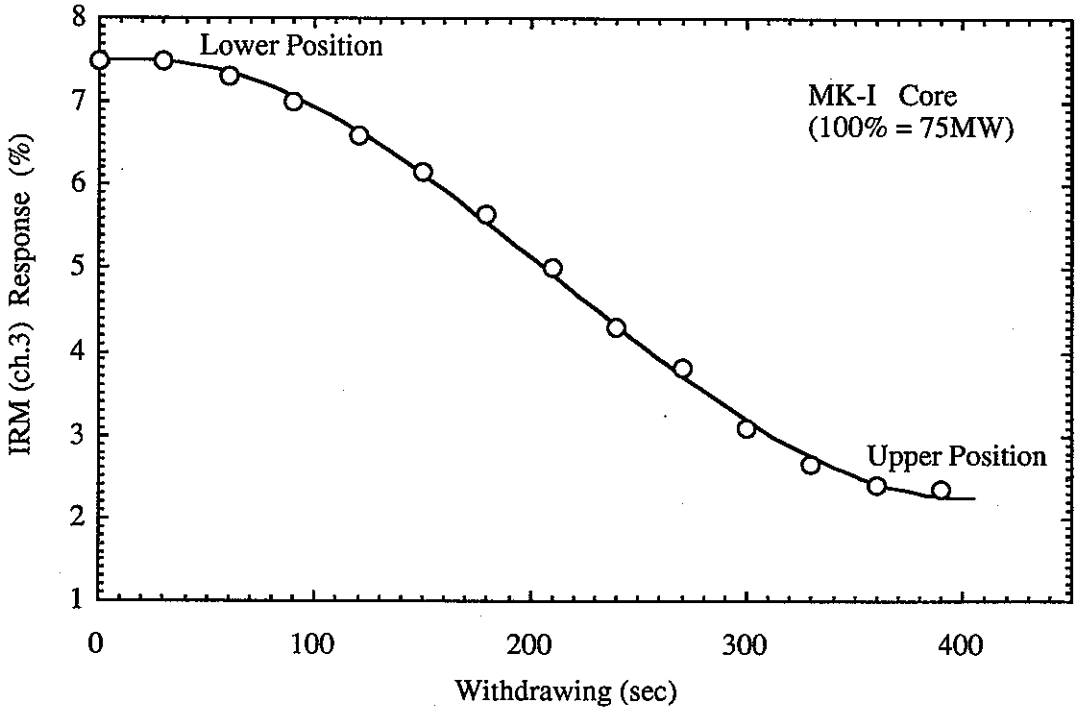

Fig. 3.4 Withdrawal Characteristic Curve of ch.3 Fission Chamber

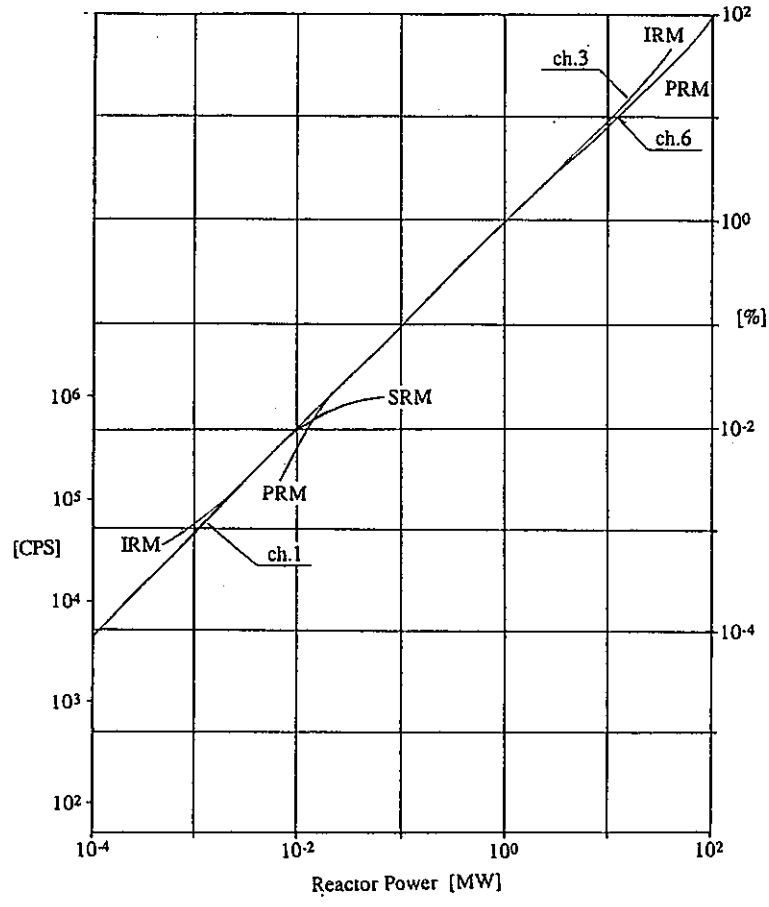

Fig. 3.5 Overlap Characteristics of NIS Response

4. NEUTRON FLUENCE MEASUREMENT WITH DOSIMETRY USING ACTIVATION METHOD

One of the most important missions of JOYO is to perform various irradiation tests to develop the fuels and the materials for FBR. In the irradiation test analysis and evaluation, neutron fluence including neutron spectral information is a key parameter and must be estimated accurately. Therefore, a neutron dosimetry technique with activation method has been developed, in cooperation with University of Tokyo, Hanbord Engineering Development Laboratory and PNC, and is now applied to all of the irradiation tests in JOYO

A procedure of JOYO neutron dosimetry is summarized as follows,

1) several activation dosimeter sets are loaded in test subassembly (rig) and are irradiated in the core region or the reflector region,

2) the irradiated test subassembly are disassembled at Fuel Monitoring Facility (FMF) and dosimeters are taken out at Material Monitoring Facility (MMF),

3) the activities of the dosimeters are measured by means of gamma-ray spectroscopy using Ge detector system and are reduced into the reaction rates, and

4) by using these measured reaction rates, the neutron spectrum at the irradiation position is unfolded with the J1-Unfolding code "NEUPAC" to obtain the neutron fluence including spectral information at the position.

More details on item 1), 3) and 4) are described after, showing CMIR-0 (Core Material Irradiation Rig) dosimeter sets as an example, in the following sections.

4.1 Dosimeter, Dosimetry Capsule

The dosimeters used in the JOYO irradiation test are listed in Table 4.1. One-tenth to one milligrams of fissionable materials and Sc are encapsulated separately in the tiny vanadium capsules and the others are fabricated in wire from with one to ten milligrams in weight.

The purities of the dosimeter materials are 99.9 to 99.999%. Almost all dosimeter materials have no impurities which obstruct the measurements of reaction rates.

These dosimeters are encapsulated into the dosimeter capsules (see Fig. 4.1), and are loaded in the irradiation subassembly (or rig) (see Fig. 4.2).

As the capsule is exposed directly to high temperature primary sodium coolant (approximately 500°C) during irradiation, all of the capsule elements are fabricated of 316-SS. To prevent oxidation of dosimeter materials, helium gas at one atmosphere pressure is sealed in the capsule.

4.2 Gamma-Spectrometric Techniques and Reaction Rate Analysis

In the JOYO neutron dosimetry measurements, to evaluate reaction rates with activation dosimeters, the activities of the dosimeters are measured by means of gamma-ray or X-ray spectroscopy using a Ge (pure) detector system (Gamma-X Ge SSD System, see Fig. 4.3 and 4.4). The detector used was an ORTEC 63 CC high-purity Germanium coaxial solid state detector. In using this system, the source-detector distance can be changed from about 3cm to a maximum 6m for varying the intensity of gamma-rays emitted from the dosimeters. The measurable activity ranged from a minimum 0.01μCi to a maximum 5mCi with reasonable counting time and counting rates. As the Gamma-X Ge SSD System has also sensitivity for very low energy photons,a several keV X-ray can be measured by using this system.

Energy calibration and efficiency calibration of the Gamma-X SSD System are carried out with standard gamma sources such as ^{137}Cs, ^{54}Mn, ^{65}Zn, ^{22}Na, ^{60}Co, and ^{152}Eu, which are supplied from "Laboratory de Metrologie des Rayonnements Ionistants (LMRI, France)".

The measured gamma spectrum data is analyzed with the BOB75 code originally developed by JAERI.

The reaction rates are calculated with the following expression for corrected activities at the end of irradiation.

$$RR = Ac \cdot \frac{1}{p \cdot a \cdot Na \cdot fi \cdot fb \cdot} \cdot \frac{1}{s}$$

$$S = \frac{\lambda}{P_0} \cdot \int_0^{t_1} P(t) \cdot e^{-\lambda (t_1 - t)} dt$$

where

RR = reaction rates (1/atom/sec)
S = saturation factor

Ac = corrected activity of dosimeter at the end of irradiation
p = purity of dosimeter material
a = isotope abundance
Na = Avogadro's number (6.020×10^{23})
fi = correction factor for impurity
fb = burn-up correction factor of dosimeter material
Po = nominal reactor power
l = decay constant
ti = irradiation time
P(t) = time dependent reactor power

In this expression, Ac is corrected for decay, weight, gamma-ray self-absorption, random summing and dead time.

The results of reaction rate measurements for the CMIR-0 dosimeter sets are listed in Table 4.2, compared with calculated ones by the unfolded spectrum.

4.3 Neutron Spectra Determination

Utilizing the measured reaction rate, the neutron spectra at dosimeter positions are unfolded in a manner shown in Fig. 4.5. The initial guess flux used as input data to the unfolding code is calculated with the following:

- Calculation code : DOT3.5 (two-dimensional discrete ordinates radiation transport code)
- Maximum Order of Pl : P_3
- Number of Angles in Sn : S30, S96
- Neutron Energy Groups : 100, 103 groups
- Cross Section Library : JSD100/JFT200 (ENDF/B-IV), JSDJ2/JFTJ2 (JENDL-2)
- Flux Normalization : Normalized to 100MWt Operation Condition

The NEUPAC (NEutron Unfolding code PACkage) unfolds neutron energy spectrum and estimates other integral quantities from reactions rates measured with dosimeters, etc.

A basic equation is $Ri = \int \sigma_i(u)\, \phi(u) du$ (i : Reaction Identification Number).

The input quantities are measured reaction rates Ri, reaction cross section $\sigma_i(u)$ and the initial guess $\phi_o(u)$ of spectrum $\phi(u)$. It is required to attach an error to every input quantity.

From the above, the spectrum $\phi(u)$ is obtained as a solution together with its uncertainty. Alternatively, the estimate and error of the integral quantity $I=\int W(u)\phi(u)du$ is obtained based on the J1 type unfolding method.

The NEUPAC code unfolds neutron spectrum and gives some additional informations such as Chi-Squares test results of input data, plotted spectrum, energy sensitivities of dosimeters and uncertainties of each integral quantity. The 103 groups cross section set based on ENDF/B-IV and V is used in neutron spectrum unfolding.

Figure 4.6 and Table 4.3 are an unfolded neutron spectrum and a 90% confidence level for each reaction rate used in the unfolding, respectively. The spectrum ratio defined as the ratio of guess spectrum to final spectrum and the improvement ratio indicating the error reduction of neutron spectrum are shown together in Fig. 4.7. A comparison of measured and calculated with a Hexagonal-Z diffusion theory code built in the JOYO core management code system "MAGI" is show in Table 4.4 and also plotted in Fig. 4.8.

Table 4.1 Standard Dosimeter Set of JOYO

Monitor Material	Form	Reaction	
		Non-Threshold	Threshold
Co	Wire (Co-V or Co-Al)	$^{59}Co(n,\gamma)$	
Sc	Vanadium Capsuled (Sc_2O_3)	$^{46}Sc(n,\gamma)$	
Ti	Wire		$^{46}Ti(n,p)$
Fe	Wire	$^{58}Fe(n,\gamma)$	$^{54}Fe(n,p)$
Ni	Wire		$^{58}Ni(n,p)$
Cu	Wire		$^{63}Cu(n,\alpha)$
Ta	Wire (Ta-V or Ta-Al)	$^{181}Ta(n,\gamma)$	
Nb	Thin Foil		$^{93}Nb(n,n')$
Np-237	Vanadium Capsuled (NpO_2)		$^{237}Np(n,f)$
U-235	Vanadium Capsuled (UO_2)	$^{235}U(n,f)$	
U-238	Vanadium Capsuled (UO_2)		$^{238}U(n,f)$
Th-232	Vanadium Capsuled (Th)	$^{232}Th(n,\gamma)$	$^{232}Th(n,f)$

Table 4.2 Comparison of Measured and Calculated Reaction Rates for before/after Spectrum Unfolding

Item / Position	Measured Reaction Rate ($\times 10^{24}$ reaction/sec/atom/100MWt)			Calculated/Measured	
	ID No.		Reaction Rate	before Unfolding	after Unfolding
Core Center Row [0] D12 (+4cm above Core Midplane)	1	^{59}Co (n,γ)	9.851E+13	1.227	1.028
	2	^{237}Np (n,f)	1.949E+15	1.297	1.055
	3	^{232}Th (n,f)	6.842E+13	1.235	0.908
	4	^{232}Th (n,γ)	7.619E+14	1.690	1.384
	5	^{235}U (n,f)	6.139E+15	1.287	1.054
	6	^{238}U (n,f)	2.203E+14	1.613	1.195
	7	^{46}Ti (n,p)	5.464E+12	1.609	1.067
	8	^{54}Fe (n,p)	4.439E+13	1.648	1.119
	9	^{58}Fe (n,γ)	2.493E+13	1.403	1.121
	10	^{58}Ni (n,p)	6.261E+13	1.553	1.066
	11	^{63}Cu (n,α)	2.607E+11	1.627	1.128
			Averaged C/E	1.472	1.102

Table 4.3 90% Confidence Level for Each Reaction Type

	90% Confidence Level (MeV)			
	No.	Reaction Type	Lower Energy	Upper Energy
Core Center Row [0] D12 (+4cm above Core Midplane)	1	^{59}Co (n,γ)	1.31087E-04	8.34572E-01
	2	^{237}Np (n,f)	4.03281E-01	3.92231E+00
	3	^{232}Th (n,f)	1.39965E+00	6.62822E+00
	4	^{232}Th (n,γ)	7.32188E-04	1.04384E+00
	5	^{235}U (n,f)	1.39982E-03	2.14496E+00
	6	^{238}U (n,f)	1.36314E+00	5.86932E+00
	7	^{46}Ti (n,p)	3.70258E+00	9.52874E+00
	8	^{54}Fe (n,p)	2.14094E+00	7.37627E+00
	9	^{58}Fe (n,γ)	3.89228E-04	7.57626E-01
	10	^{58}Ni (n,p)	1.78493E+00	7.29298E+00
	11	^{63}Cu (n,α)	4.66739E+00	1.12569E+01

Table 4.4 Unfolded Neutron Flux and Fluence for CMIR-0

	D11 Z=-282mm	D12 Z=+4mm	D13 Z=+268mm	Units
ϕ Total	2.425×10^{15} (8.88)	4.075×10^{15} (3.64)	2.217×10^{15} (8.05)	$n/cm^2/sec/100MWt$
ϕ >1.0MeV	3.123×10^{14} (10.4)	7.353×10^{14} (10.3)	3.267×10^{14} (10.5)	
ϕ >0.1MeV	1.496×10^{15} (10.9)	3.009×10^{15} (9.71)	1.525×10^{15} (10.3)	
Dpa Rate	6.838×10^{-7} (7.63)	1.430×10^{-6} (6.82)	6.982×10^{-7} (7.14)	dpa/sec/100MWt
Φ Total	5.827×10^{21} (8.88)	9.791×10^{21} (3.64)	5.327×10^{21} (8.05)	n/cm^2
Φ >1.0MeV	7.504×10^{20} (10.4)	1.767×10^{21} (10.4)	7.850×10^{20} (10.5)	
Φ >0.1MeV	3.595×10^{21} (10.9)	7.230×10^{21} (9.71)	3.664×10^{21} (10.3)	
Φ DPA	1.643 (7.63)	3.436 (6.82)	1.678 (7.14)	dpa

(NOTE) • Z : Distance from Core Midplane in mm

• Figures in parentheses : one standard deviation in %

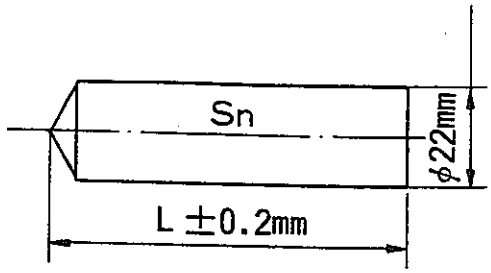

Spacer No.	Spacer Length (mm)
S_1	215
S_2	218
S_3	377.5
S_4	442
S_5	461.5
S_6	571
S_7	760

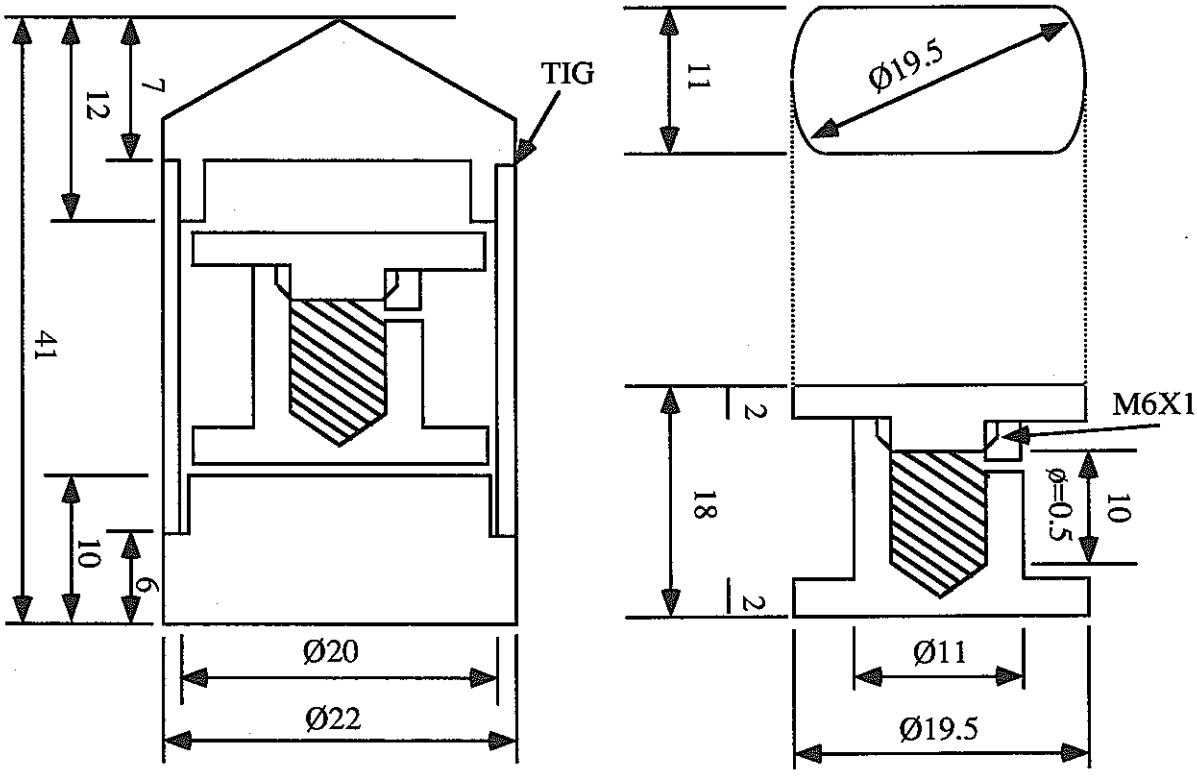

Fig. 4.1 Dosimeter Capsule and Its Spacer Used for CMIR-0

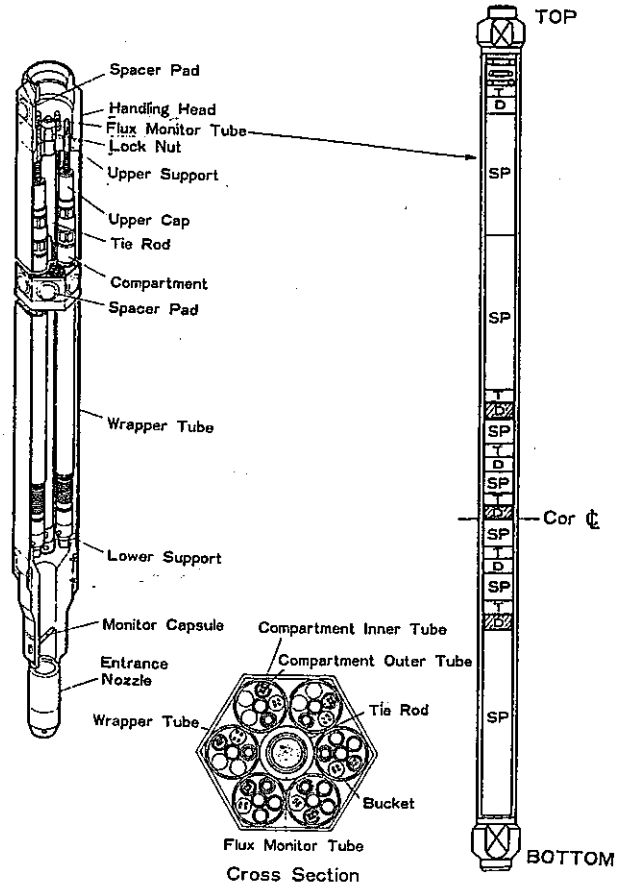

Fig. 4.2 CMIR and Flux Monitor Tube

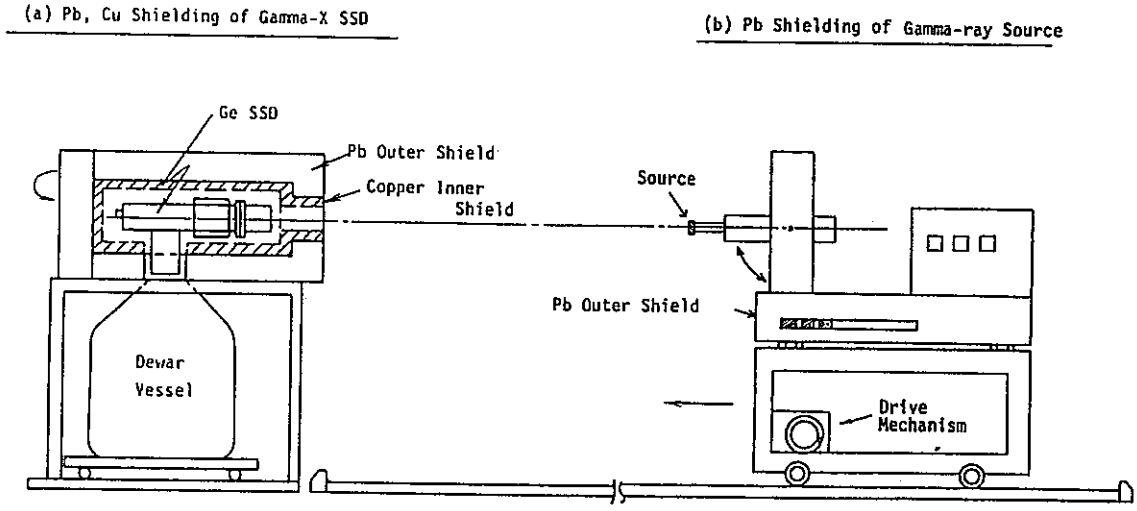

Fig. 4.3 Gamma-X Ge SSD System

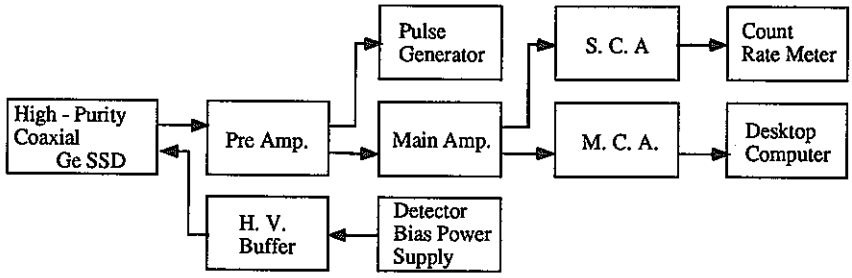

High - Pulity Coaxial Ge SSD	: ORTEC High - Pulity Germanium (HP Ge) Coaxial Solid State Detecor Detector Size 45øx40L Total Active Volume 63 cm Absorbing Layers Al 0.5mm Window to Detector Distance ~3m
Pre Amp.	: ORTEC Model 120-4 Preamplifier
H. V. Buffer	: NAIG High Voltage Buffer D-133S
Pulse Generator	: CANBERRA Model 807 Pulser
Main Amp.	: ORTEC Model 572 Spectroscopy Amplifier
Detector Bias Power Supply	: ORTEC Model 459 5kV Detector Bias Supply
M. C. A.	: NAIG E series Multichannel Analyzer
Desktop Computer	: YHP 9845B
S. C. A.	: ORTEC Timing Single Channel Analyzer Model 455
Count Rate Meter	: ORTEC Ratemeter Model 441

Fig. 4.4 Block Diagram of Gamma-X SSD System

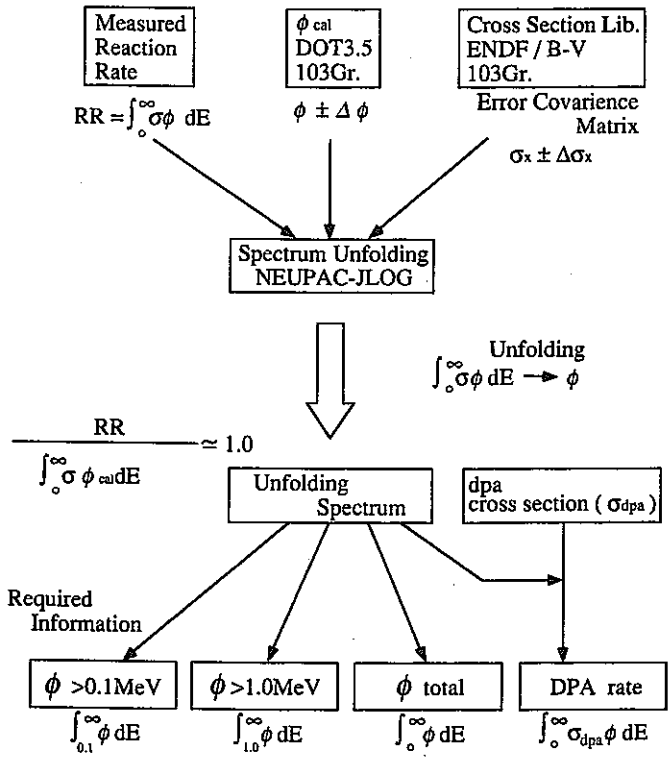

Fig. 4.5 Calculation Flow of NEUPAC

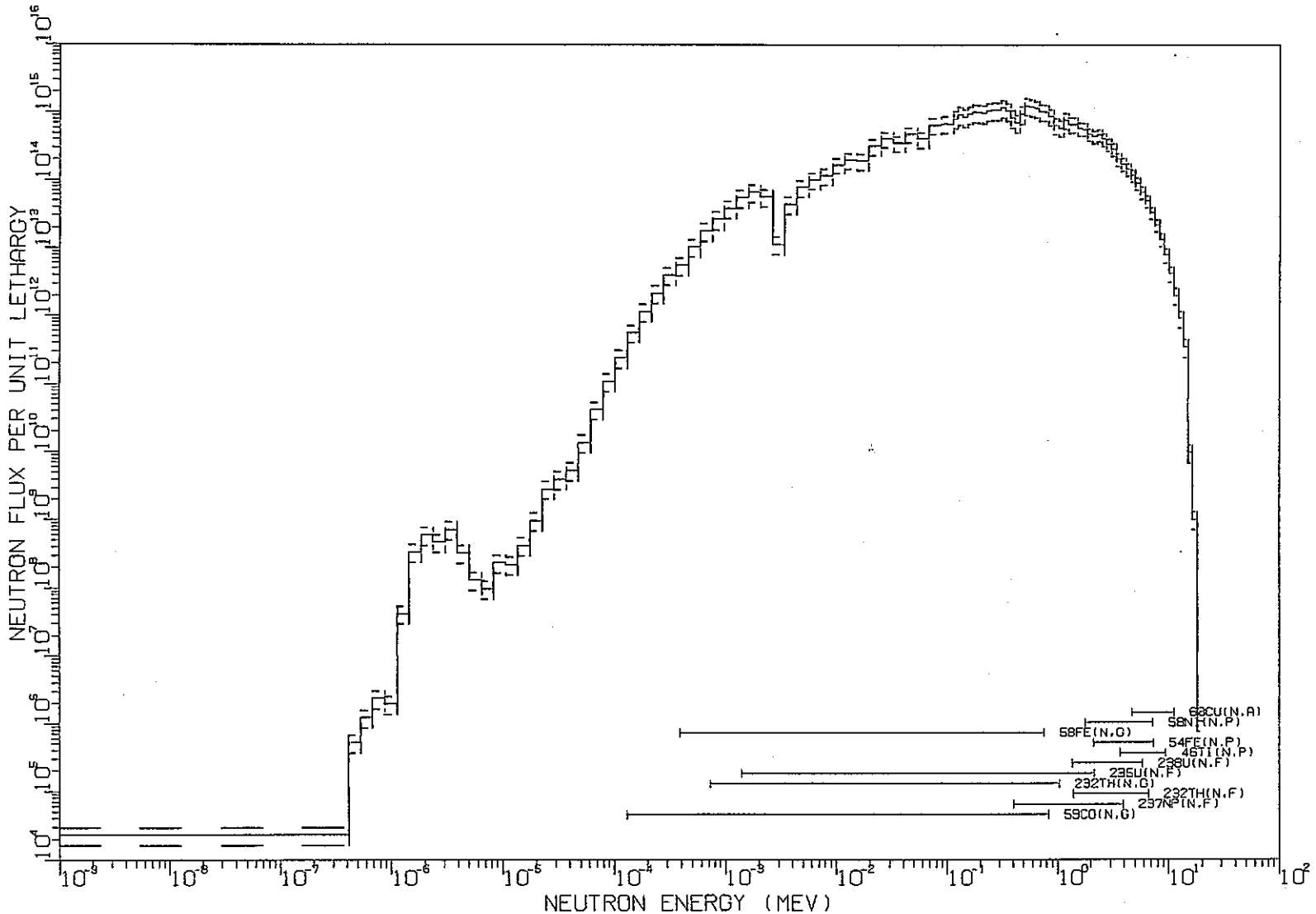

Fig. 4.6 Unfolded Neutron Spectrum at Core Center Level of CMIR-0

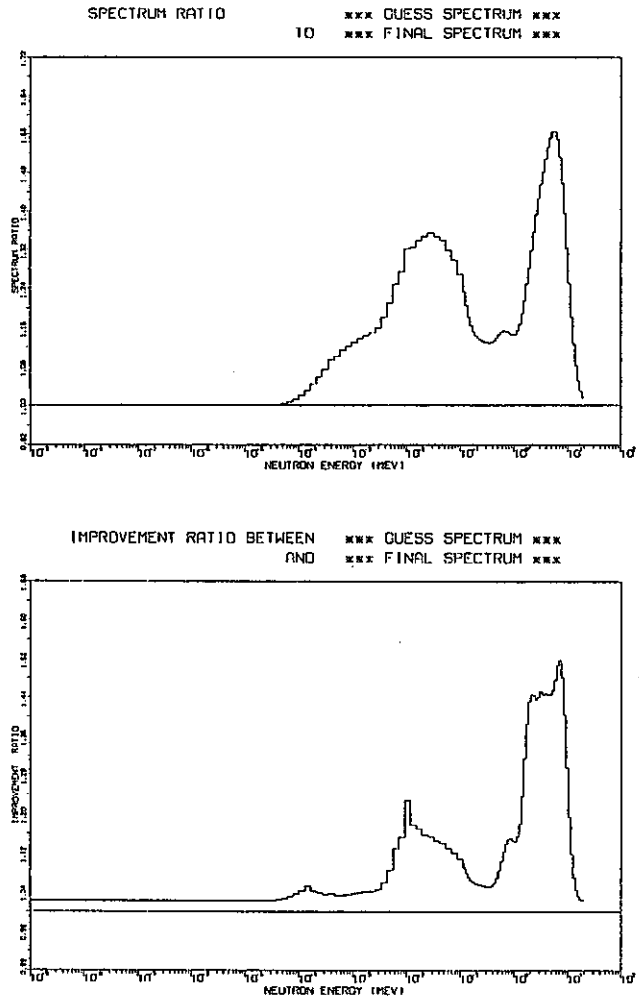

Fig.4.7 Spectrum Ratio and Improvement Ratio of unfolded Spectrum

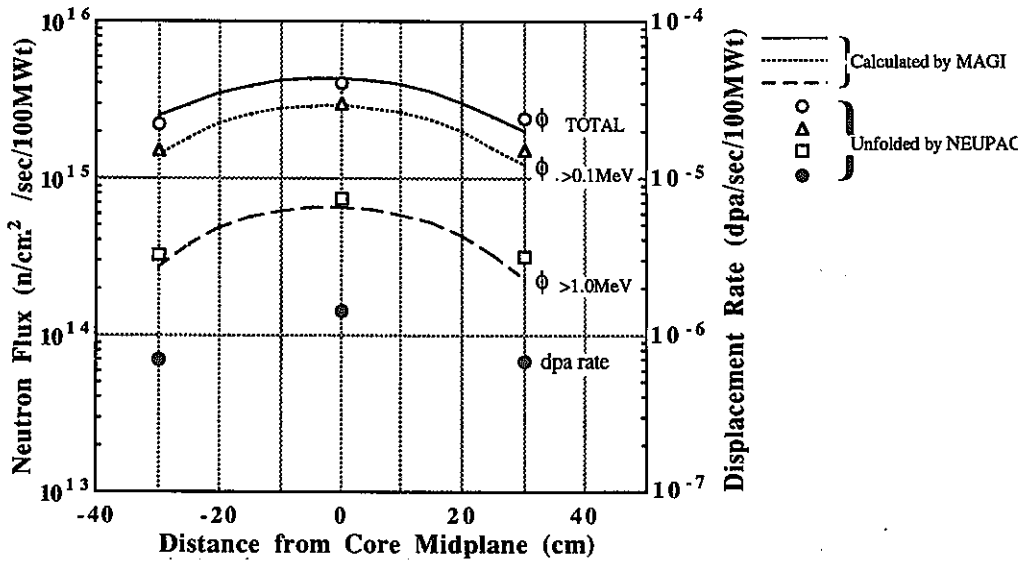

Fig. 4.8 Comparison of Axial Flux Distributions by NEUPAC and MAGI for CMIR-0

5. HELIUM ACCUMULATION FLUENCE MONITOR (HAFM)

A dosimetry applicable to long-term irradiation tests is required essentially both in developing high burn-up fuels and in reactor surveillance work because in an activation method used extensively in the neutron dosimetry, residual activity is saturated with irradiation time and can not retain the whole irradiation history particularly in the irradiation test for period of time longer than a several times of its half life.

A helium accumulation method is one of the most prospective means to measure a neutron fluence in such long-term irradiation because the number of helium atoms produced by (n,α) is simply proportional to the fluence owing to the fact that the measured end-product, helium, is stable and is not itself burned up by neutron irradiation. The stability of the helium also means that the analyses can be performed later, with no concern that time delay will compromise accuracy.

A concept of HAFM is illustrated in Fig. 5.1. In simplest terms, a HAFM consists of a sensor material which is irradiated and subsequently analyzed for the helium produced by (n,α) reactions. The helium-generating materials are chosen for the differing energy responses of their helium production cross sections. For fast reactor and other high-temperature environments, it is advantageous to encapsulate the sensor materials to prevent adverse chemical or physical interaction with the surroundings, and to prevent loss of helium generated by the irradiation.

The most prospective material for the capsule is vanadium, because of its mechanical strength, low induced radioactivity, chemical stability, and relatively low helium production cross section. The quantitative analysis of helium in the encapsulated HAFM is performed by vaporizing the entire capsule and its contents in the mass spectrometer vacuum system to release the helium. Adjustments are made for the helium generated in the capsule material, based on calculations or on measurements of the helium generated in pieces of the encapsulation material irradiated at the same time.

Utilizing the measured helium atoms for irradiated dosimeters, the neutron spectra are unfolded in almost the same manner as the activation method as described in section 4.3.

In JOYO, the feasibility study on HAFM application to the fast reactor dosimetry was started in 1986. As a first step, we began an irradiation test of sample HAFMs encapsulated boron, aluminum and beryllium as helium production material in vanadium

capsule in 1989 and a helium quantitative analysis system with a mass spectrometer was fabricated completely in 1990 (now under system calibration test).

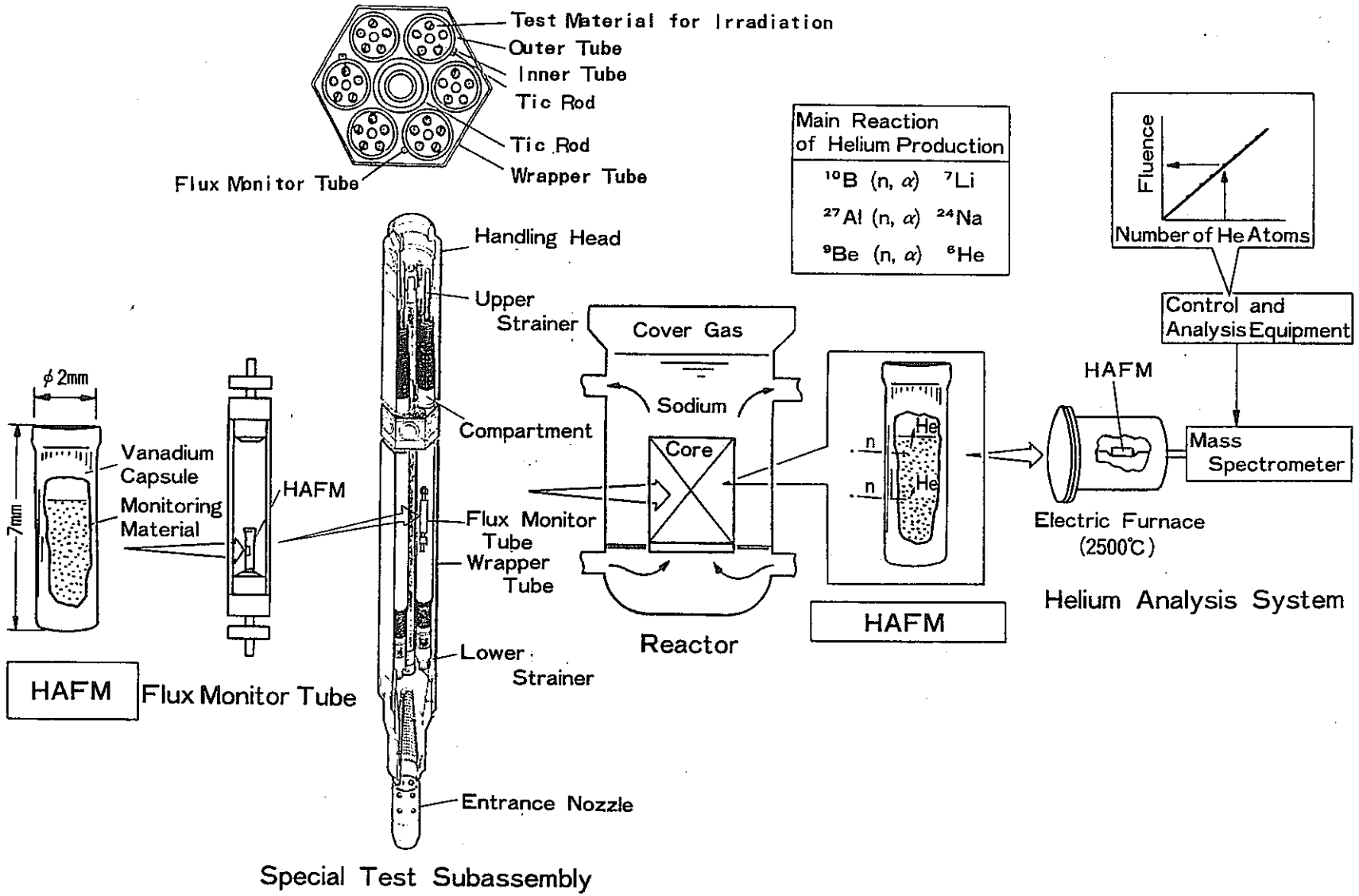

Fig. 5.1 Concept of Helium Accumulation Fluence Monitor (HAFM)

6. FUEL FAILURE DETECTION (FFD) SYSTEM

Fuel Failure Detection (FFD) and Failed Fuel Detection and Location (FFDL) are important for FBR plants not only to achieve a high availability and to secure the operational reliability, but also to conduct special test attended with a fuel failure. At the present time every FBR plant has an FFD system which consists of both a Delayed Neutron Monitor (DNM) and a Cover Gas activity Monitor (CGM).

Run-To-Cladding Breach (RTCB) and Power-To-Melt (PTM) tests are planned in JOYO. These tests are expected to contribute to the improvement in the performance of FBR fuels; the results of RTCB test is useful for the consideration of the increase in the fuel life and those of PTM test is useful for that in the fuel power density. As part of the preparation works for these tests, the FFD system has been upgraded and a series of simulated fuel failure test has been and will be conducted on the schedule shown in Fig. 6.1.

6.1 System Description

Two types of FFD systems are provided in JOYO as shown in Fig. 6.2.

One is two DNMs which are located adjacent to each piping of the A and the B primary cooling loops for detecting the delayed neutrons emitted from fission products such as ^{87}Br, ^{88}Br, ^{137}I and ^{138}I, which are released from breached fuel elements to sodium and transferred to the primary piping beside the DNM.

Another is two types of CGMs composed of a cover gas precipitating system (Precipitator), by which the fission product of ^{88}Rb i.e., beta decay of ^{88}Kr in the cover gas, is detected, and a newly developed On-Line Gamma-ray Monitor (OLGM). The special feature of OLGM is the ability to identify the amount of the isotopes contained in the cover gas by the gamma-ray spectroscopy.

(1) DNM

The DNM is installed along each of the two hot leg pipings as shown in Fig. 6.3.

The DNM at the A loop consists of the neutron shielding of polyethylene and boral, lead blocks, graphite blocks, and two kinds of neutron detectors, BF_3 proportional counters and boron-lined counters as shown in Fig. 6.4. The graphite block are used as a neutron moderator in order to make the system more sensitive for delayed neutron. On the other hand, the lead blocks are piled up to protect the counters and also to reduce the noise

signals from high gamma radiation, which is emitted from activated primary coolant sodium. In addition to these two surrounding materials, the neutron shield of boron-aluminum plates are installed outside of the lead blocks to remove thermal neutron around the DNM block. The polyethylene neutron shield is installed after the reactor critical test to reduce the background of the core neutrons leaking through the primary piping penetration. In the graphite blocks, four BF_3 counters and two boron lined detectors are installed. The block diagram of the detectors is illustrated in Fig. 6.5. In order to assure a broad sensitivity range for the DNM system, the BF_3 counters having a high neutron sensitivity are employed to detect a small amount of fission products and the boron-lined detectors are installed for covering a large breach of the fuel element.

The DNM at the B loop consists of the neutron shield of borated polyethylene blocks, canned B_4C powder and cadmium sheet, lead blocks, a polyethylene block, and two types of neutron detectors, BF_3 proportional counters and boron-lined counters as shown in Fig. 6.6. The polyethylene block, which contains a BF_3 counter, two boron-lined detectors and a spare, is to moderate the delayed neutrons from the primary coolant and to raise sensitivity of the system. The lead block is a gamma shield to prevent the detectors counting the gamma pile up signals. The borated polyethylene, the B_4C powder and the cadmium neutron shields are installed inside of the lead blocks to moderate neutrons and to remove resulting thermal neutrons around the DNM block.

The transit time of fission products from failed fuel in the core to the DNMs is evaluated to be approximately 30 seconds by the experiment using U-Ni fission product source.

(2) Precipitator

The precipitator system consists of piping systems, two vapor traps, a compressor, and a precipitator as shown in Fig. 6.7. The argon cover gas is extracted from the reactor vessel and driven to the precipitator through the piping in one inch diameter by a compressor.

The cover gas is introduced into a precipitator chamber after trapping sodium mist and vapor with two vapor traps. When gaseous fission products enter the precipitator with the cover gas, the Rb and Cs produced with beta decay of the respective Kr and Xe isotopes are positively charged. If negative voltage is applied to the precipitating wire, it is possible to collect these daughter nuclides on the charged wire.

The precipitator is composed by a beta-scintillation counter, a precipitating wire and a chamber, a wire drive motor and gear system, insulation plates and iron shield, as

illustrated in Fig. 6.8 and 6.9. The wire is charged to 500 volts against the precipitator chamber to collect beta decayed nuclides. The wire is driven from the chamber to the beta-scintillation counter at fixed intervals, and the beta-scintillator counts beta-particles emitted from the precipitated daughter nuclides of fission products.

$$^{88}Kr \xrightarrow[28h]{\beta^-} {}^{88}Rb \xrightarrow[18\,\mathrm{min}]{\beta^-} {}^{88}Sr(stable)$$

$$^{138}Xe \xrightarrow[17\,\mathrm{min}]{\beta^-} {}^{138}Cs \xrightarrow[32\,\mathrm{min}]{\beta^-} {}^{138}Ba(stable)$$

After beta counting, the wire is driven to the wire drum, which stores wire about one hundred times longer than one interval length. The activity on the wire is decayed during the stay at the wire drum. The precipitator has three nozzles, a sample gas inlet, a clean argon gas purge line and a gas outlet nozzle. Clean argon gas flows from scintillator side to the chamber through the wire guide hole to prevent the sample gas flowing to the detector and to reduce the background. The iron shield reduces the background of the sample gas in the chamber.

(3) OLGM

A schematic diagram of OLGM is illustrated in Fig.6.10. This system is composed of a charcoal bed, a gamma-ray shielding, a germanium detector, valves and pipings which connect the charcoal bed to cover gas inlet and outlet pipings and a fresh argon gas supply line. A principle of the system is as follows;

(1) At first, as cover gas flows through the charcoal bed at the room temperature, xenon and krypton isotopes are selectively adsorbed in the charcoal bed at high efficiencies compared with ^{41}Ar and ^{23}Ne which obstruct a precise gamma-ray analysis of FP nuclides, due to a difference of the adsorption coefficient between noble gases (see Fig. 6.11).

(2) Next, the charcoal bed is flushed with a small amount of fresh argon to release the undesirable radioactive argon and neon isotopes due to the same principle as item (1).

A prototype OLGM was connected with JOYO at the first failed fuel simulation test to demonstrate its performance. Based on the results obtained at the demonstration test, OLGM has been designed, fabricated and installed on JOYO. OLGM is equipped with two charcoal bed to enable measurements in short interval time, and with a germanium detector cooled by a closed-cycle cryogenic refrigerator using helium for saving the time, man power and man-rem to feed liquid nitrogen. A flow sheet of this system is shown in

Fig. 6.12. This system was successfully calibrated and used at the fission product source test.

6.2 Operational Experience at Special Testings

(1) First Fuel Failure Simulation Test

The test was carried out with an irradiation subassembly comprising six compartments in which two plenum pre-defected fuel pins, a sibling fuel pin and a plenum pre-defected dummy rod with tag gas capsule were contained. A configuration of this test subassembly is shown in Fig. 6.13. Pre-defect was produced by machining a slit of 0.1mm width and 1.0mm length at gas plenum region through the cladding tube made of 316-SS. The plenum slit was then sealed with fusible alloy having melting point of 300°C to allow fission gas release and sodium ingress through the defect at reactor start-up. Fuel pin used in the test contained the plutonium-uranium mixed oxide fuel, whose specification is the same as that of the JOYO MK-II driver fuel pin.

The test subassembly was irradiated at the first row of the JOYO MK-II core during the period of April 17 to April 19, 1985. The gaseous fission products in the cover gas which released through the plenum slit were successfully monitored by both OLGM and the precipitator during entire period of this test.

The prototype OLGM with 4 grams of charcoal in the charcoal bed was hand-made and connected with JOYO at this test to demonstrate the detection capability of the fission gas activities in the cover gas.

At the early stage of the test, various operational parameters of OLGM were determined with a characteristic test. Figure 6.14 shows the gamma-ray spectra obtained both for before and after the flushing with fresh argon, and the effect of the flushing can be seen clearly comparing these two figures. Major characteristics are summarized also in Fig. 6.10.

With prototype OLGM under the operational condition determined above, fission gas isotopes in the cover gas were measured every 30 minutes from reactor start-up to the end of wet sipping test. Measured activities of xenon and krypton isotopes in the cover gas are shown in Fig. 6.15, Fig. 6.16 and 6.17 .

(2) Fission Product Source Test

A Fission Products Source (FPS) was irradiated in the middle of June, 1988 during the 15'th cycle operation of the JOYO MK-II core to provide the data on calibrating

the FFD system, clarifying the transition behavior of the gaseous fission products in the reactor, and verifying the flux tilting and the triangulation methods to optimize the FFDL system of FBRs.

1) Fission Product Source

As the fission product source, a special test subassembly which was composed of thirty U-Ni alloy pins with no cladding and sixty-one dummy pins made of stainless steel was loaded in the core. The U-Ni alloy pins which contain 3.5 wt% of 20% enriched uranium were employed for the test, because the amount of fission products released into the coolant should be well-defined. Schematic diagram and specifications of FPS are shown in Fig. 6.18 and in Table 6.1, respectively.

2) Test procedures

Three FPS tests (FPS-1, FPS-2 and FPS-3) were conducted at 1MWt constant reactor power. FPS was loaded alternately at positions of core address [000] (core center), [4A4] (the 4th row position nearest from the reactor outlet piping of the primary cooling loop A and adjacent to the control rod) and [4D4] (that of the B loop) for FPS-1,2 and 3 tests, respectively. FPS locations are illustrated in Fig. 6.19 and major plant conditions are summarized in Table 6.1.

The flow rate of the primary coolant was changed step by step to clarify DNMs' sensitivity by means of subtracting the background from the measured DNMs' counting rates.

The flux tilting test was performed to determine whether the DNM and the CGM signals from FPS could be modulated by the local flux perturbations induced by moving the control rod adjacent to FPS. In FPS-2 (or FPS-3) test, the control rod at the position addressed [3A3] ([3D3]), adjacent to [4A4] ([4D4]) where FPS was located, was fully inserted into or withdrawn out of the core and the other control rods were all moved to the even position in the opposite direction to maintain the constant reactor power of 1MWt.

3) Test Results

The outlines of the FPS test results are described, taking FPS-2 as an example, in this section. Figure 6.20 shows the representative trend data obtained with FPS-2 test.

The DNM(A) signal shows stepwise reduction with reduction of the primary coolant flow rate. This phenomenon can be explained as follows; the number of delayed

neutron emitters in the coolant passing through DNM(A) decreases with the flow rate of primary coolant sodium, because the maximum half life of delayed neutron emitters is shorter than one minute, while the time required for the transport of delayed neutron emitters from the core to DNM(A) is approximately 30 seconds. From these results, the delayed neutrons from FPS are certainly detected by DNMs and net counting rates of DNMs can be obtained by subtracting backgrounds from measured counting rates of DNMs. Similar results are obtained for DNM(B) with FPS-3 test and for both DNM(A) and DNM(B) at FPS-1 test.

On the contrary, DNM(B) (or DNM(A)) signals showed no significant changes during the FPS-2 (FPS-3) test operation. These results mean that the delayed neutron emitters did not reach DNM(B) (DNM(A)) which was located in the opposite direction of the FPS at FPS-2 (FPS-3) test, because the FPS position was near the coolant outlet piping A (B) of the reactor vessel and little mixing of the coolant occurred at the upper plenum of the reactor vessel. Thus, the availability of FFDL, sub-regionalization, by the delayed neutron triangulation method is verified.

As for the CGM signals, precipitator and OLGM are able to detect noble fission product gasses in the cover gas with an enough signal to noise ratio. OLGM is able to monitor eight isotopes of xenon and krypton, including nuclides with a short half life such as ^{137}Xe whose half life is 3.8 minutes. In addition, fission product gas activities of the cover gas are found to vary depending on the flow rate of the primary coolant sodium.

As a result of the series of FPS tests, it is demonstrated clearly that the DNM responses and the activities of short life fission products in the cover gas can be changed sensitively, corresponding to the insertion patterns of control rods. Moreover, this fact suggests that the flux tilting method can be employed as a kind of sub-FFDL system in JOYO.

4) Analysis and Evaluation

An analytical model for the relationship between the DNM response and the release rate of fission products is shown in Fig. 6.21. This analytical model is built in the fission products behavior analysis code "FFDL-88" developed by PNC. A calculation flow of the DNMs response at the series of FPS test is shown in Fig. 6.22 with the used date base. Among data in the figure, the recoil range data for fission fragments in the U-Ni FPS has been measured by using the well-know neutron flux field of the thermal reactor CP-5 (see Fig. 6.23) and also verified by the test in EBR-II.

The calculated counts rate are fitted to the experimental data in order to determine the values of ε, the sensitivity of DNM, and transit time T from the breached fuel in the core to DNM system. The values of ε and T are tabulated in table 6.2 and the calculated DNM responses show good agreement with the measured ones as can be seen in Fig. 6.24, which demonstrates the validity of the analytical model. Using the evaluated ε and T, the detectable lower limit of the DNM system is estimated for 0.1cm^2 of the surface area of a breached fuel pin.

The sensitivity of the precipitator is determined to be 3×10^5 (cps/μCi/cc^{88}Kr), by comparing the measured precipitator response with OLGM. Using this value, the precipitator responses for the failure of a fresh fuel pin is estimated to be 90 times higher than the background at 100MWt operation. Finally, it is found that any fuel failure can be detected successfully by the precipitator.

On the other hand, an analytical model for the relationship between the activities of fission products in the cover gas and their release rates is expresses in Fig .6.25. This analytical model is also built in the FFDL-88 code. The calculation flow of the fission products activities in the cover gas is show in Fig. 6.26 with used nuclear data base.

First of all, calculation are conducted for the FPS-1 test, taking a disengagement rate constant λd, a cover gas leak rate constant (to the dump tank) λl and a cold trap efficiency λCT as unknown parameters and the calculated activities in the cover gas are fitted to the measured ones in other to evaluate the values of λd, λl and λCT. The λl and λCT and are determined to be 1.7×10^{-5} sec^{-1}, and 1×10^{-4} sec^{-1}, respectively, and the λd is determined for each flow rate of the primary sodium. Figure 6.27 shows these λd values versus the primary flow rate. In the next step, some calculations are performed both for the FPS-2 tests and the FPS-3 test employing the each value of λ defined by the FPS-1 test. Figure 6.28 shows the measured activities of fission products in the cover gas with calculated curves for the FPS-2 test. As can be seen in the figure, the calculation shows fairly good agreement with the measured result.

As a conclusion of the analysis, it is successfully shown that both of the analytical model and the FFDL-88 code are valid. The similar result is also obtained for the FPS-3 test.

5) Summary

The FPS test was successful in that most of the objectives were achieved. The following are the representative results;

(a) both of the cover gas and the delayed neutron monitoring systems were successfully calibrated to expand the irradiation test capability of JOYO such as RTCB and RBCB tests,

(b) major constants for the cover gas and the delayed neutron activity models were determined to confirm validity of computer codes, particularly disengagement rate constant of fission product gas from the coolant to the cover gas was found to depend on the flow rate of the primary coolant, and

(c) failed fuel location by the flux tilting and the triangulation method was demonstrated, particularly the flux tilting method by an on-line gamma ray monitor was found to be very useful.

Table 6.1 Test Specification

Test ID	FPS-1	FPS-2	FPS-3
Objective	Calibration	• Calibration • Triangulation Test • Flux Tilting Test	
FPS Location	[000]	[4A4]	[4D4]
FPS Specfication	Contents : 3.5wt%U (20wt% E.U.) in Ni Surface Area : 4585cm^2		
Plant Operation Conditions	Power : 1% of Rated Power Coolant Temp. : 250°C Primary Flow rate : 100%, 30%, 100% Control Rod Pattern* : Even, Full In, Full Out		
Monitoring System	FFD CGM ; Precipitator, Online Gamma-Ray Monitor FFD DNM		

* Position of the Control Rod Adjacent to FPS

Table 6.2 Determination of Transit Time and Efficiency

• Transit Time : T (s) at Full Flow Rate

FPS Location	DNM(A)	DNM(B)
[000]	30	40
[4A4]	21	——
[4D4]	——	40

• DNM Efficiency : ε (cps/(dps/cc))

DNM(A)		DNM(B)		
ch. 1	ch. 2	ch. 1	ch.2	ch.3
BF_3	BF_3	B_{10}	B_{10}	BF_3
8.7	7.8	3.3	5.6	3.8

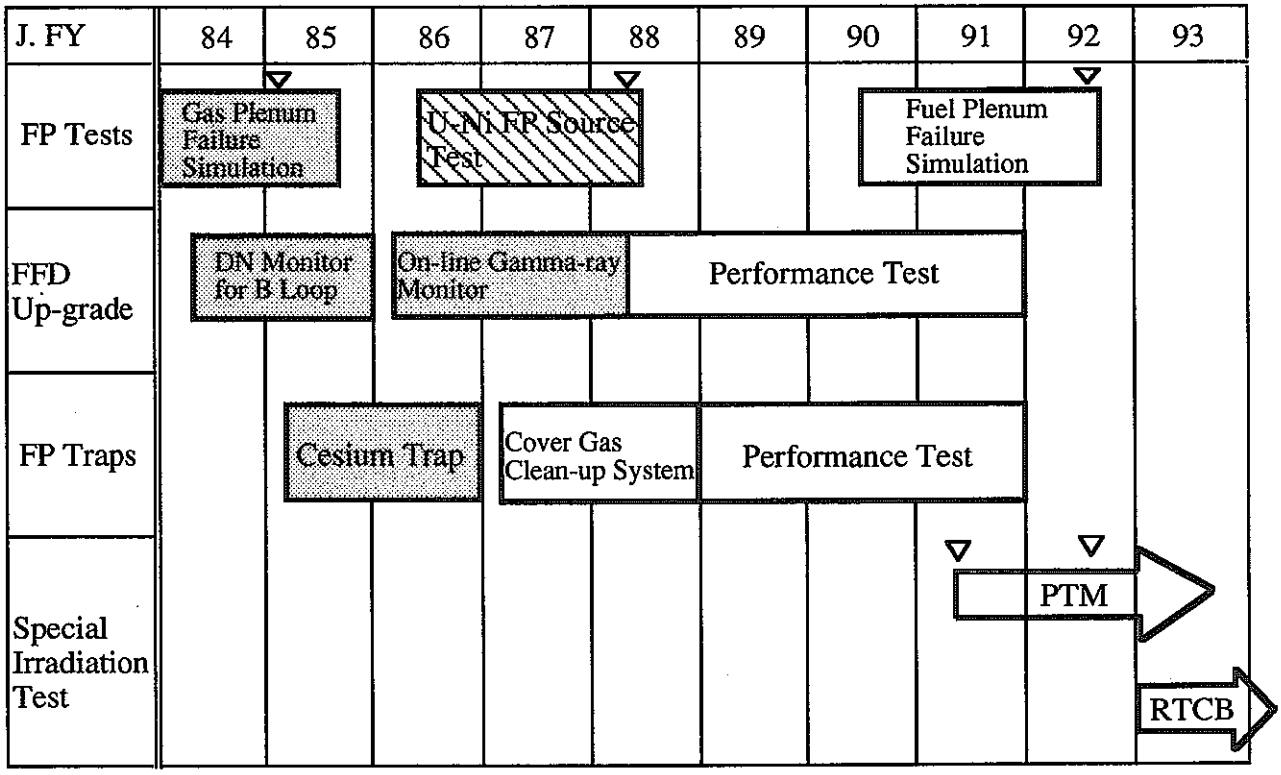

Fig. 6.1 Schedule of Preparations for RTCB and PTM Tests

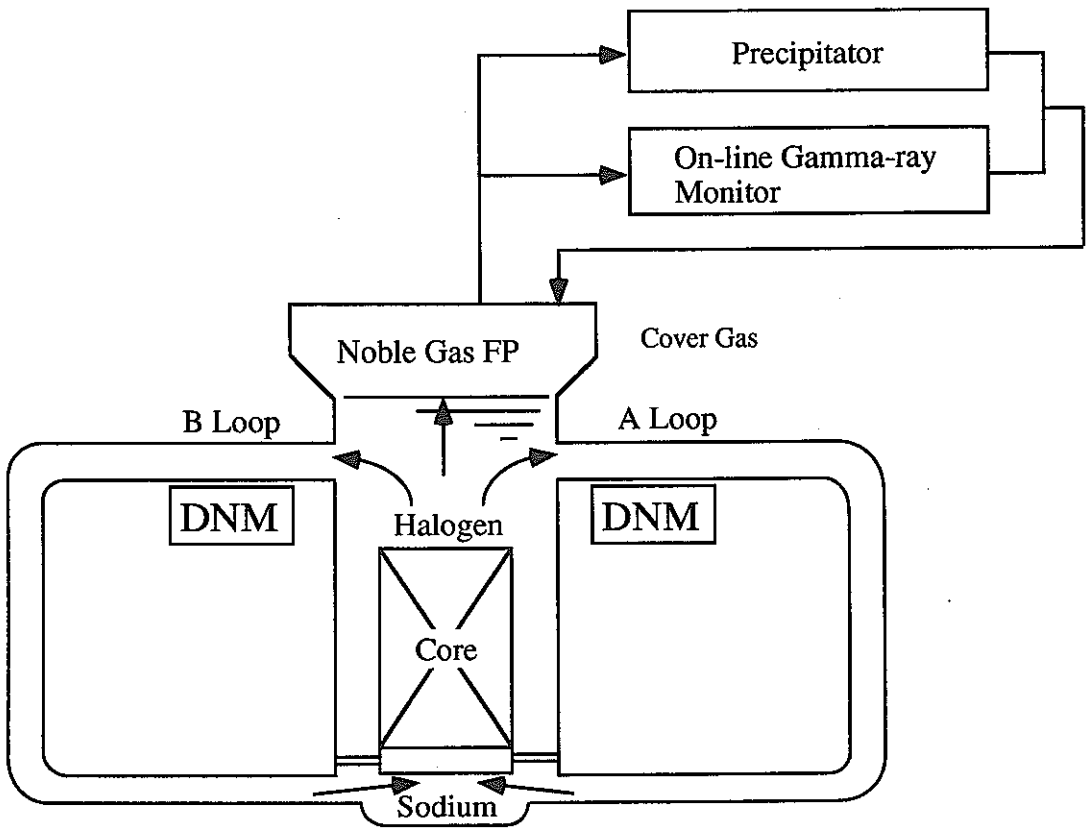

Fig. 6.2 Schematic Diagram of FFD Systems in JOYO

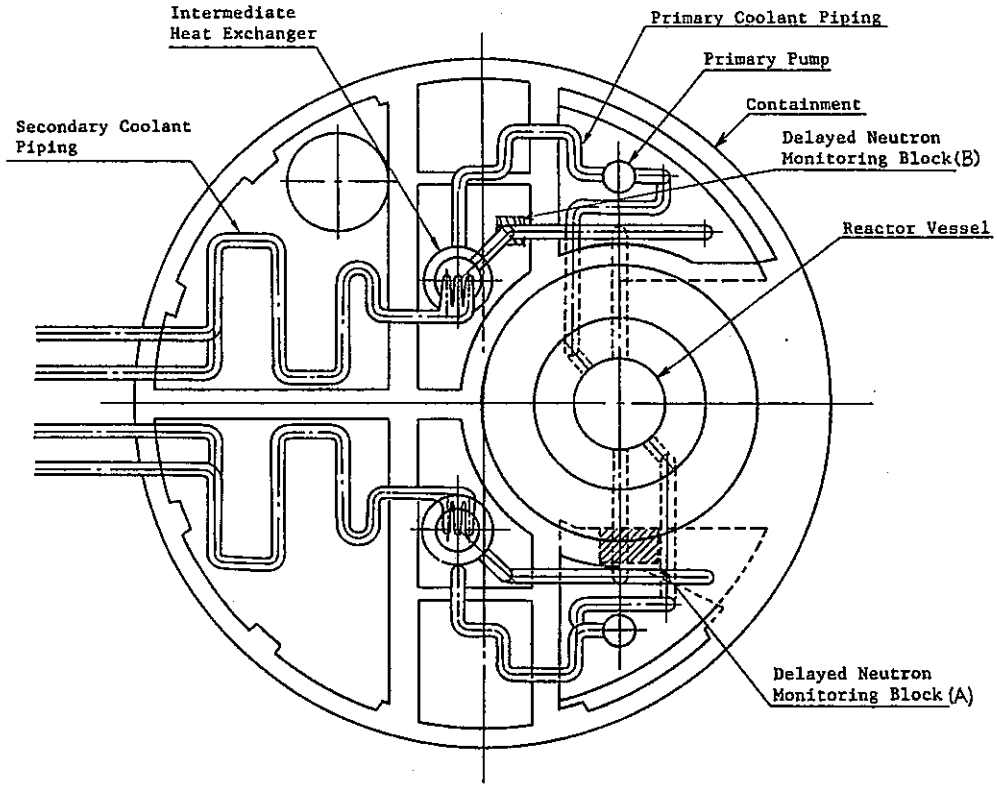

Fig. 6.3 FFD • DNM Block Layout

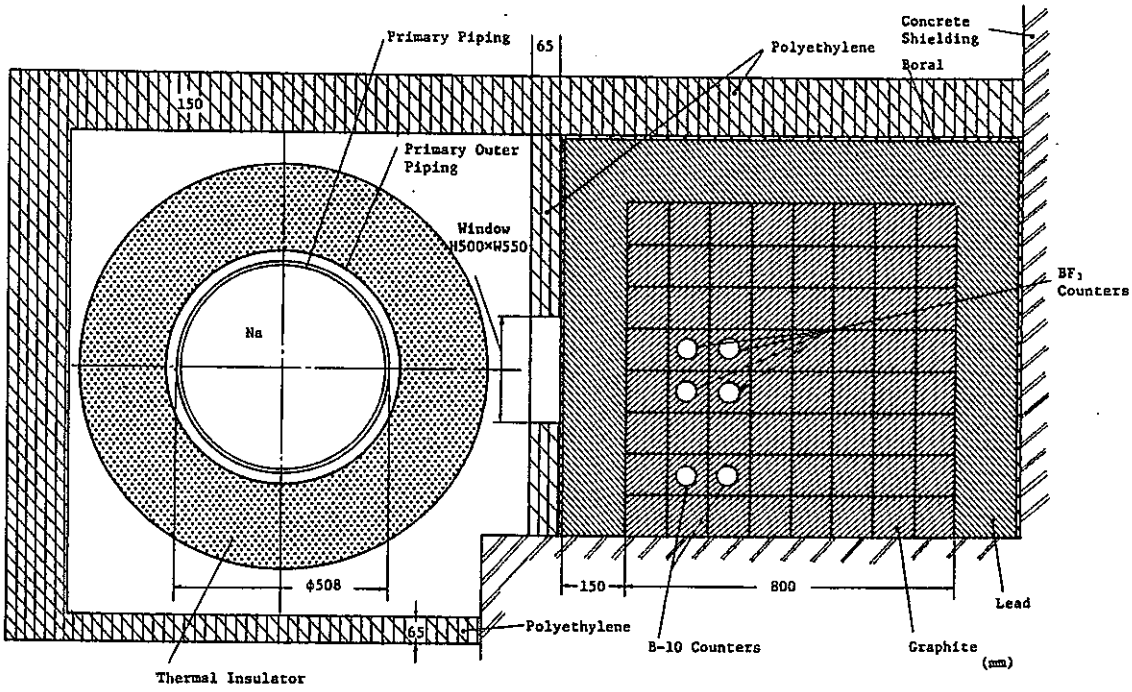

Fig. 6.4 Section Diagram of DNM (A) Block

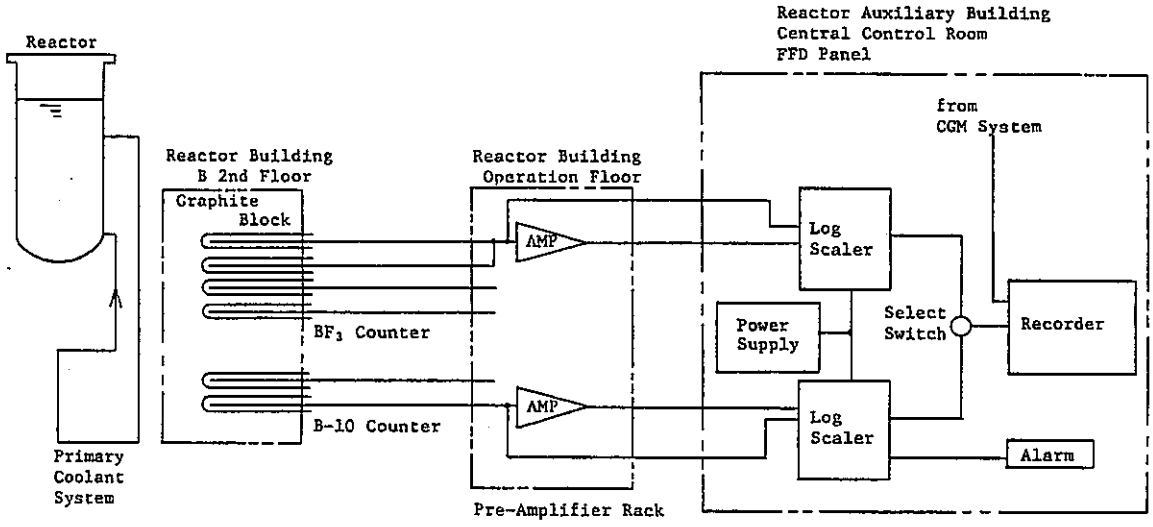

Fig. 6.5 Block Diagram of Delayed Neutron Monitoring System

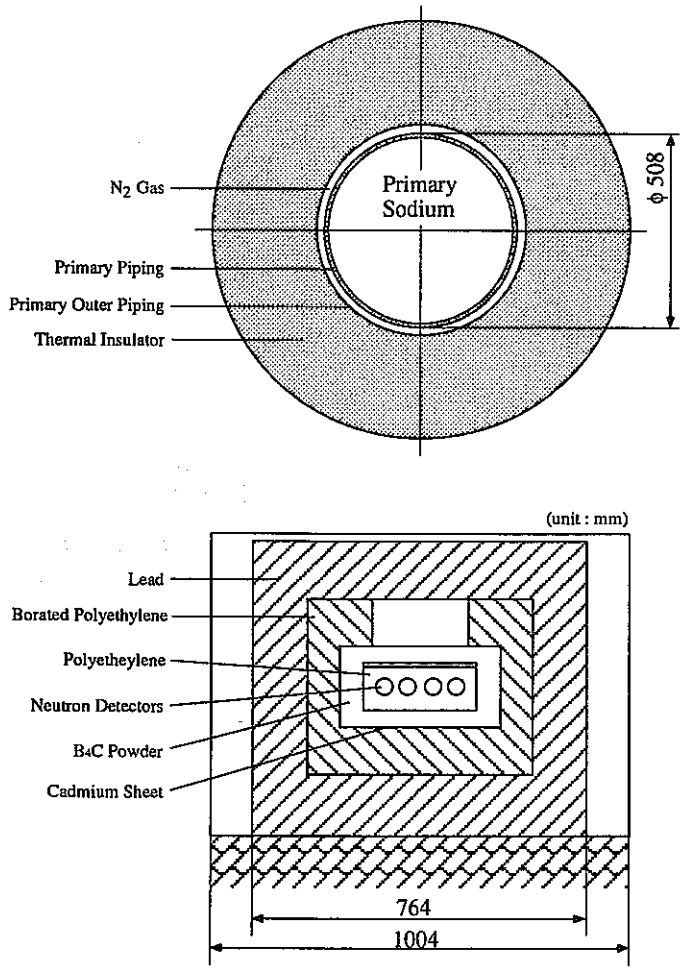

Fig. 6.6 Cross Sectional View of DNM (B) Block

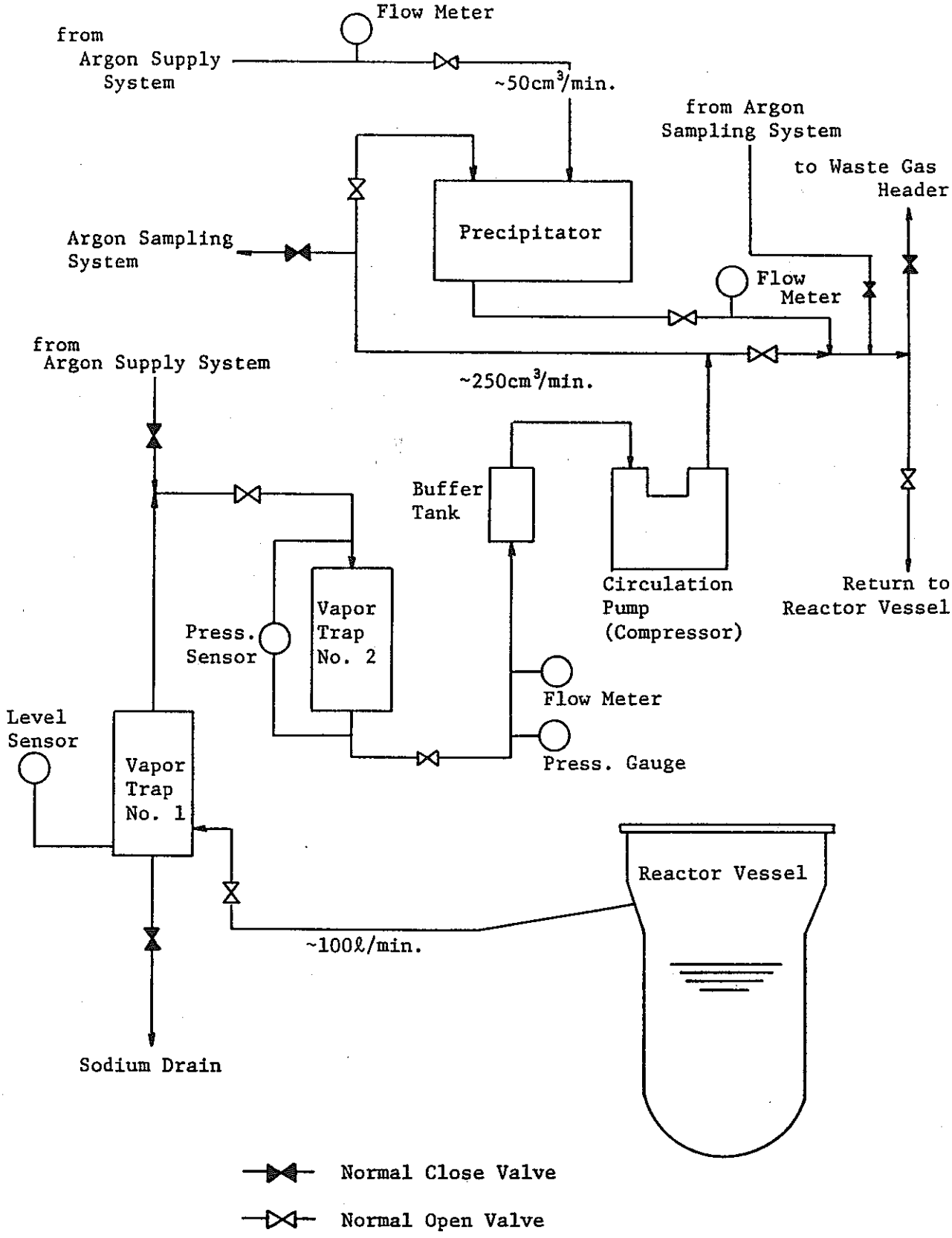

Fig. 6.7 Block Diagram of Fuel Failure Detection Cover Gas Monitoring System

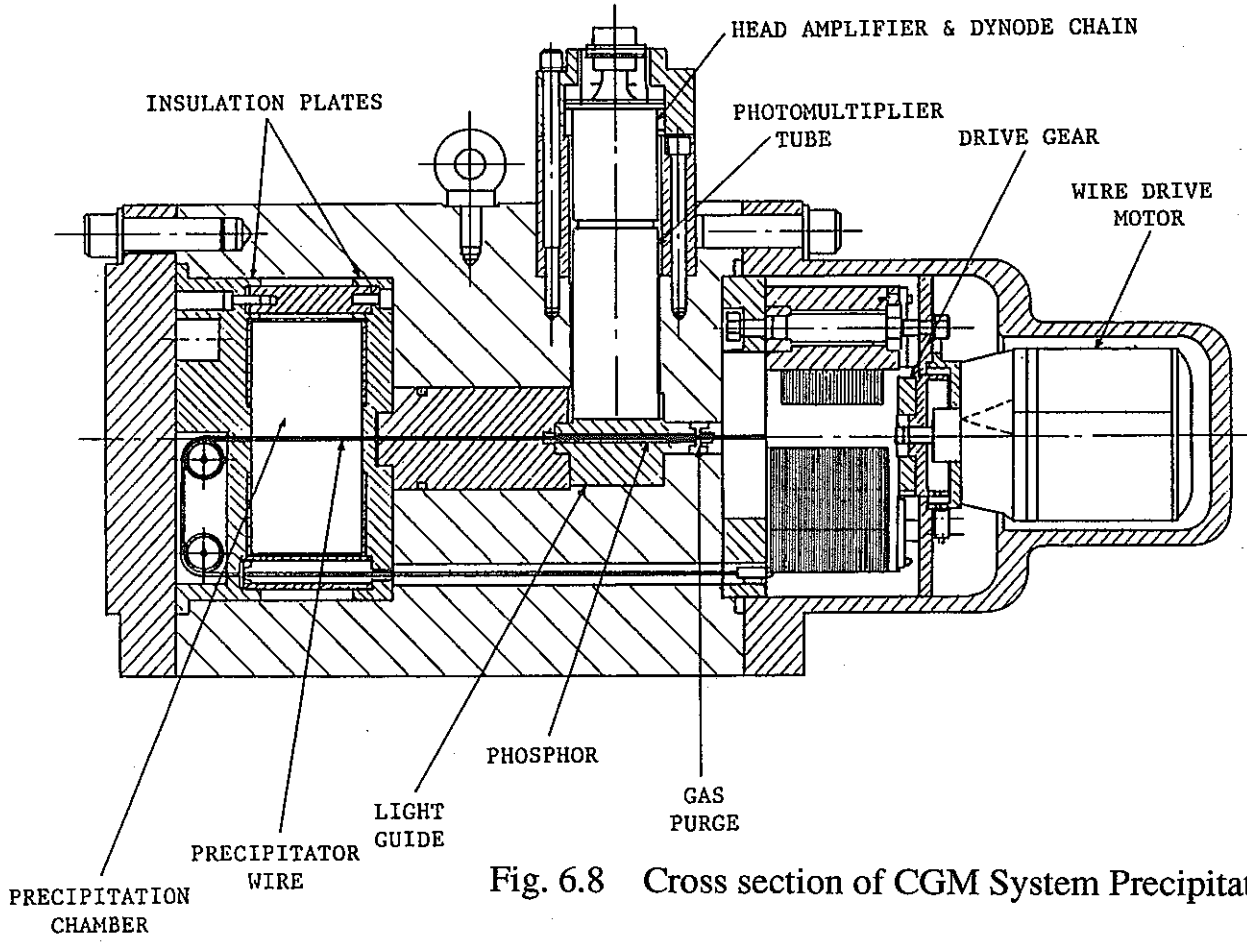

Fig. 6.8 Cross section of CGM System Precipitator

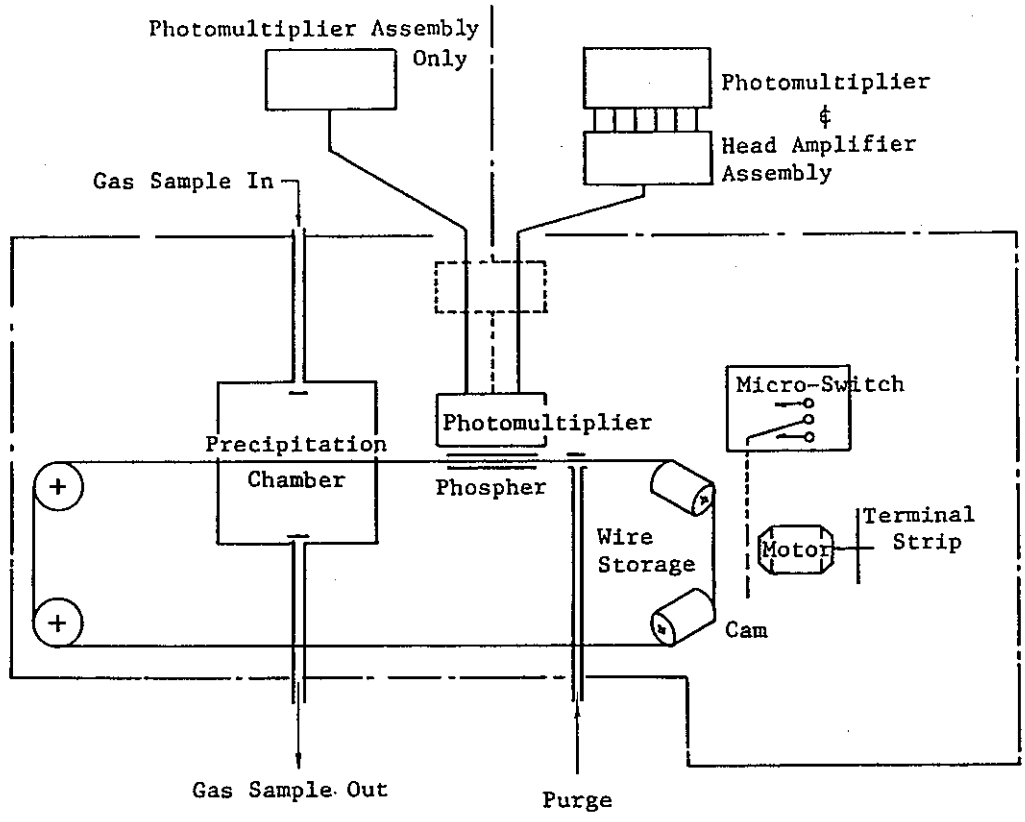

Fig. 6.9 Diagrammatic Layout of CGM System Precipitator

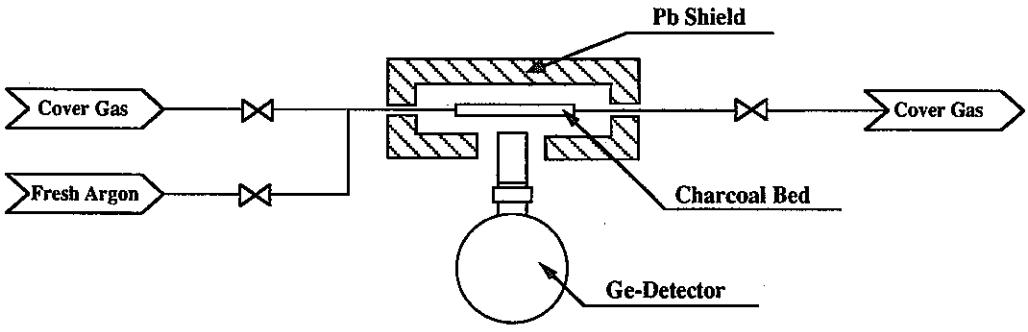

Schematic Diagram

- **Advantages**
  - **Xe and Kr gasses are concentrated up to 100 times and 10 times, respectively.**
  - **A small amount of fresh argon purges out selectively ^{41}Ar and ^{23}Ne.**
- **Measured Nuclides : ^{133}Xe, ^{135}Xe, ^{135m}Xe, ^{137}Xe, ^{138}Xe, ^{85m}Kr, ^{87}Kr, ^{88}Kr**
- **Detectable Lower Limit : 1 ~ 10 pCi/ cc**

Fig. 6.10 On-line Gamma-Ray Monitor

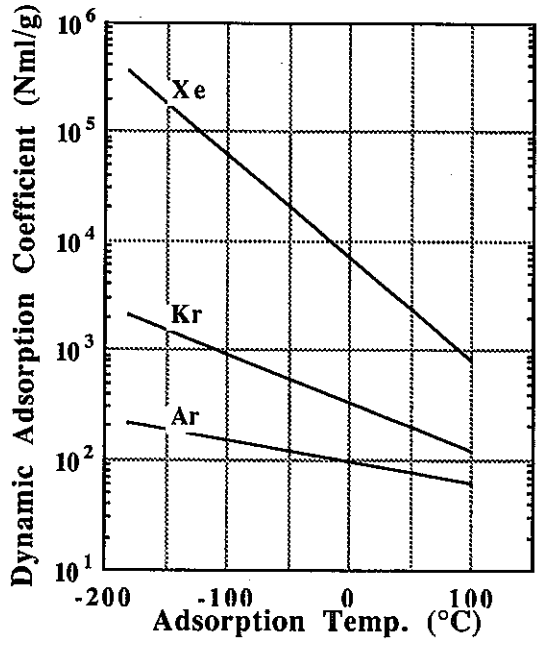

Fig. 6.11 Adsorption Characteristic of Noble Gases

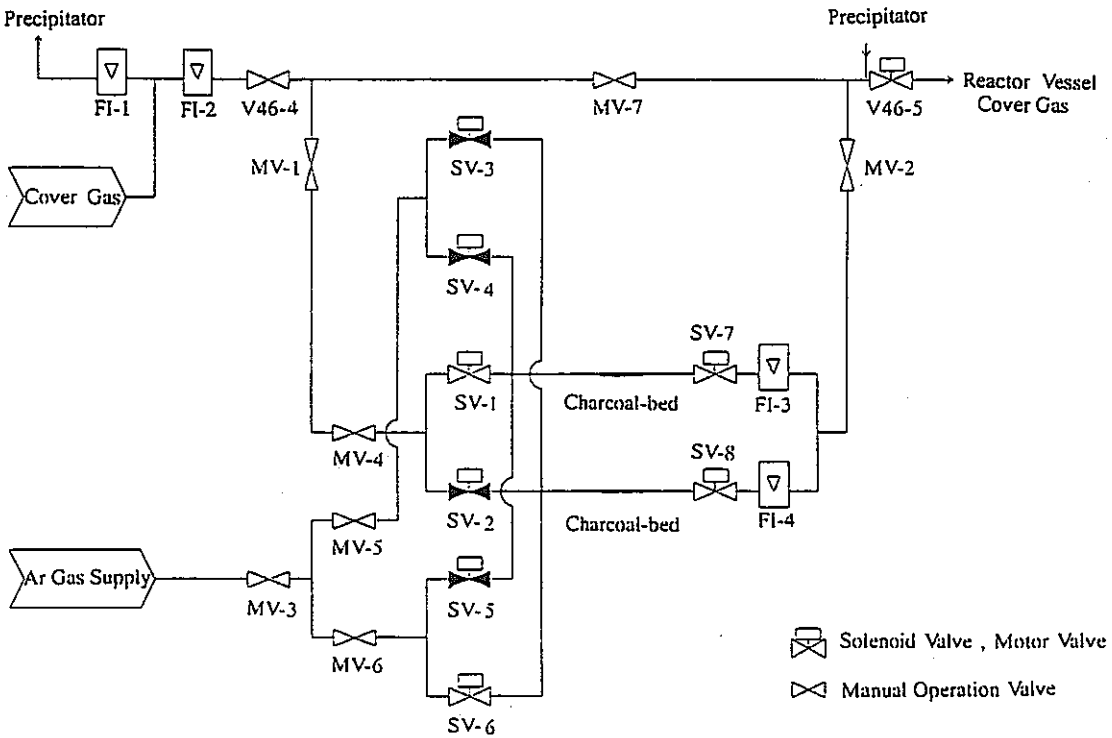

Fig. 6.12 Flow Sheet of On-line Gamma-Ray Monitor

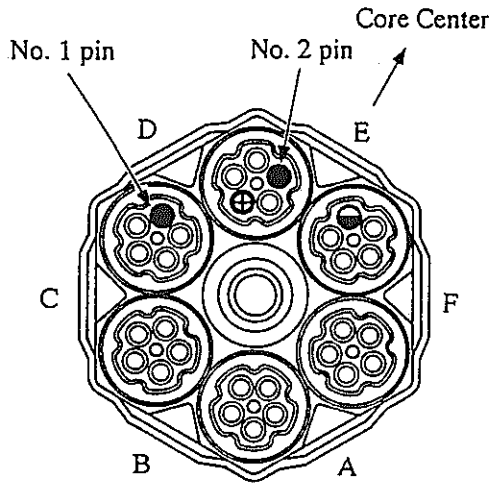

Plenum Predefected Pins with 0.1mm x 1mm Slit

Sibling Pin

Plenum Predefected Dummy Rod with Tagging Gas

Dummy Rod

Fig. 6.13 Schematic Diagram of test Pins Configuration

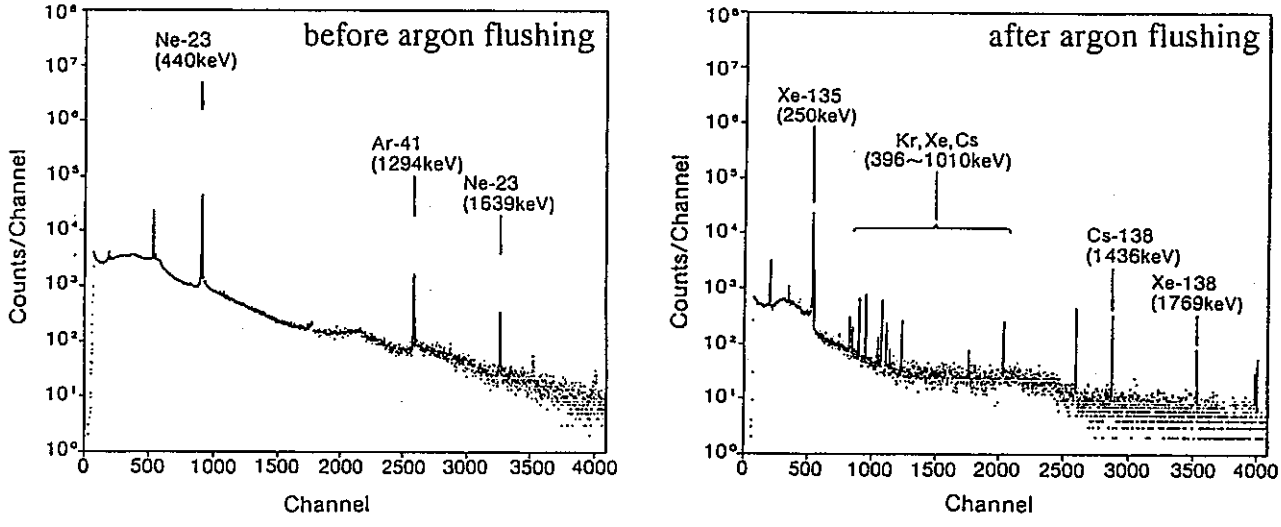

Fig. 6.14 Effect of Argon Flushing on Gamma-Ray Spectrum

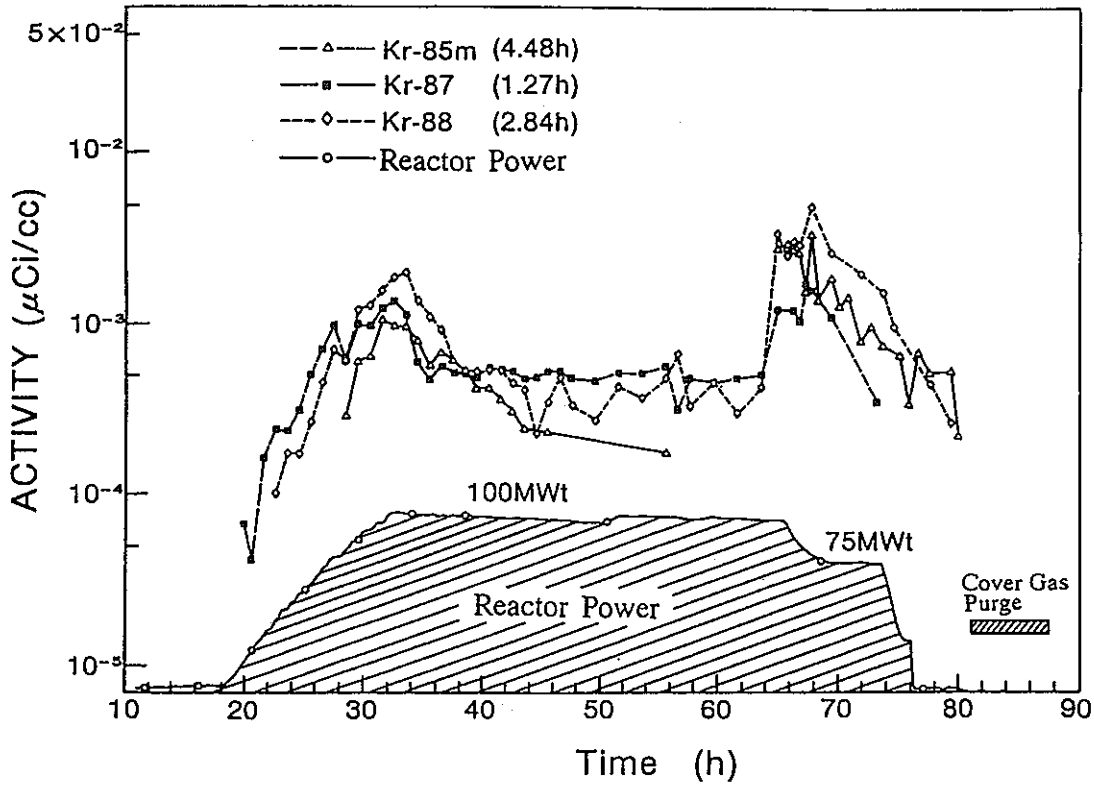

Fig. 6.15 Activities of Krypton Isotopes in Cover Gas during Reactor Operation of the Test

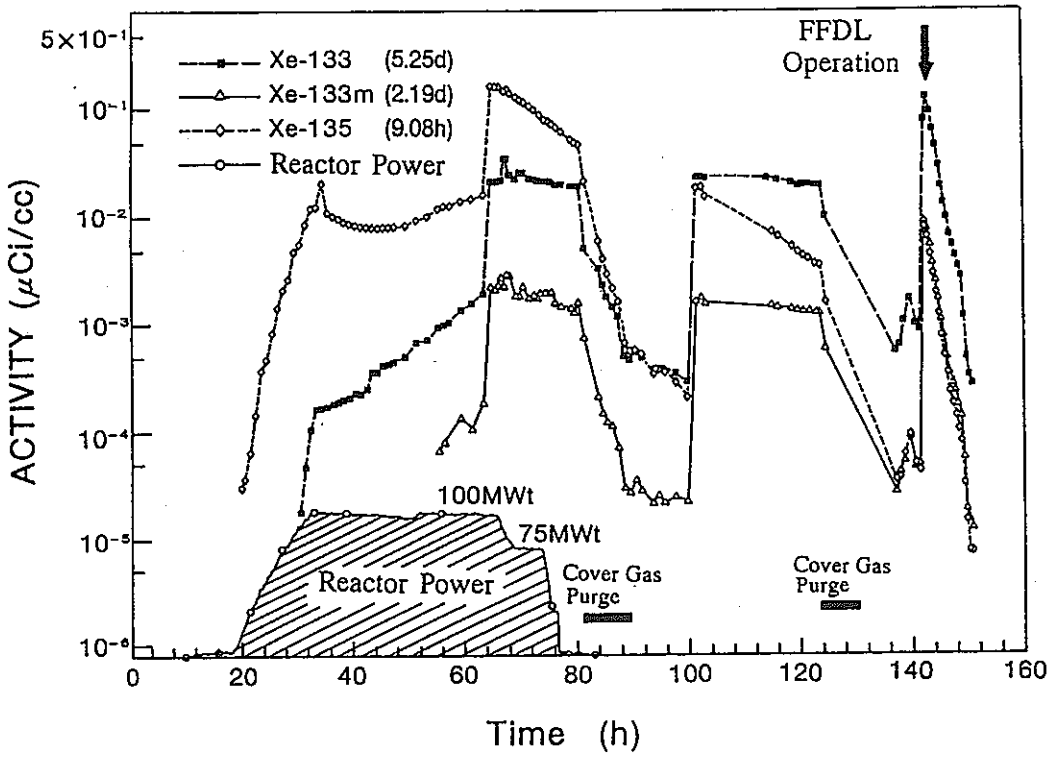

Fig. 6.16 Activities of Xenon Isotopes with Long Half Life Time in Cover Gas during the Test

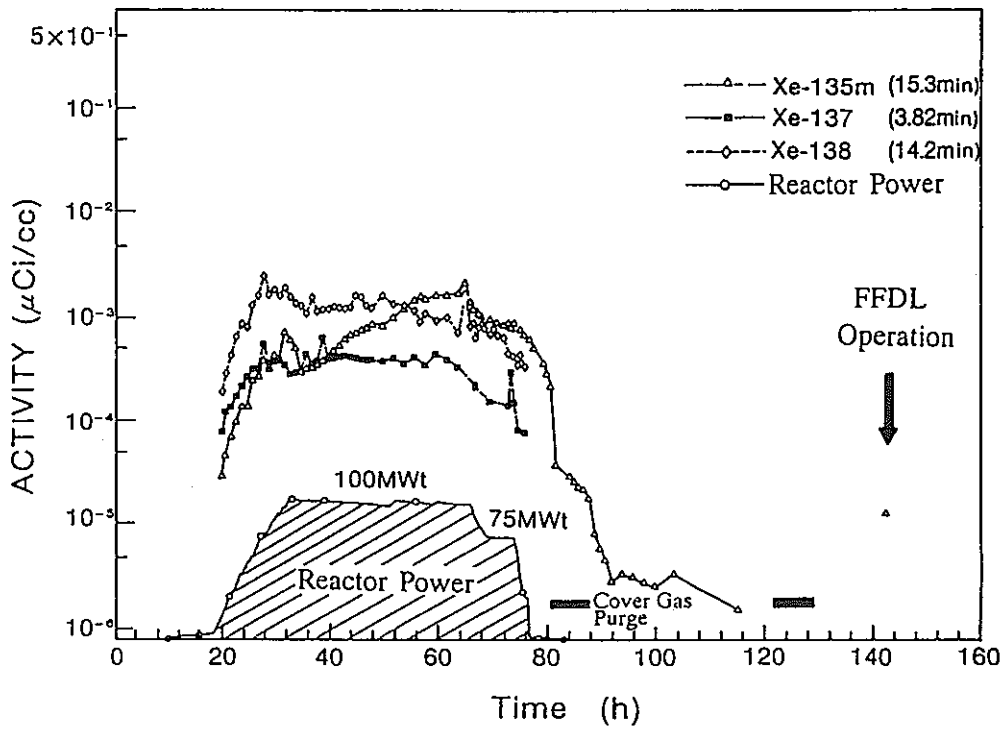

Fig. 6.17 Activities of Xenon Isotopes with Short Half Life Time in Cover Gas during the Test

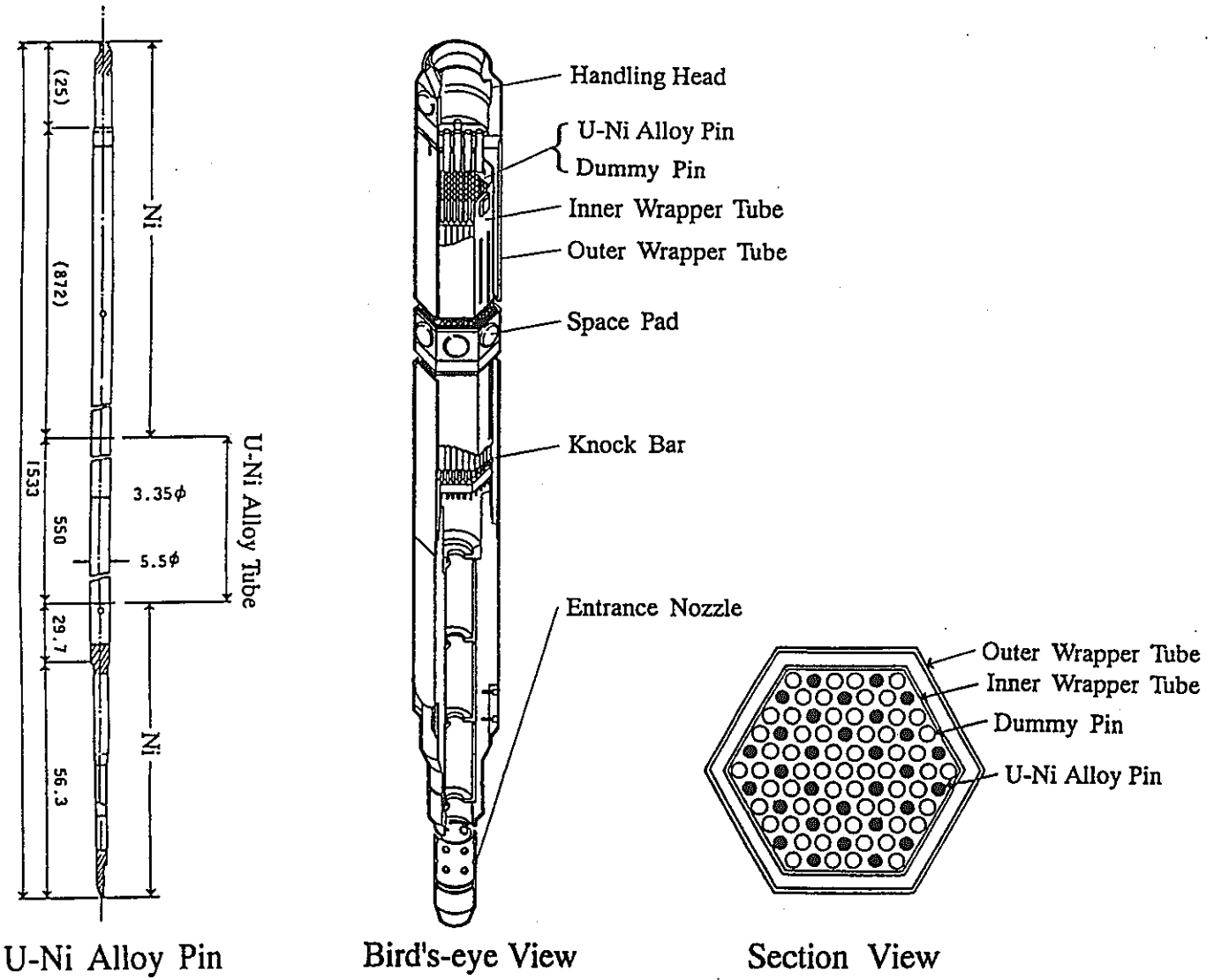

Fig. 6.18 Diagrams of FPS

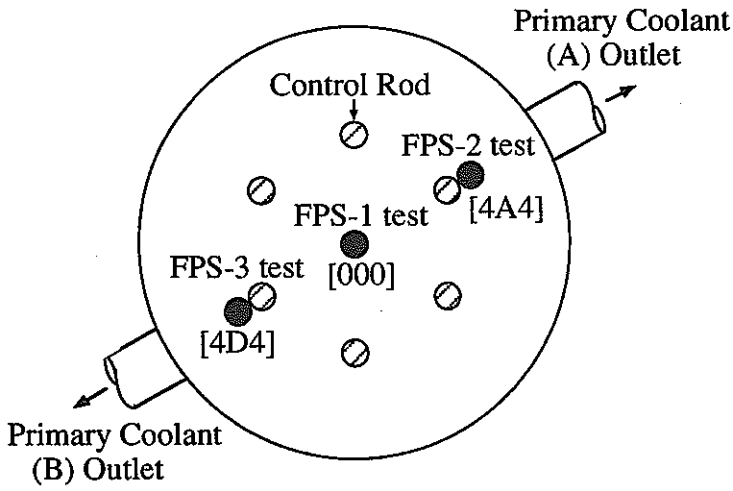

Fig. 6.19 FPS Location for Each FPS Test

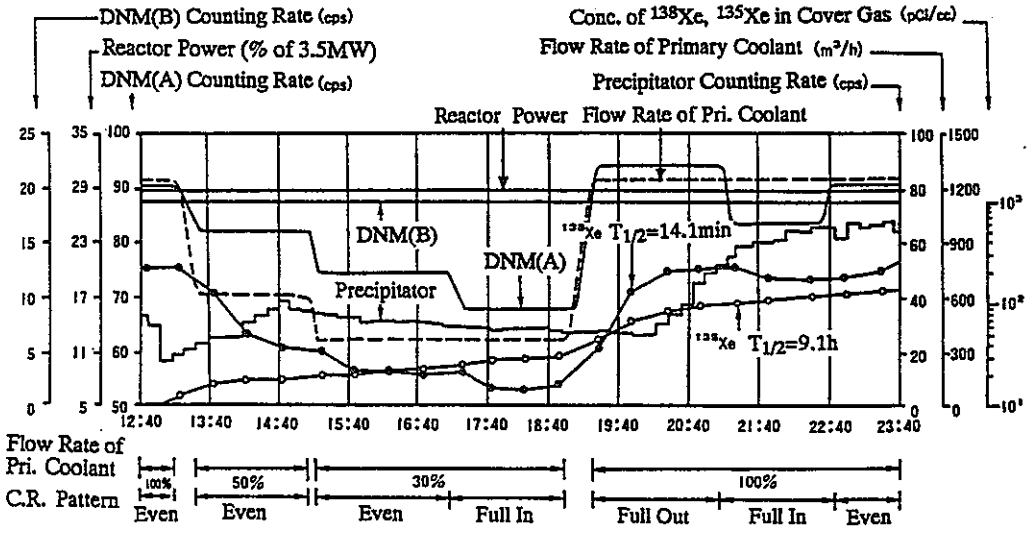

Fig. 6.20 Major Trend Data for FPS-2 Test

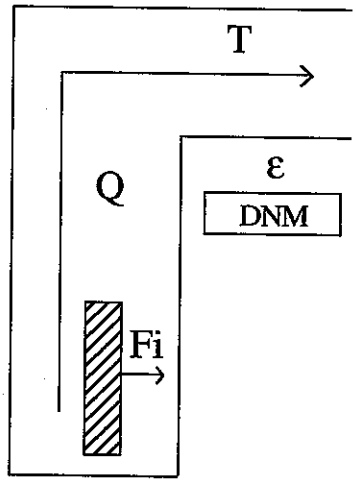

C : DNM Counting Rate (cps)
ε : Efficiency of DNM (cps/(dps/cc))
Fi : Release Rate of i-th Nuclide from FPS to Coolant (n/s)
λi : Decay Constant of i-th Nuclide (s^{-1})
ηi : Probability of DN Emission, Fraction (-)
Q : Flow Rate of Pri. Coolant (cc/s)
T : Transit Time from FPS to DNM (s)
D : Delayed Neutron Emitter
P : Parent of Delayed Neutron Emitter

$$C = \frac{\varepsilon}{Q} \cdot \sum_i \left\{ F_i^P \cdot \frac{\lambda_i^P}{\lambda_i^D - \lambda_i^P} \cdot \left(e^{-\lambda_i^P \cdot T} - e^{-\lambda_i^D \cdot T} \right) + F_i^D \cdot e^{-\lambda_i^D \cdot T} \right\} \cdot \lambda_i^D \cdot \eta_i^D$$

Fig. 6.21 Analytical Model of DNM Response

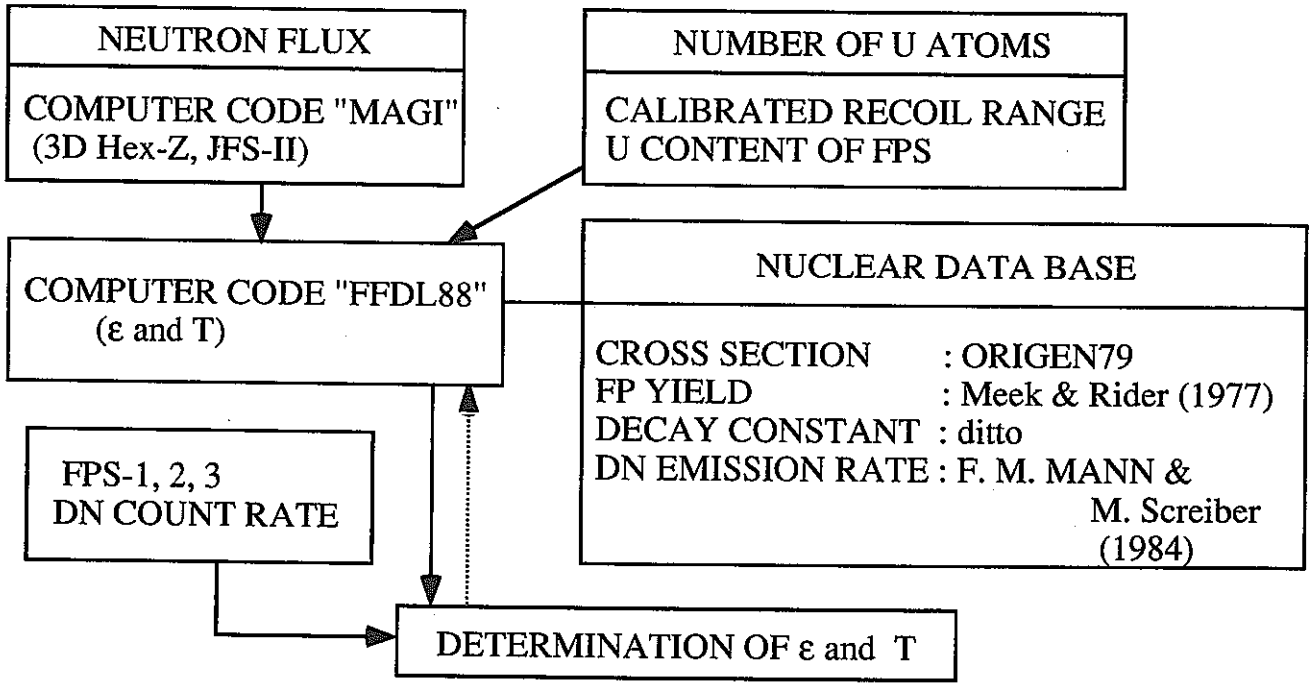

Fig. 6.22 Calculation Flow of DNM Response

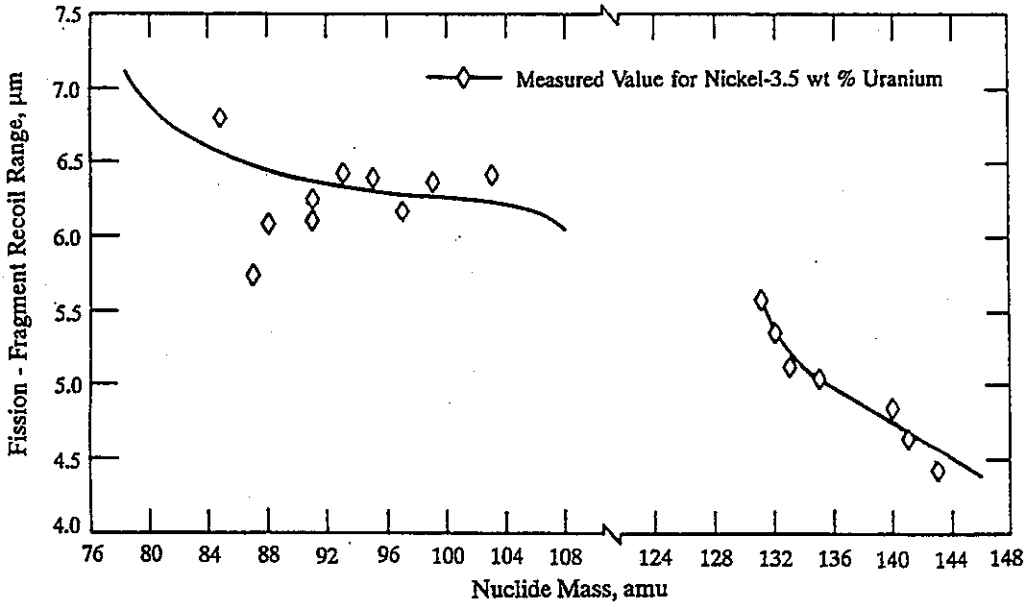

Fig. 6.23 Recoil Range of Nuclide in FPS Calibrated in CP-5 (1)

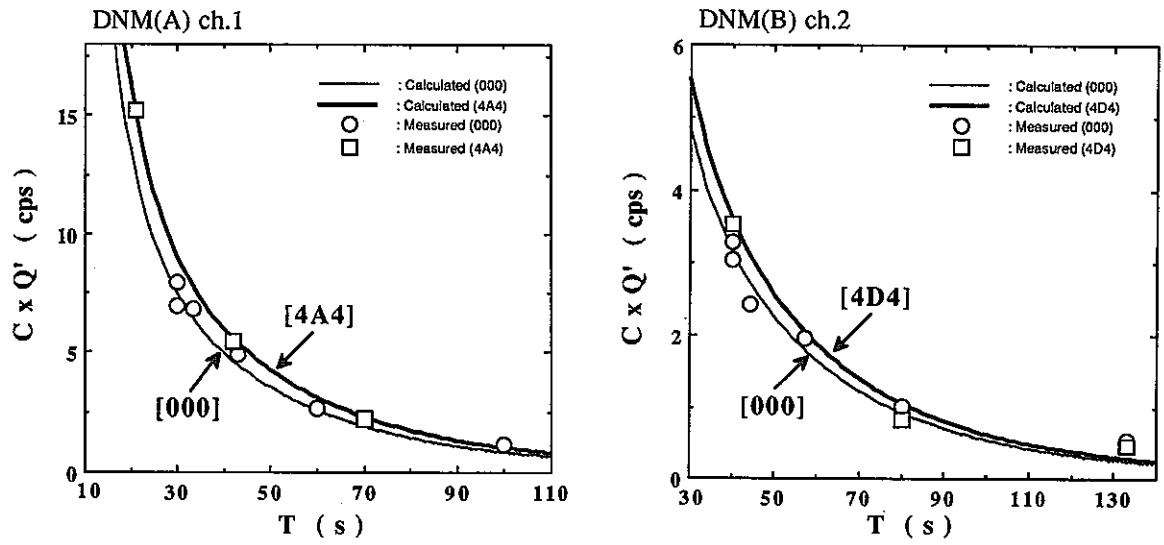

Fig. 6.24 Comparison of Experimental and Calculated Responses for Delayed Neutron

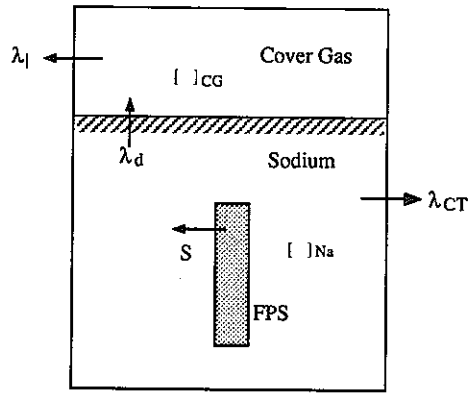

$$\frac{d[1]_{Na}}{dt} = S_1 - [1]_{Na}(\lambda_1 + \lambda_{CT})$$

$$\frac{d[2]_{Na}}{dt} = S_2 + f_{1,2}[1]_{Na}\lambda_1 - [2]_{Na}(\lambda_2 + \lambda_d)$$

$$\frac{d[3]_{Na}}{dt} = S_3 + f_{1,3}[1]_{Na}\lambda_1 + f_{2,3}[2]_{Na}\lambda_2 - [3]_{Na}(\lambda_3 + \lambda_d)$$

$$\frac{d[2]_{CG}}{dt} = [1]_{Na}\lambda_d - [2]_{CG}(\lambda_2 + \lambda_l)$$

$$\frac{d[3]_{CG}}{dt} = [3]_{Na}\lambda_d + f_{2,3}[2]_{CG}\lambda_2 - [3]_{CG}(\lambda_3 + \lambda_d)$$

[i]= number of fission-product atom i
1= I or Br
2= metastable Xe or Kr
3= Xe or Kr
[ ]Na = sodium phase
[ ]CG = argon-cover-gas phase

λi = decay constant of atom i, (s^{-1})
λCT = cold-trap efficiency, (s^{-1})
λd = disengagement-rate constant, (s^{-1})
λl = cover-gas-leak-rate constant, (s^{-1})
f = branching ratio (-)

Fig. 6.25 Analytical model of FP Activity in the Cover Gas

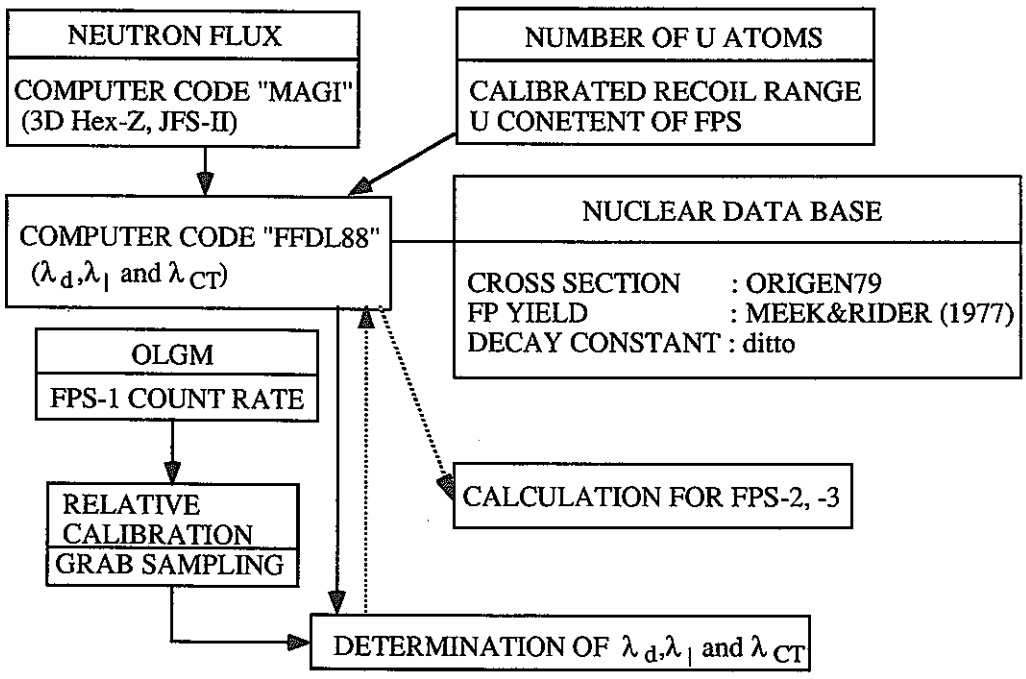

Fig. 6.26 Calculation Flow of FP Activity in the Cover Gas

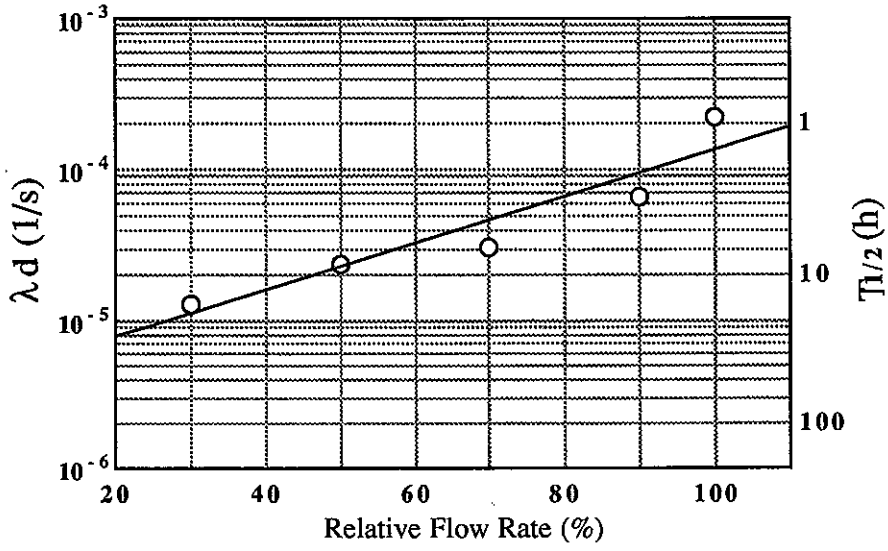

Fig. 6.27 Disengagement-Rate Constants depending on Primary Coolant Flow Rate

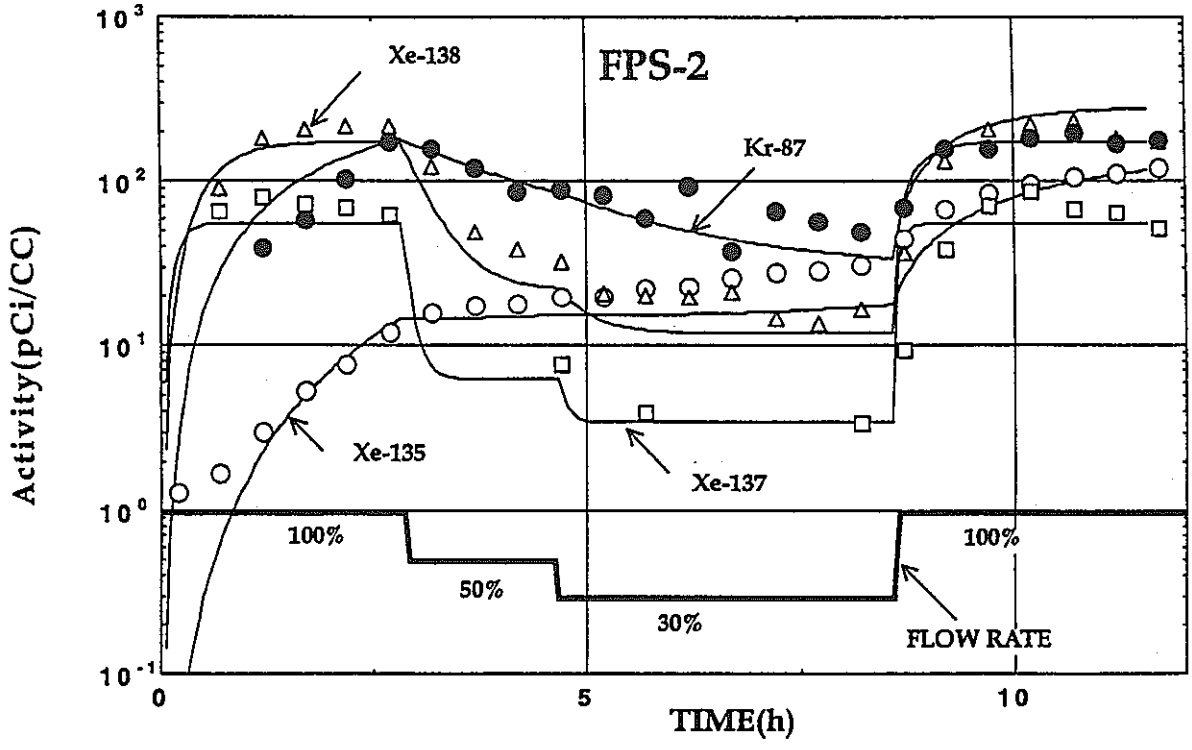

Fig. 6.28 Comparison of Measured and Calculated Activities of FP in Cover Gas

7. FAILED FUEL DETECTION AND LOCATION (FFDL) SYSTEM

FFDL system must have function as an indicator to withdrawal of the fuel subassembly which contains any failed pins for refueling, if necessary. Therefore it is considered to be more important from the viewpoint of plant availability rather than that of safety in LMFBR. At the present time every LMFBR plant has an FFDL system employing one of the following methods; a selector valve, a gas tagging or a sipping methods.

Installation of an FFDL system to JOYO was planned in 1976 to select the sipping method because of its applicability to JOYO; a sipping system can be installed on the rotating plug at the top of the reactor vessel and can access the fuel subassembly in the same manners as the fuel handling machine, where a selector valve system required the large modification of the upper part of the reactor vessel and a gas tagging system required the modification of a fuel pin design to include a capsule containing tagging gas. R&Ds, fabrication, extensive functional tests and a performance test for the sipping method have been conducted for over ten years at JOYO.

Recently, the sipping methods combined with the flux tilting method and the delayed neutron triangulation method is begun to investigate as a reference FFDL system in the design study of the Japanese demonstration FBR, because of its low cost and less impact on the plant design.

7.1 System Description

An overview of FFDL employing the sipping method and a flow sheet of gas circulation unit are shown in Fig. 7.1 and Fig. 7.2.

The sipping and sniffing mechanism of FFDL is illustrated in Fig. 7.3. FFDL is mounted on the rotating plug and is addressed to a subassembly with the primary flow rate set at 75%, where Pa is the pressure at the entrance nozzle of the subassembly and Pb is the pressure at the failed part. When a sipping port is coupled to the top of subassembly and the sodium flow in the subassembly is blocked, Pb becomes nearly equal Pa and larger than Pb and some volume of sodium is introduced into the fuel pin through the failure hole, when a difference between Pb' and Pb is larger than 0.5 kg/cm^2. After lapse time of 3 minutes, the sipping port is left the top of subassembly, while sodium is introduced into the sodium tank. Then the pressure balance of the fuel pin is restored to the initial state, and some volume of sodium or gas in the fuel pin is released through the failure hole, and sampled sodium contains some FP nuclides. Five minutes later sodium

level in the sodium tank attains the level of sodium free surface in the reactor vessel. At this time the sodium inventory in the sodium tank is 5 liters. Then, by introducing the carrier argon gas to flow into the sampled sodium, FP gas contained in the sipped sodium is transferred into the carrier gas. Radioactivity of this circulating gas is measured by NaI scintillation counter and Ge detector. After measurement, sodium and circulating gas are returned to the reactor vessel. Those procedures take 30 minutes for a subassembly. The FP extraction mechanism with the FFDL device is schematically shown in Fig. 7.4.

7.2 Demonstration Test at JOYO

In order to demonstrate the performance of the FFDL system, an in-pile simulation test was carried out by using two identically slitted fuel pins, as described section 6.2 (1). The representative results of the test and the analyses are as follows:

(1) In the FFDL operation, a signal level of the test assembly is several hundreds times higher than that of the background which is obtained for other normal fuel subassemblies (see Fig. 7.5). Thus, FFDL is confirmed to have capability to identify the failed fuel with a defect at gas plenum.

(2) Measured volume of ^{133}Xe released to cover gas from test pins by FFDL operation is 50% of the predicted with an assumption of 0.05 as the FP release-to-birth ratio. Consequently, FP extraction mechanism for the defect at upper gas plenum of the fuel pin is confirmed to hold true.

(3) Measured volume of ^{133}Xe introduced into the gas circulation unit is 10% of the predicted. This low sampling efficiency may be due to the dead time of 7 seconds between release of the sipping port from the assembly and sodium introduction (see Fig. 7.3). Most of the FP gas in the test pins might be released during this dead time.

Further tests of the FFDL for pins with a slit at fuel column are now planned to be carried out in the end of 1992.

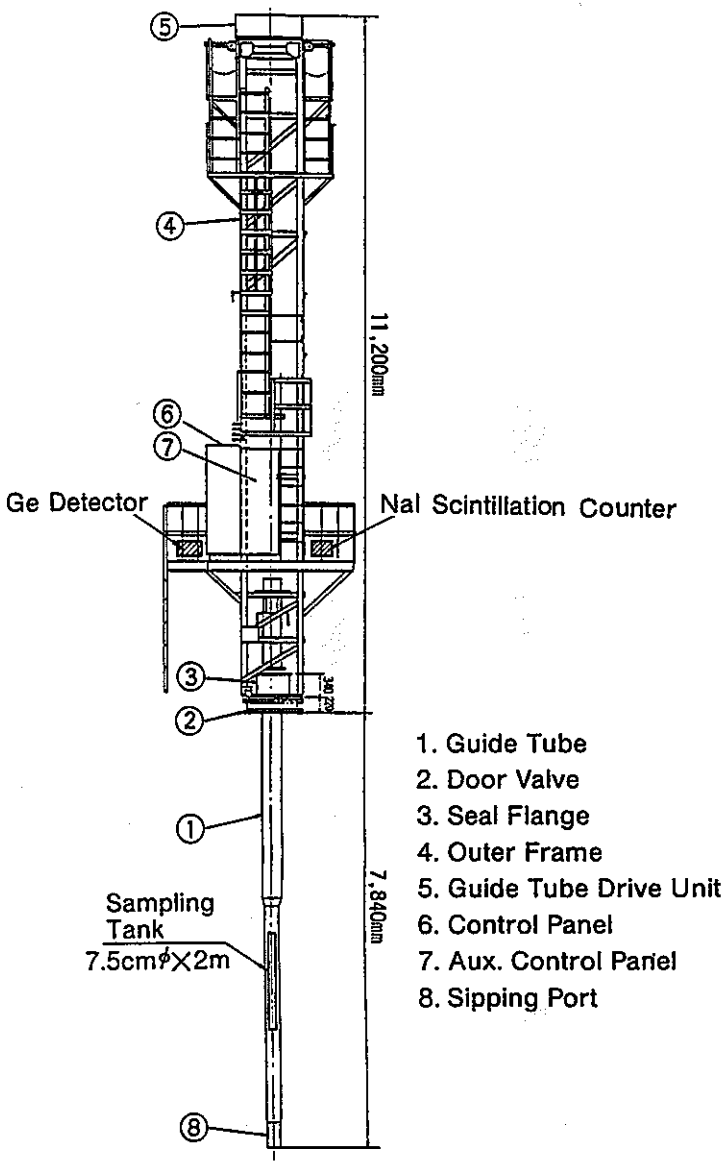

Fig. 7.1 Overview of FFDL System

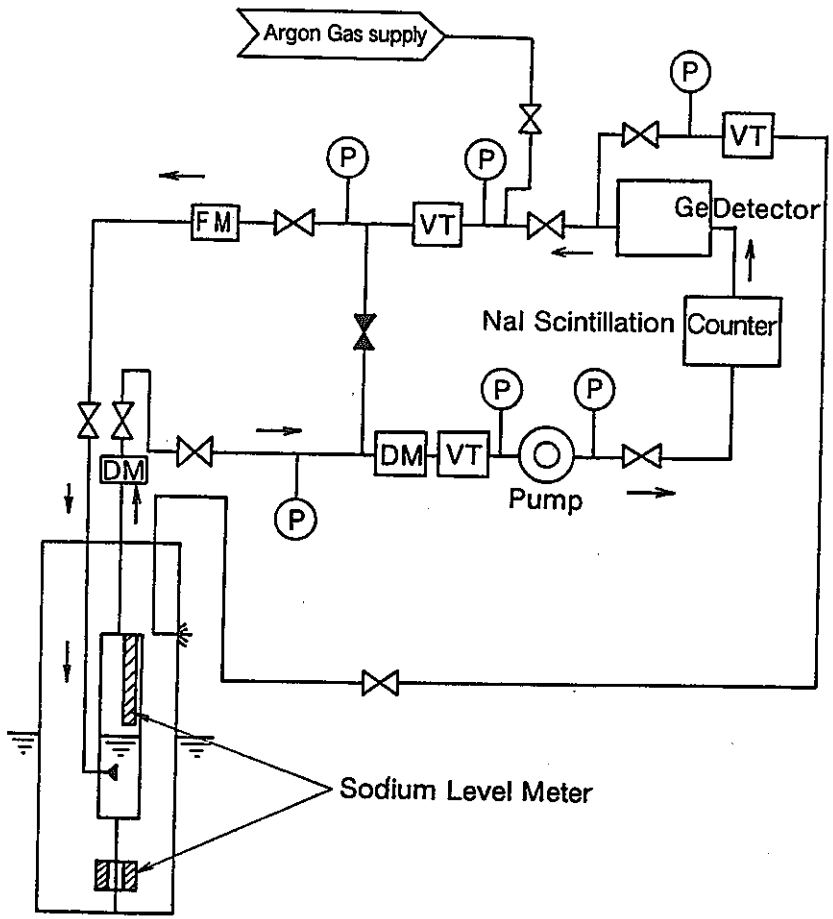

Fig. 7.2 Flow Diagram of Gas Circulation Unit

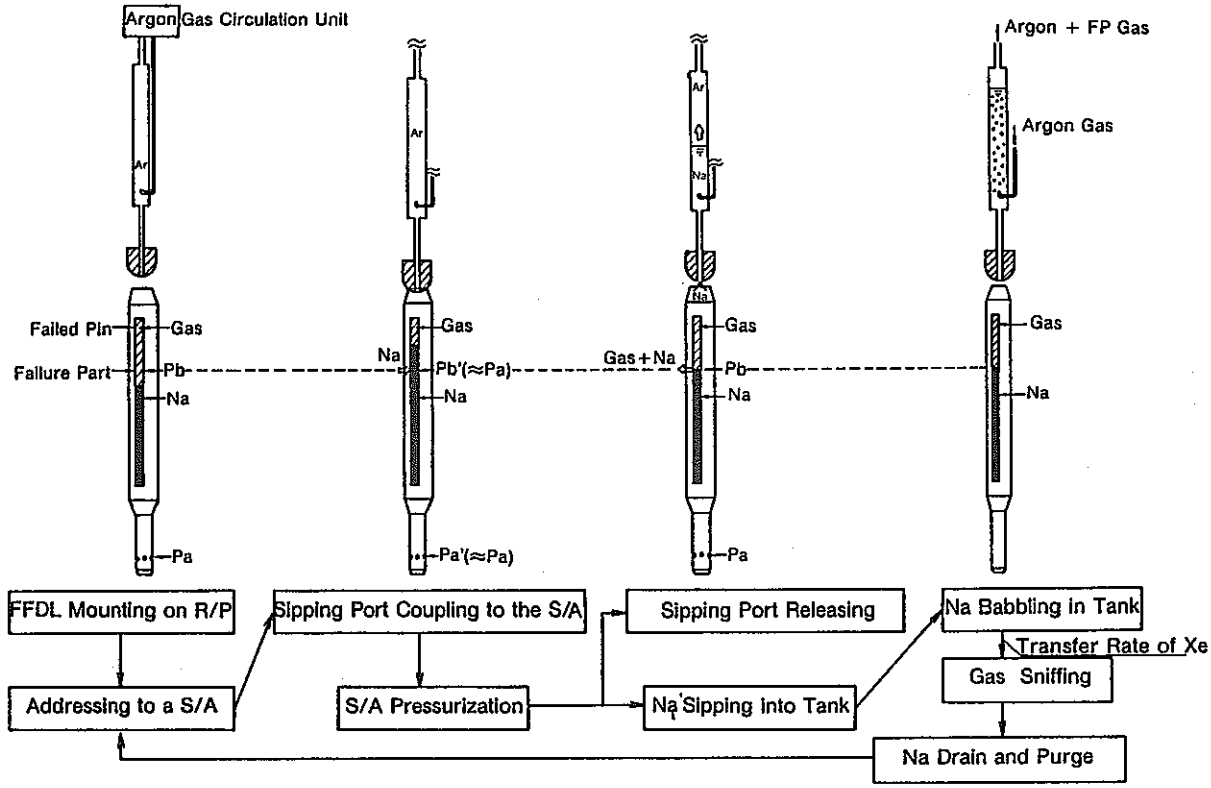

Fig. 7.3 Sipping and Sniffing Mechanisms of FFDL

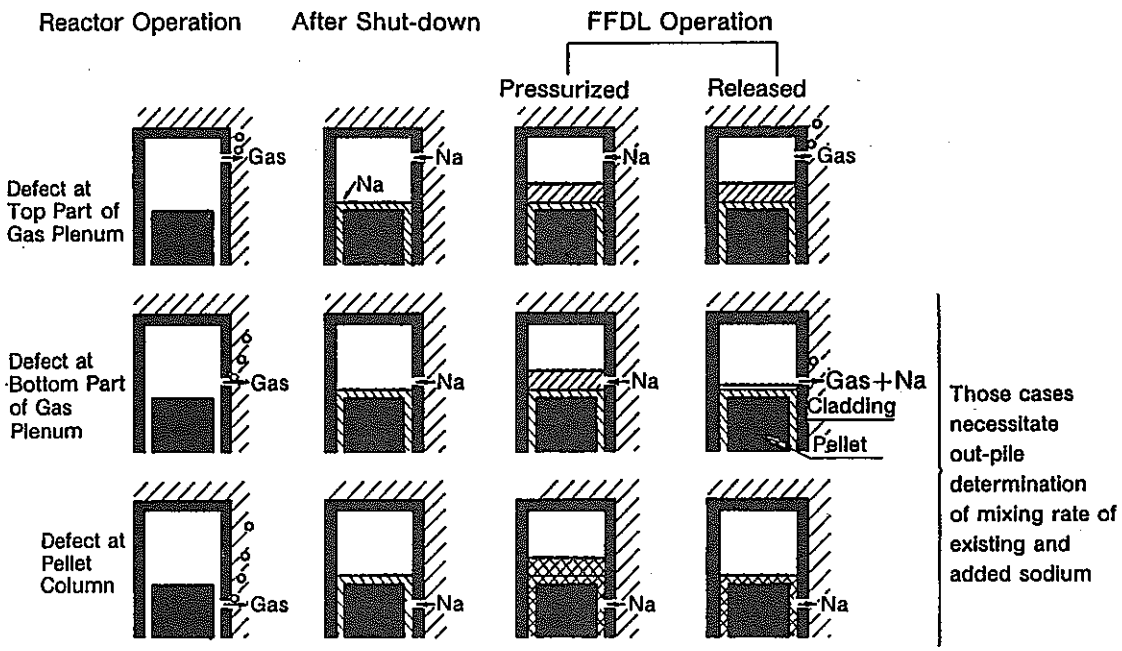

Fig. 7.4 Three Possible Locations of Breaching and the FP Extraction Mechanisms by FFDL Operation

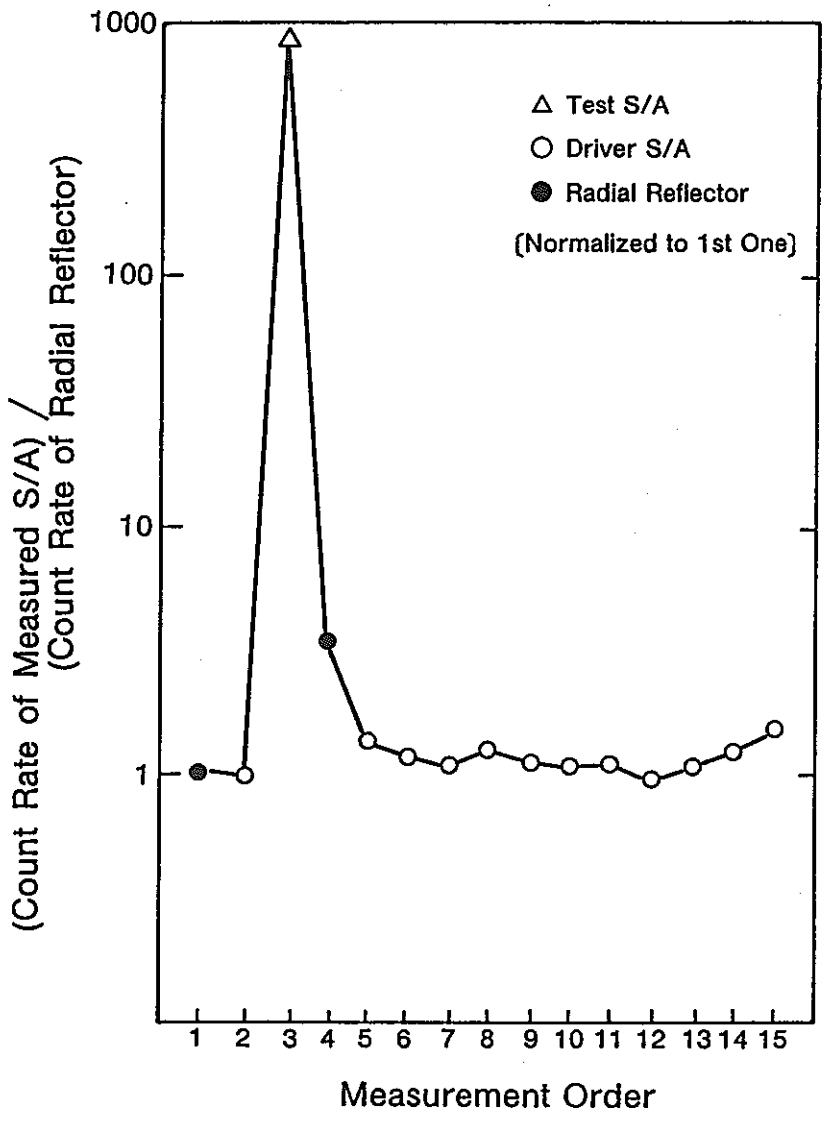

Fig. 7.5 Relative Count Rate of ^{133}Xe Gamma-ray (Photo Peak at 81keV) from Examined Subassemblies

8. BURN-UP DISTRIBUTION MEASUREMENT OF JOYO SPENT FUEL

The non-destructive analysis (NDA) of spent fuels based on gamma spectroscopy has been developed and applied in JOYO for conducting the integrity check and the burn-up management of the spent fuels on site.

8.1 Equipment Description

The burn-up measurement is conducted on the spent fuel contained in a stainless steel can in the spent fuel cooling pond in JOYO with a equipment shown in Fig. 8.1. The equipment consists of a fuel scanning device which holds a spent fuel can, moves it up and down and rotates it circumferentially, a pure germanium detector system, a gamma ray collimation system which consists of a collimator pipe, slits and absorbers arranged as shown in Fig. 8.2, a neutron detector part, and instrumentations shown in Fig. 8.3.

8.2 Measurement Procedure

The spent fuel subassembly storaged in the spent fuel cooling pond after the sodium cleaning and canning processes is moved to and set up on the fuel scanning device by the spent fuel transfer machine under water. The measurement procedures are described with some results, hereafter.

(1) Burn-up Monitor

To obtain a relative distribution of fission products in the fuel, the fuel irradiated at the core region is set at the collimated head position, and is measured by the Ge detector system for 500 seconds of live time. A gamma ray spectrum obtained by the Ge detector system is transferred to the HP9845B micro computer and subsequently analyzed with the "GAMMA-V" code, originally produced by Toshiba Co. and improved by PNC, both for the identification of nuclide and for the determination of a net counting rate for each nuclide. A typical gamma ray spectrum is shown in Fig. 8.4.

The burn-up of over 10 spent fuels have been already measured by this method. The measured count rates for the fuels, standardized by considering cooling periods, are plotted against the burn-ups calculated by the MAGI code system; three dimensional Hex-Z diffusion theory; in Fig. 8.5, resulting in that ^{144}Ce-^{144}Pr is the best and ^{106}Ru-^{106}Rh is better to be used as an index nuclide for burn-up monitor based by the NDA method.

(2) Burn-up Distribution

To obtain the axial distribution of target nuclide in the fuel, photo-peak area in the gamma ray spectrum is discriminated by a single channel analyzer (SCA) and is continuously accumulated in the multi-channel scalar (MCS) along with axial scanning of the fuel subassembly.

This method is applicable only for the high energy gamma ray because the Compton scattering effect obstructs to count the photo-peak area accurately. As an example of the high energy photo-peak, 2186keV gamma ray of ^{144}Pr is shown in Fig. 8.4 and a ^{144}Pr distribution measured with its photo-peak is also shown in Fig. 8.6. On the other hand, in the ^{137}Cs measurement with the 661keV photo-peak counts, the results are sometimes strongly contaminated by Compton scattered gamma ray as shown in Fig. 8.7 (a). A simple method explained in Fig. 8.8 is newly developed to correct the Compton scattering effect in the gamma spectrometry and is applied in practical use. An example of the corrected ^{137}Cs distribution is shown in Fig. 8.7 (b).

A circumferential distribution can be also obtained in almost the same manner as the axial one but with 3.6 degrees per second for the rotational speed and 0.5 second per channel for the MCS setting. Figure 8.9 shows a circumferential gross gamma distribution obtained from a spent fuel subassembly which has been irradiated adjacent to the control rod.

(3) Measurement of Fuel Stack Length

In order to measure the fuel stack length, gamma ray measurements are conducted in the same manner as item (1) at the positions of ten to twenty axial levels with a interval of 1mm around the suspected top and the bottom of fuel column, respectively, as shown in Fig. 8.10. Measured changes of the fuel stack length are plotted against the row number of the core at which the fuel has been irradiated, as can be seen in Fig. 8.11, resulting in showing that the densification of the fuel is getting more apparent as the linear heat rate of the fuel increases.

8.3 Summary

The technology of the relative burn-up monitoring and of the burn-up distribution measurement are established by the NDA system.

Measurements and studies will be conducted by the NDA method on spent fuels in JOYO aiming at the extension of data base for the verification of codes for nuclide production & decay such as "ORIGEN" and for clarifying the irradiation behavior of FBR fuels.

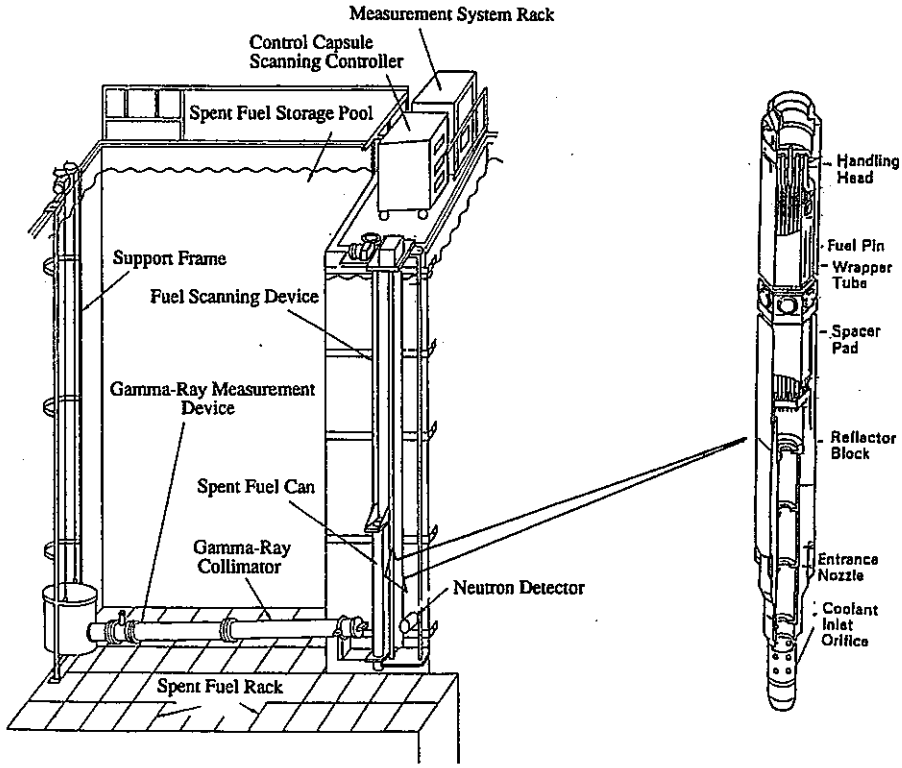

Fig. 8.1 Schematic Diagram of Scanning Device Arrangement at Gamma-Neutron Scanning Test

(in mm)

Mode	Movable Slit	Movable Absorber
Open	10	0
Close	2	20

Slit (in mm)

Slit	Width	Length
Object	30	110
Intermediate	20	80
Detector	10	20

Fixed Absorber (in mm)

Element	Thickness
Pb	10.00
Sn	1.01
Cu	0.53

Mark	Description	Material
1	Detector Vessel	SUS 304
2	Detector Slit	Pb
3	Movable Absorber	Pb
4	Collimator Pipe	SUS 304
5	Intermediate Slit	Pb
6	Object Slit	Pb
7	Movable Slit	SUS 304
8	Static Absorber	Pb, Sn, Cu
9	Spent Fuel Can	SUS 304
10	Ge Detector&Dewar	-

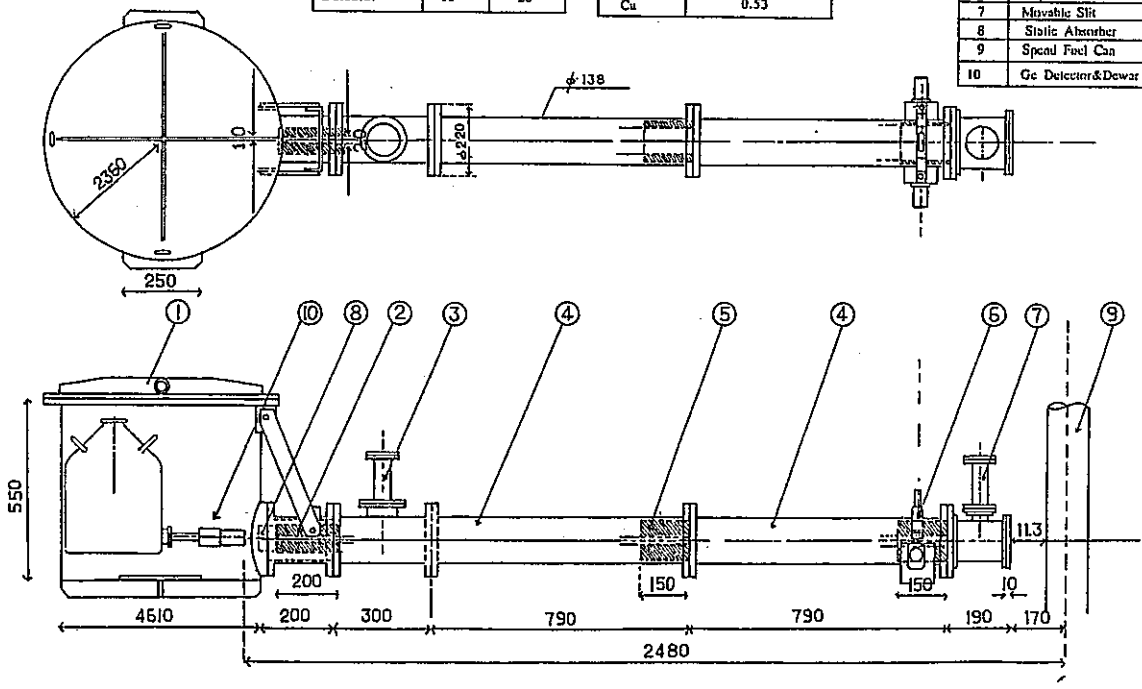

Fig. 8.2 Schematic Diagram of Collimation System

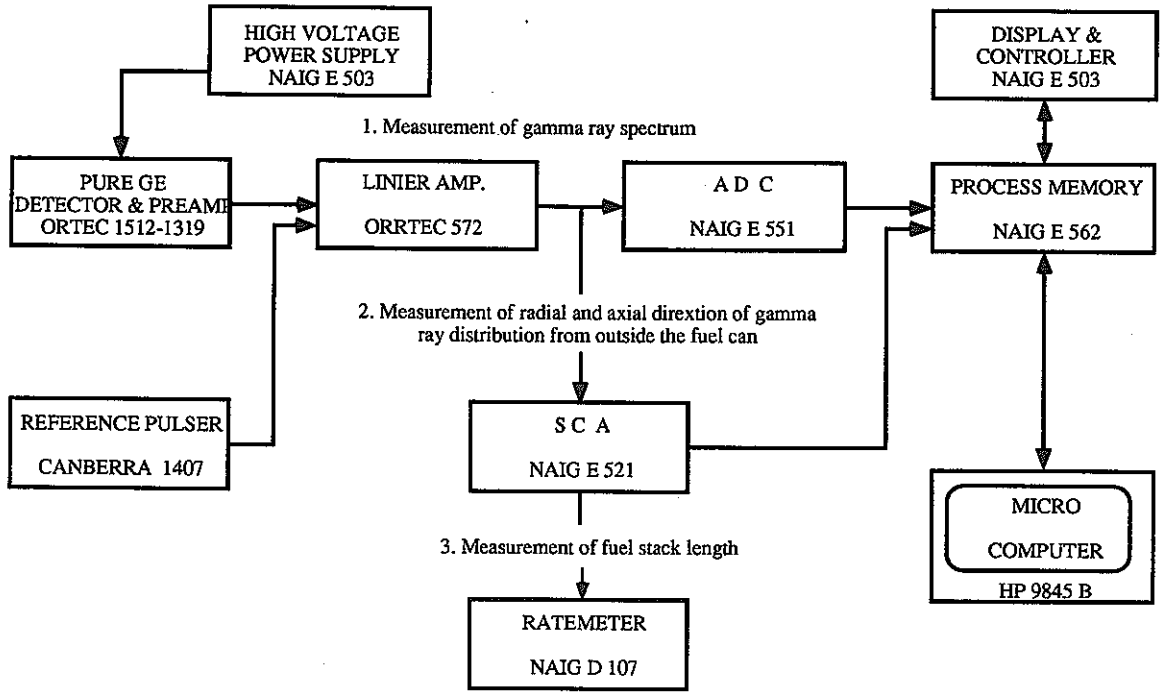

Fig. 8.3 Electronic Block Diagram of Gamma Ray Instrumentation for measuring of Spent Fuel Subassembly

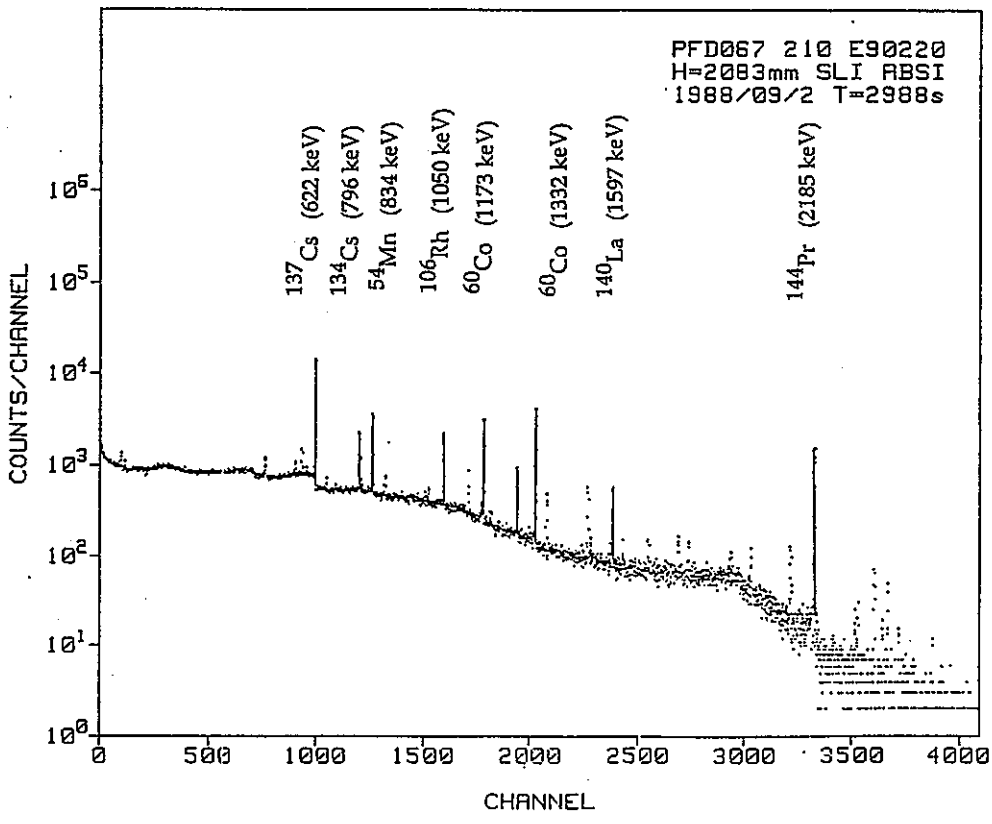

Fig. 8.4 Typical Gamma Spectrum of Spent Fuel Subassembly

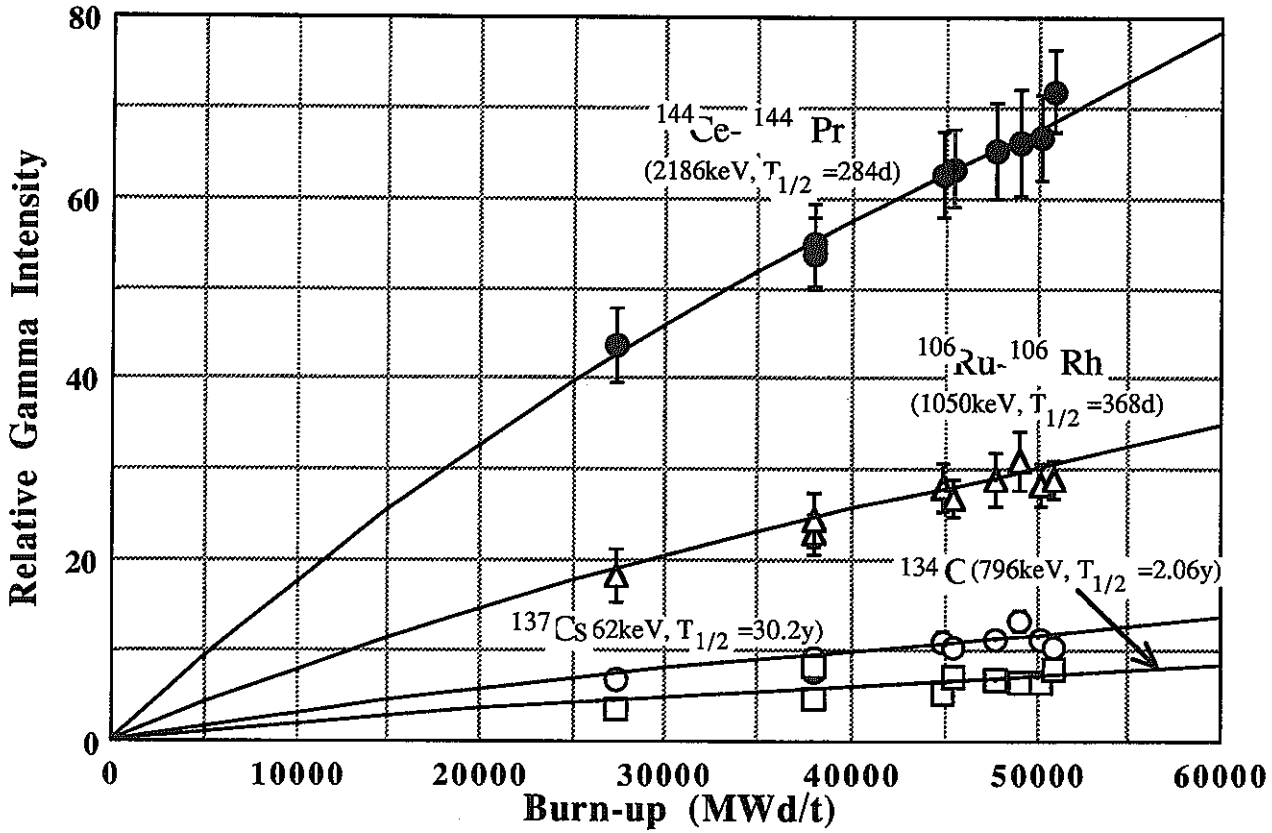

Fig. 8.5 Relation between Measured Activity and Burn-up Calculated by MAGI

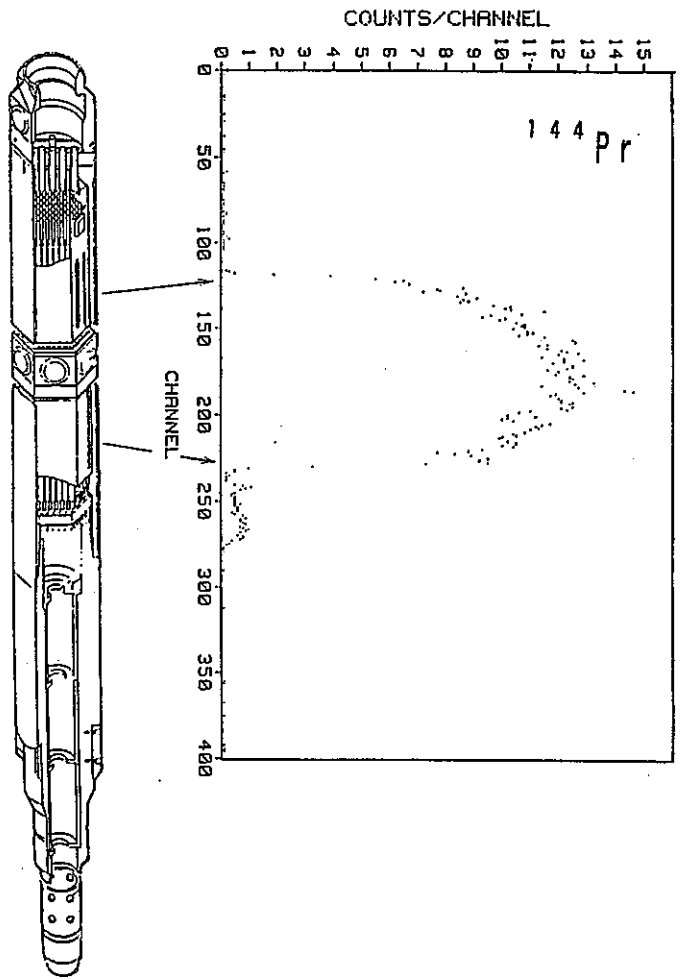

Fig. 8.6 Axial Distribution of ^{144}Pr

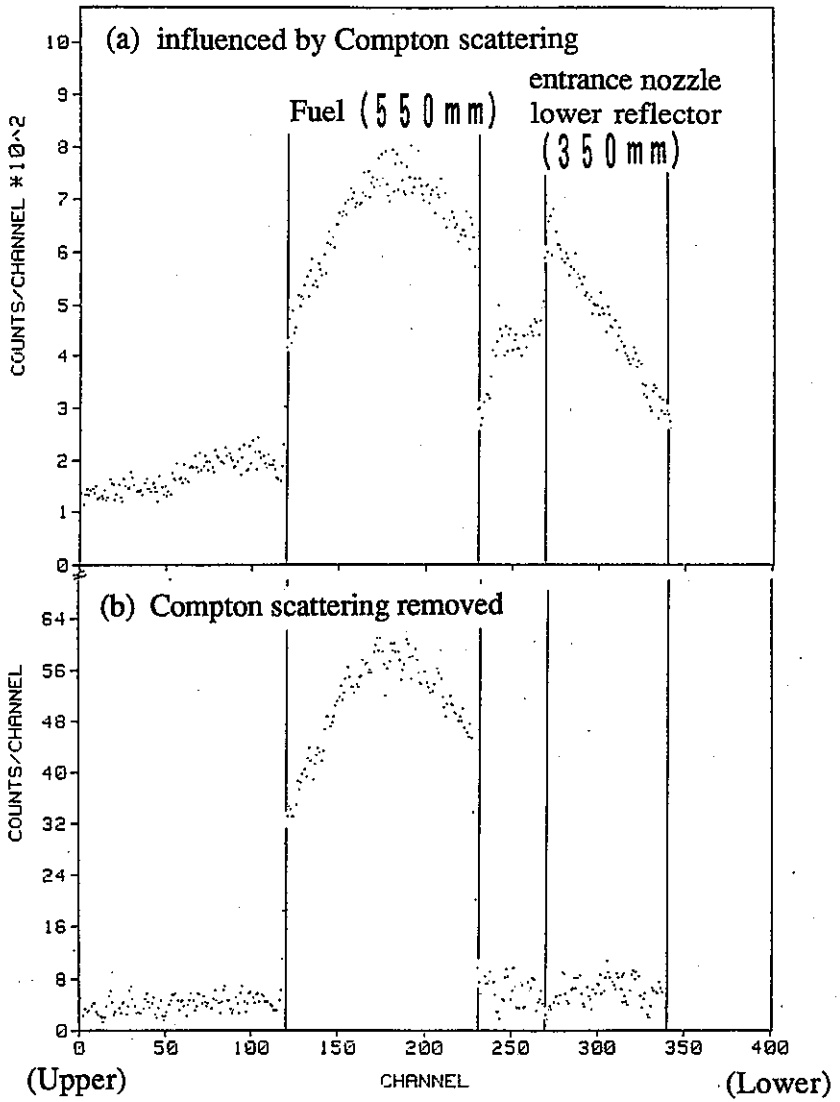

Fig. 8.7 Axial Distribution of ^{137}Cs for PFD024 S/A before and after Correction of Compton Scattering

(1) Measurement of gamma ray spectrum at fixed position

(2) Discrimination of photo peak area, net area and main background (BG) area

(3) Determination of sub-BG area by considering sub-BG area equal to main BG area

(4) Measurement of axial distribution with photo peak area

(5) Measurement of the same as (4) on sub-BG area

(6) Subtraction (5) from (4)

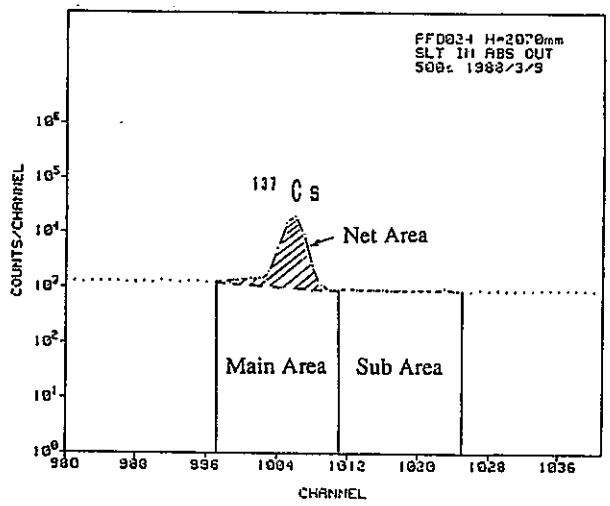

Fig. 8.8 Correction Method of Compton Scattering Effect

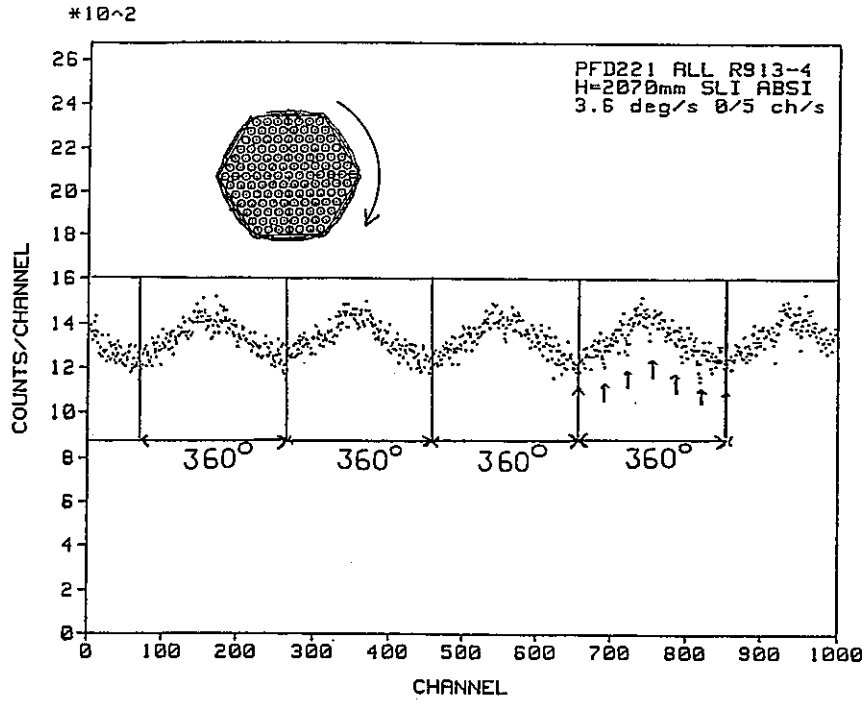

Fig. 8.9 Circumferential Distribution of Gamma Intensity at the Fuel Center Level

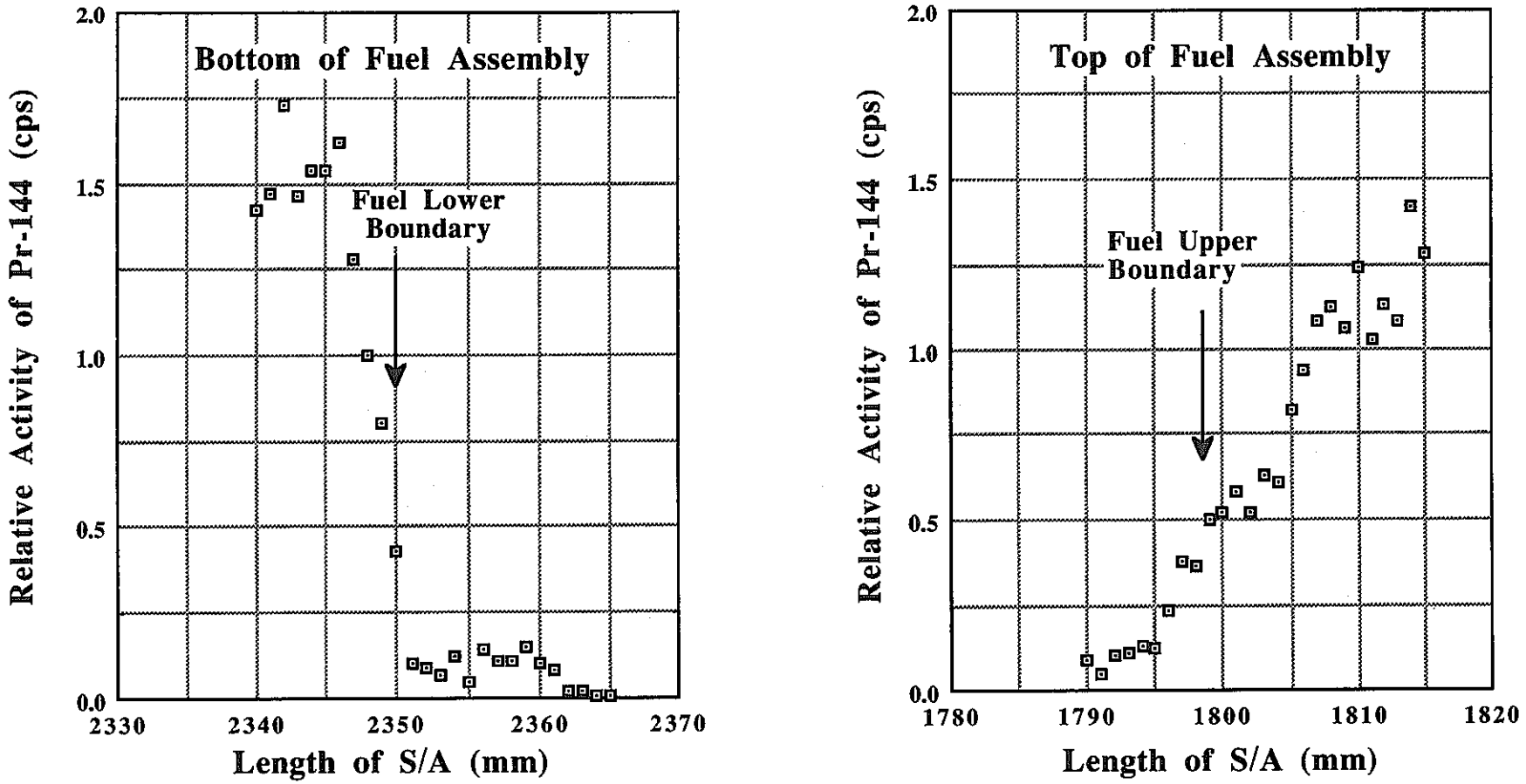

Fig. 8.10 Relative Activities at Top and Bottom of Fuel Stack

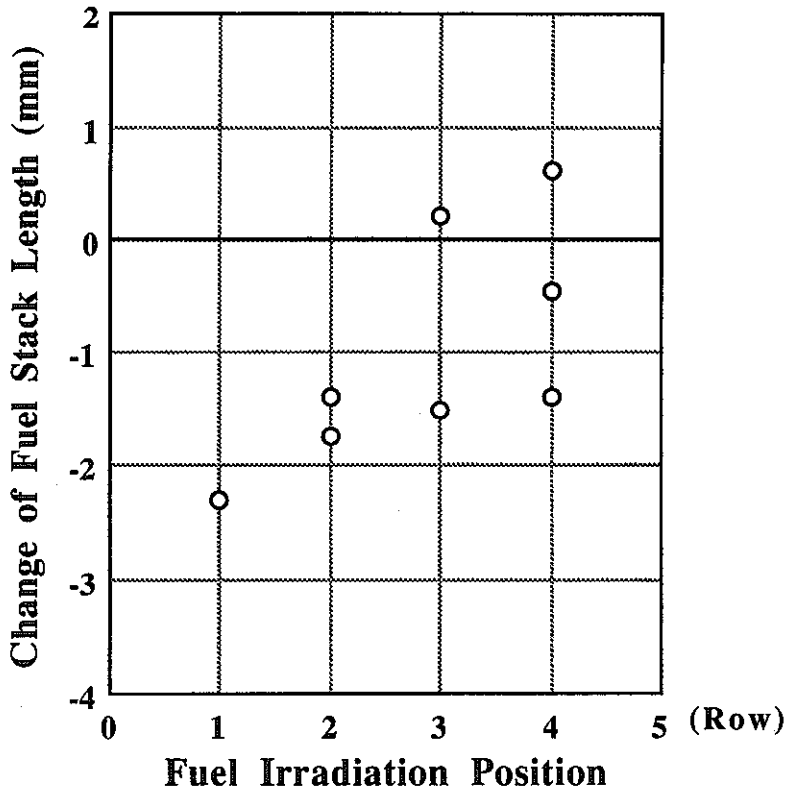

Fig. 8.11 Changes of Fuel Stack Length

9. MEASUREMENT OF RADIOACTIVE CORROSION PRODUCTS (CP)

The sodium cooled fast reactor JOYO has been operated for 14 years or more (about 4 years of effective full power years) since the initial criticality in April 1977 and the cumulative reactor output has now been achieved over $1.5X10^5$MWd. Since JOYO has not yet experienced any operation with breached fuels, the radio active contamination with FPs has not become an issue in the plant system. Then, during annual plant inspections, to prevent the hazard of radiation exposure from long-lived ^{22}Na, all primary sodium in the main circulating loops is drained into a sodium tank. Under these conditions, the spatial gamma dose rate distribution is dominated by the radioactive CPs which have deposited on inner surfaces of primary piping and components. This means that most personnel exposure has come from these CPs.

At the 6 annual inspections (the end of MK-I operation: July 1982; MK-II 4th: Feb., 1984; 5th: Sept.,1985; 6th: April,1987; 7th: Sept.,1988, 8th:May,1990), radioactive CP deposits on inner surfaces of the primary main piping (A-loop)were measured at 14 locations shown in Fig. 9.1, using a Ge solid state detector system. The geometrical layout for measurement points and sodium piping is illustrated in Fig.9.2. The detector system was calibrated by the use of a piping mock-up with two planer type standard gamma sources, ^{54}Mn and ^{60}Co, as shown in Fig. 9.3, so that absolute amounts of CP deposits could be obtained from the gamma spectra. As an example of the resulting gamma spectra, that for location CP-001 is given in Fig. 9.4.

In every annual inspection, gamma dose rates from radioactive CP deposits on inner surfaces of primary main piping and components are measured by using calcium sulfate ($CaSO_4$) thermo-luminescence dosimeters (TLDs). Gamma dose rate distribution near the piping is measured in detail for 93 locations, at one meter intervals along loop(A) from the outlet to the inlet of the reactor vessel. For each location TLDs are placed every 90 degrees around the thermal insulator cover. The geometrical conditions for the measurements is almost the same as those for the radioactive CP deposit mentioned above.

Along with these measurements, a corrosion product behavior analysis code has been developed and verified with the measured radiation data, in order to analyze the distribution of corrosion product in the primary cooling system. Further, to estimate the radiation exposure of maintenance personal, a three dimensional analysis code for the primary piping cell radiation distribution has been also developed by PNC.

Summary of results so far obtained are as follows.

(1) The radiation source of the primary cells is deposited corrosion product, and the dominant nuclides are ^{54}Mn and ^{60}Co.

(2) Deposited corrosion products are built-up along with the reactor operation time, and the activity is increasing together with the accumulated thermal power as shown in Fig. 9.5.

(3) The calculated activities shows good agreement with the measured of corrosion products which deposits on the piping in the order of $1\mu Ci/cm^2$ for ^{54}Mn and $0.1\mu Ci/cm^2$ for ^{60}Co.

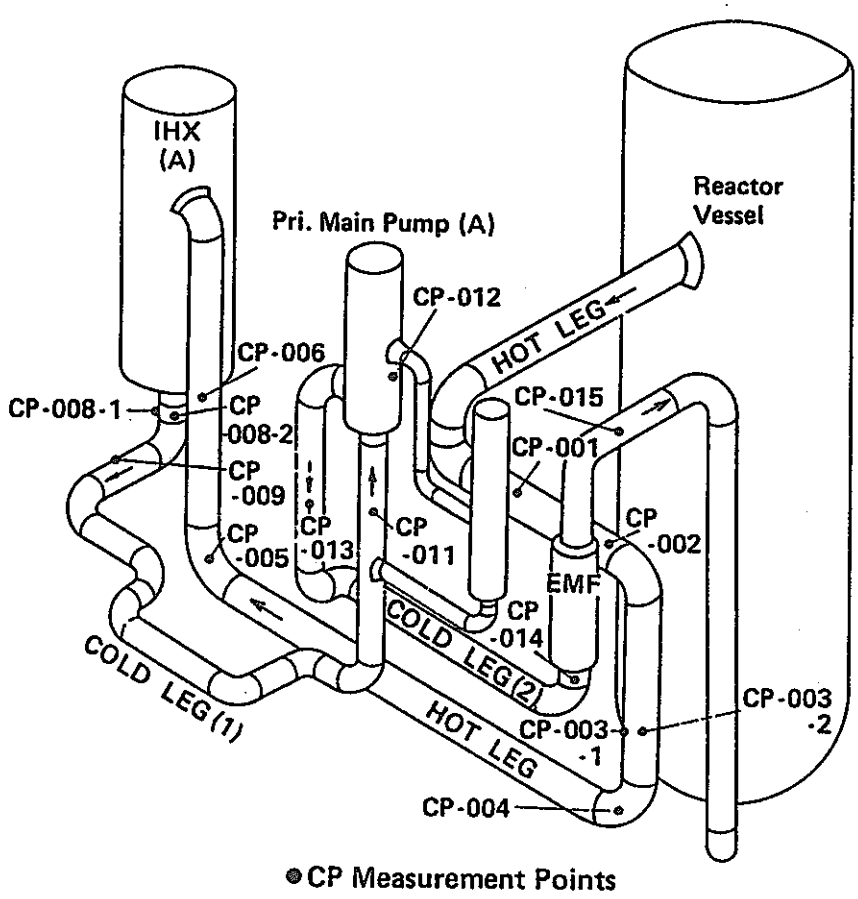

Fig. 9.1 Measurement Points for CP Deposits

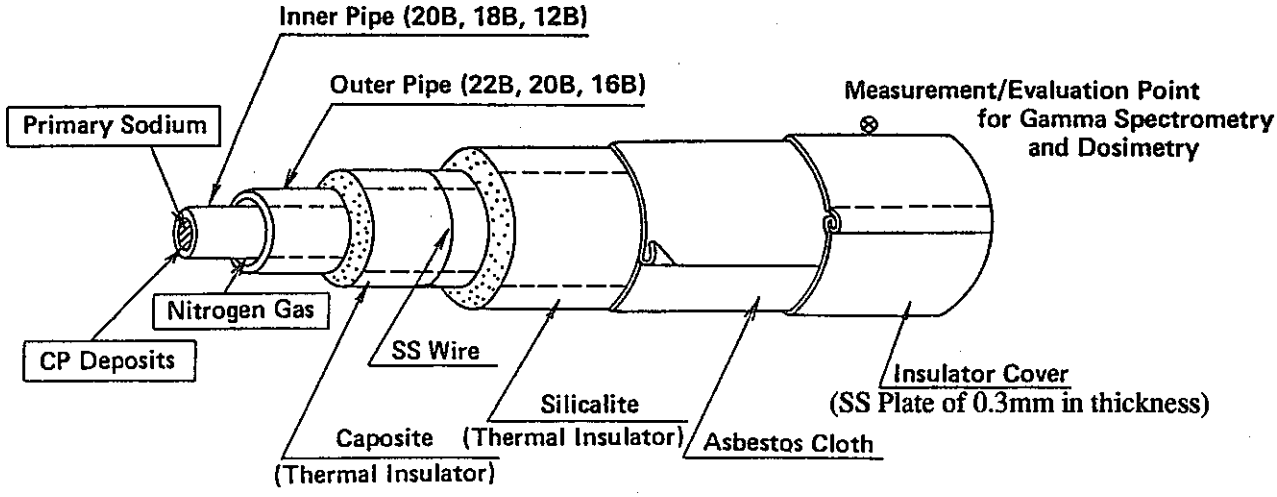

Fig. 9.2 Geometrical Layout of Measurement Points and Sodium Pipe

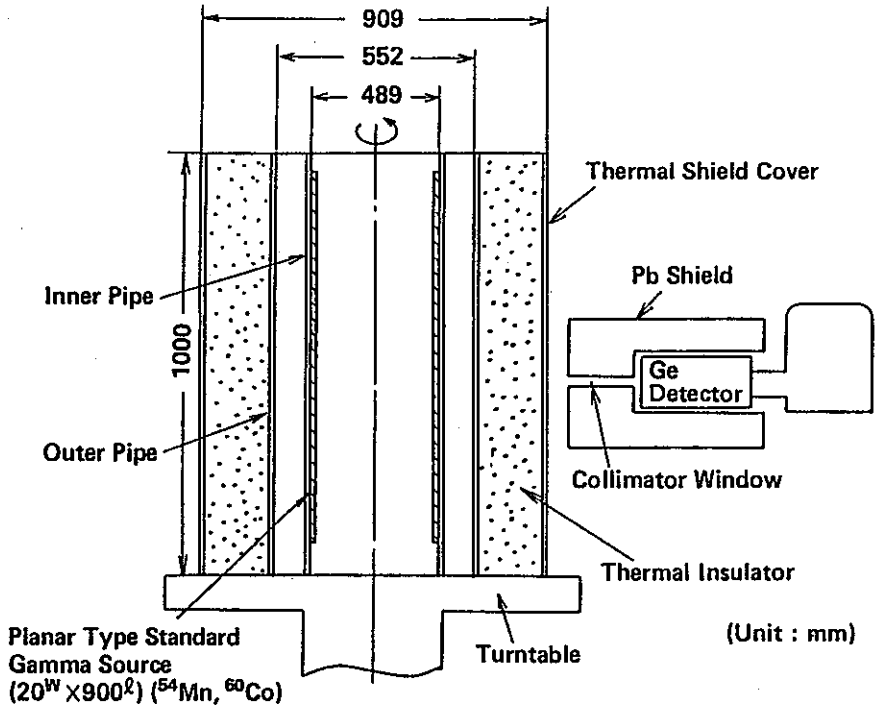

Fig. 9.3 Pipe Mock-up Arrangement for Calibration of CP Measurement System

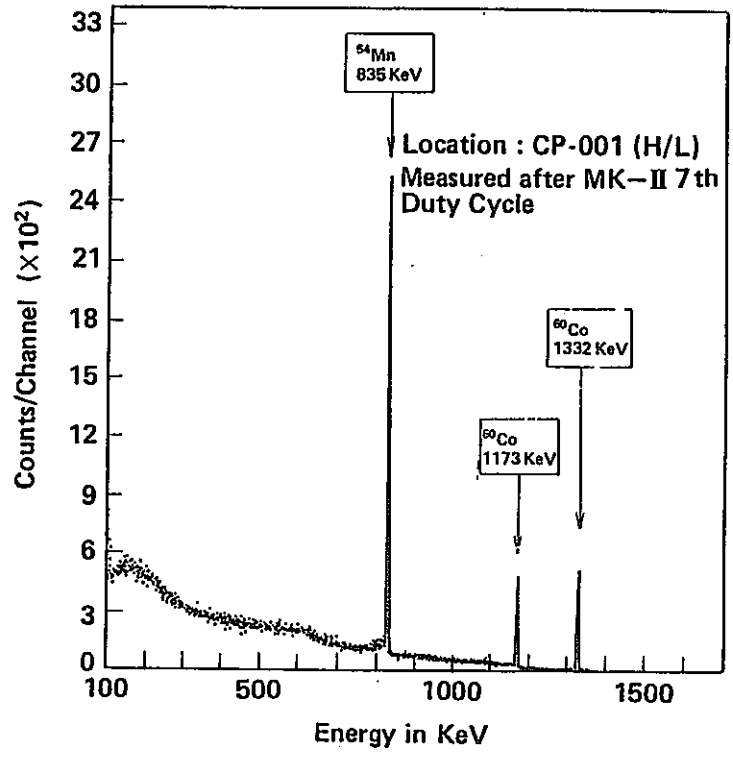

Fig. 9.4 Typical Gamma-ray Spectrum of CP

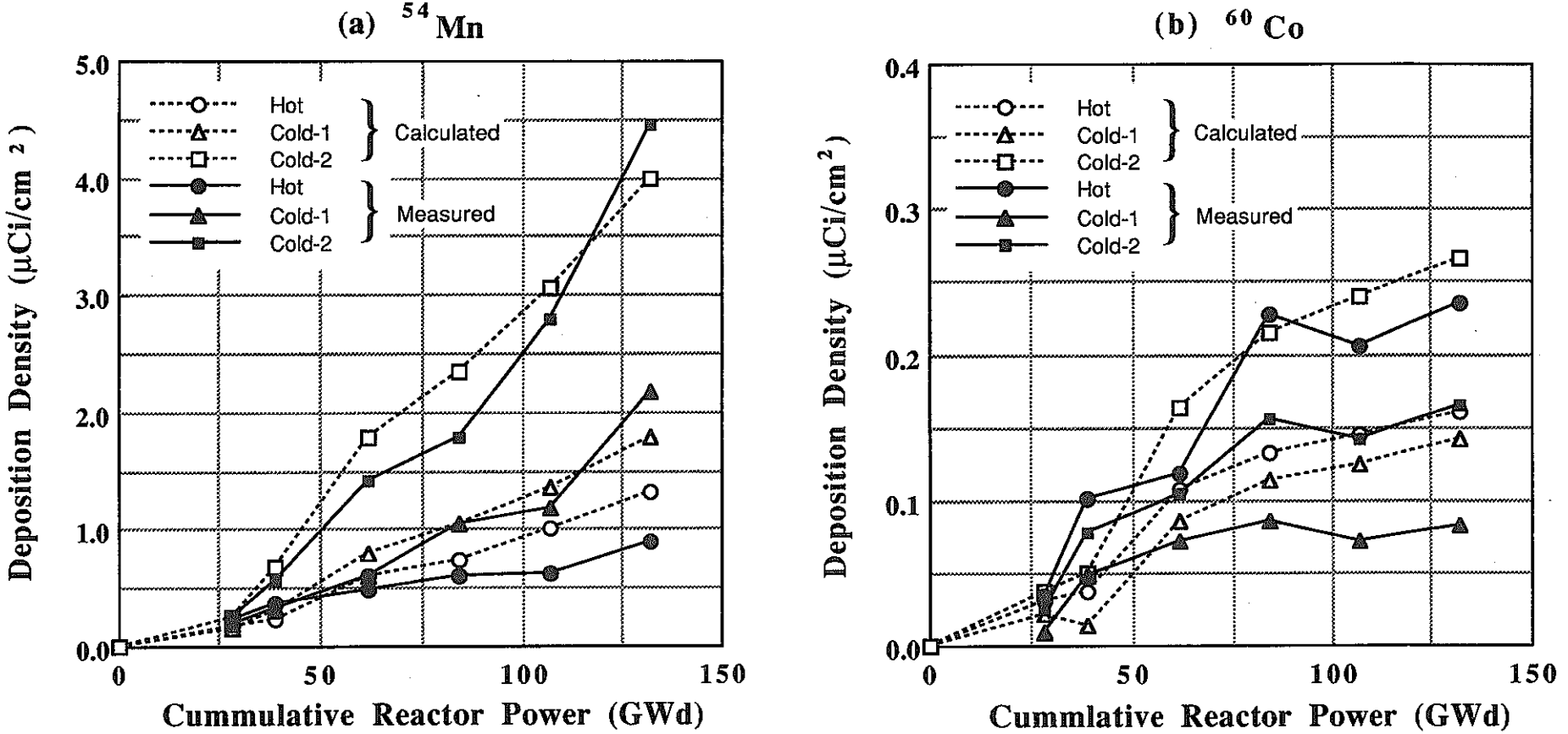

Fig. 9.5 Comparison of Measured and Calculated CP Build-up in Primary Main Cooling Piping (A)

ACKNOWLEDGMENT

The authors wish to thank T. MASUI of Inspection Development Company Ltd. for his supporting work in measurements, analyses and discussions described in this report.